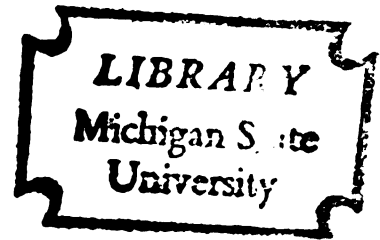


THE EFFECT OF ACTUAL AND INHERENT AUSTENITE  
GRAIN SIZE ON IMPACT PROPERTIES OF MEDIUM  
CARBON STEELS

Dissertation for the Degree of Ph. D.  
MICHIGAN STATE UNIVERSITY  
MICHAEL WESLEY WISTI  
1975



This is to certify that the  
thesis entitled  
THE EFFECT OF ACTUAL AND INHERENT AUSTENITE GRAIN  
SIZE ON IMPACT PROPERTIES OF MEDIUM CARBON STEELS

presented by  
Michael Wesley Wisti

has been accepted towards fulfillment  
of the requirements for  
Ph.D. degree in Metallurgical Engineering

A handwritten signature in cursive script, appearing to read "Howard N. Howard".

Major professor

Date 8/7/75



CH 7734

ABSTRACT

THE EFFECT OF ACTUAL AND INHERENT AUSTENITE GRAIN  
SIZE ON IMPACT PROPERTIES OF MEDIUM CARBON STEELS

By

Michael Wesley Wisti

The effect of actual and inherent austenite grain size on impact properties was determined for two heats of AISI 1040 and two heats of AISI 1046 steel. One heat of each AISI grade was inherently fine grain and the other was inherently coarse grain by the McQuaid-Ehn criterion. All steels were subjected to several austenitizing treatments which varied the austenite grain size from ASTM No. 0 to ASTM No. 10. Impact properties were determined using half-width Charpy V-notch specimens heat treated by air-cooling, or quenching and tempering to a hardness of 26-28 R<sub>c</sub>. Tensile properties were also determined for the quenched and tempered specimens.

All quenched and tempered specimens produced impact properties which are excellent for most applications since the highest energy transition temperature was -65°C. Inherently fine grain steels had slightly lower transition temperatures than inherently coarse grain steels, but the upper shelf energy was approximately equal. Specimens quenched from actual fine grained austenite showed a slight improvement in upper shelf energy, generally about 10%, but up to 100% in one case; however, the transition temperature was not affected.

Impact properties of air-cooled specimens were extremely sensitive to actual prior austenite grain size. Specimens cooled from coarse austenite grains had energy transition temperatures between 25-45°C. Room temperature impact energy was increased 100-400% by cooling from actual fine grained austenite.

Tensile test results of quenched and tempered specimens showed percent reduction in area slightly improved, or increased 100% in one case, by quenching from actual fine grained austenite. Only specimens austenitized at low temperatures for short times produced sharp yield point behavior, and the degree of sharp yield was increased with increasing aluminum content. All other quenched and tempered tensile properties were equivalent for both actual or inherent, coarse and fine grain steels.

Explanations are advanced to account for the slightly improved impact properties exhibited by inherently fine grain steels, as well as the sharp yield point behavior produced by certain heat treatments. The discussion encompasses a review of austenite grain coarsening theories, deoxidation practices involved in steelmaking, and the relationship between prior austenite grain size and ferrite size and shape in tempered martensite. A possible mechanism is suggested which involves the precipitation of aluminum nitride on lattice defects. This may account for the slight improvement in impact properties and the more pronounced sharp yield point behavior produced by aluminum killed steels. A possible beneficial stress relieving effect produced by sharp yielding is also suggested.

THE EFFECT OF ACTUAL AND INHERENT AUSTENITE GRAIN  
SIZE ON IMPACT PROPERTIES OF MEDIUM CARBON STEELS

By

Michael Wesley Wisti

A DISSERTATION

Submitted to  
Michigan State University  
in partial fulfillment of the requirements  
for the degree of

DOCTOR OF PHILOSOPHY

Department of Metallurgy, Mechanics, and Materials Science

1975

## ACKNOWLEDGMENTS

During the completion of this research project several people have sacrificed their time and offered constant encouragement. My wife, Lori, has been a continual source of support and without her encouragement the work would not have been completed. My sons, Mike Jr. and Leif, have been tolerant and understanding throughout the course of this project. My major professor, Dr. Howard Womochel, was a major source of encouragement and his totally positive approach made the work a pleasurable experience.

In the experimental portion of this work much help was provided by industry. The steel was obtained through the efforts of the late Chuck Gahagen of Youngstown Steel Corporation and Bill Brown of Republic Steel Corporation. Salt bath heat treating facilities were provided by the Lansing Heat Treating Company, and the impact testing was performed at Central Foundry Division, General Motors Corporation. The scanning electron microscope and microprobe work was performed at Oldsmobile Division, General Motors Corporation by Leo Tankersley and Jim Roman. To these people and their companies, I am extremely grateful for the courteous manner in which the use of these facilities was extended.

My committee members, Drs. Gary Cloud, Frank Blatt, D. J. Montgomery, William Bradley and Robert Summitt, offered many helpful suggestions during the course of this work. I am especially grateful for the many hours they spent editing the final draft of the thesis.

## TABLE OF CONTENTS

	Page
LIST OF TABLES .....	vi
LIST OF FIGURES .....	viii
CHAPTER I. INTRODUCTION .....	1
1.1. Economic Considerations .....	3
1.2. Historical Summary .....	4
1.3. Grain Size Control .....	7
1.4. Transition Temperature .....	10
1.4.1. Notch Effect .....	11
1.4.2. Specimen Size .....	12
1.4.3. Strain Rate .....	12
1.4.4. Chemical Composition .....	12
1.4.5. Microstructure .....	13
1.5. Fracture .....	14
1.6. Description of Fractures .....	16
1.7. Brittle Fracture .....	16
1.8. Ductile Fracture .....	18
1.9. Use of SEM in Fractography .....	18
1.10. Objectives .....	18
1.11. Summary .....	20
CHAPTER II. PROCEDURE .....	22
2.1. Chemical Analysis .....	22
2.2. Grain Coarsening Characteristics .....	24

	Page
2.3. Selection of Austenitizing Temperatures .....	32
2.4. Heat Treating .....	33
2.5. Hardness .....	35
2.6. Microstructure .....	36
2.7. Specimen Preparation .....	36
2.8. Impact Testing .....	37
2.9. Instrumented Impact Testing .....	40
2.10. Tensile Testing .....	42
2.11. Examination of Fractures .....	43
CHAPTER III. EXPERIMENTAL RESULTS .....	44
3.1. Quenched Hardness .....	44
3.2. Tempered Hardness .....	45
3.3. Hardness of Air-Cooled Specimens .....	45
3.4. Microstructure of Quenched Specimens .....	48
3.5. Microstructure of Quenched and Tempered Specimens .....	48
3.6. Microstructure of Air-Cooled Specimens .....	57
3.7. Impact Testing .....	66
3.8. Load-Time and Energy-Time Curves .....	73
3.9. Macroscopic Examination of Fractures .....	82
3.10. Microscopic Examination of Fractures .....	88
3.11. Microscopic Examination of Inclusions .....	92
3.12. Sharp Yield Point .....	99
CHAPTER IV. DISCUSSION .....	104
4.1. Grain Growth .....	104
4.2. Grain Size Control During Heat Treating .....	107
4.2.1. Quenching and Tempering .....	107
4.2.2. Air-Cooling .....	108

	Page
4.3. Effect of Grain Size on Impact Properties .....	109
4.3.1. Effect of Actual Austenite Grain Size on Impact Properties .....	109
4.3.2. Effect of Inherent Grain Size on Impact Properties .....	112
4.4. The Charpy Impact Test .....	115
4.5. Instrumented Impact Testing .....	118
4.6. Fracture Appearance .....	118
4.7. Sharp Yield Point .....	119
4.8. General Remarks .....	124
CHAPTER V. CONCLUSIONS .....	128
BIBLIOGRAPHY .....	134

## LIST OF TABLES

Number	Page
1	Effect of Inherent and Actual Grain Size on Impact Properties . 1
2	Chemical Analysis of Steel in Weight Percent ..... 23
3	Nitrogen and oxygen analysis in parts per million ..... 24
4	Grain Coarsening Characteristics ..... 26
5	Time-Sensitive Grain Coarsening ..... 26
6	Average Grain Size for Austenitizing Treatments Selected ..... 32
7	Rockwell "C" hardness of specimens quenched from the austenitizing temperature shown ..... 44
8	Knoop hardness number of specimens quenched from the austenitizing temperature shown ..... 46
9	Rockwell "C" hardness after quenching and tempering. Specimens were quenched from the austenitizing temperature shown. .... 46
10	Knoop hardness number after quenching and tempering. Specimens were quenched from the austenitizing temperature shown. .... 47
11	Rockwell "B" hardness of specimens air-cooled from the austenitizing temperature shown..... 47
12	Charpy V-notch impact energy in ft. lbs. for quenched and tempered AISI 1040 steel ..... 67
13	Charpy V-notch impact energy in ft. lbs. for quenched and tempered AISI 1046 steel ..... 67
14	Inflection point transition temperature for half-width, quenched and tempered Charpy V-notch specimens ..... 72
15	Charpy V-notch impact energy in ft. lbs. for air-cooled specimens ..... 74
16	Inflection point transition temperature for half-width, air-cooled Charpy V-notch specimens ..... 74

Number	Page
17 Percent brittle fracture for quenched and tempered specimens ..	77

## LIST OF FIGURES

Number	Page
1 Relation of Austenite Grain Size to Toughness at 50 R <sub>c</sub> .....	3
2 Impact properties v.s. grain size at 50 R <sub>c</sub> .....	6
3 Impact properties v.s. hardness for coarse and fine grain steels	6
4 Effect of austenite grain size on toughness and transition temperature at 27 R <sub>c</sub> .....	6
5 Aluminum nitride v.s. temperature for steel heated one hour and quenched from the temperature indicated .....	9
6 Effect of microstructure on impact properties .....	14
7 Schematic representation of a flow curve intersecting cleavage and fracture curves .....	15
8 The effect of testing temperature on the fracture strength, yield strength, and ductility of steel .....	15
9 Grain Coarsening Characteristics .....	27
10 Grain coarsening characteristics of Youngstown #66797 (IC). First column top to bottom: austenitized at 1500, 1600, 1700 and 1800°F. Second column top to bottom: austenitized at 1900, 2000, 2100 and 2200°F. (100x) .....	28
11 Grain coarsening characteristics of Youngstown #95313 (IF). First column top to bottom: austenitized at 1500, 1600, 1700 and 1800°F. Second column top to bottom: austenitized at 1900, 2000, 2100 and 2200°F. (100x) .....	29
12 Grain coarsening characteristics of Republic #5023766 (IC). First column top to bottom: austenitized at 1500, 1600, 1700 and 1800°F. Second column top to bottom: austenitized at 1900, 2000, 2100 and 2200°F. (100x) .....	30
13 Grain coarsening characteristics of Republic #5054025 (IF). First column top to bottom: austenitized at 1500, 1600, 1700 and 1800°F. Second column top to bottom: austenitized at 1900, 2000, 2100 and 2200°F. (100x) .....	31

Number	Page
14 Effect of transfer time from cooling medium to fracturing a standard Charpy V-notch specimen .....	39
15 Typical load-time and energy-time curves from instrumented impact testing .....	41
16 As-quenched martensite structure for Youngstown #66797 (IC) (AISI 1040) Top: austenitized at 2000°F., 4 hours. Bottom: austenitized at 1500°F., 2 minutes (1000x), nital etch .....	49
17 As-quenched martensite structure for Youngstown #95313 (IF) (AISI 1040) Top: austenitized at 2100°F., 4 hours. Bottom: austenitized at 1500°F., 5 minutes (1000x), nital etch .....	50
18 As-quenched martensite structure for Republic #5023766 (IC) (AISI 1046) Top: austenitized at 2100°F., 4 hours. Bottom: austenitized at 1500°F., 2 minutes (1000x), nital etch .....	51
19 As-quenched martensite structure for Republic #5054025 (IF) (AISI 1046) Top: austenitized at 2100°F., 4 hours. Bottom: austenitized at 1500°F., 5 minutes (1000x), nital etch .....	52
20 Quenched and tempered structure for Youngstown #66797 (IC) (AISI 1040) Top: austenitized at 2000°F., 4 hours. Bottom: austenitized at 1500°F., 2 minutes (1000x), nital etch .....	53
21 Quenched and tempered structure for Youngstown #95313 (IF) (AISI 1040) Top: austenitized at 2100°F., 4 hours. Bottom: austenitized at 1500°F., 5 minutes (1000x), nital etch .....	54
22 Quenched and tempered structure for Republic #5023766 (IC) (AISI 1046) Top: austenitized at 2100°F., 4 hours. Bottom: austenitized at 1500°F., 2 minutes (1000x), nital etch .....	55
23 Quenched and tempered structure for Republic #5054025 (IF) (AISI 1046) Top: austenitized at 2100°F., 4 hours. Bottom: austenitized at 1500°F., 5 minutes (1000x), nital etch .....	56
24 Quenched and tempered structure for Youngstown #66797 (IC) (AISI 1040) Tempered at 1300°F., 24 hours. Top: austenitized at 2000°F., 4 hours. Bottom: austenitized at 1500°F., 2 minutes (1000x), nital etch .....	58
25 Quenched and tempered structure for Youngstown #95313 (IF) (AISI 1040) Tempered at 1300°F., 24 hours. Top: austenitized at 2100°F., 4 hours. Bottom: austenitized at 1500°F., 5 minutes (1000x), nital etch .....	59

Number	Page
26 Quenched and tempered structure for Republic #5023766 (IC) (AISI 1046) Tempered at 1300°F., 24 hours. Top: austenitized at 2100°F., 4 hours. Bottom: austenitized at 1500°F., 2 minutes (1000x), nital etch .....	60
27 Quenched and tempered structure for Republic #5054025 (IF) (AISI 1046) Tempered at 1300°F., 24 hours. Top: austenitized at 2100°F., 4 hours. Bottom: austenitized at 1500°F., 5 minutes (1000x), nital etch .....	61
28 Air-cooled structure of Youngstown #66797 (IC), (AISI 1040). Top: austenitized at 2000°F., 4 hours. Bottom: austenitized at 1500°F., 2 minutes (100x), nital etch .....	62
29 Air-cooled structure of Youngstown #95313 (IF), (AISI 1040). Top: austenitized at 2100°F., 4 hours. Bottom: austenitized at 1725°F., 4 hours (100x), nital etch .....	63
30 Air-cooled structure of Republic #5023766 (IC), (AISI 1046). Top: austenitized at 2100°F., 4 hours. Bottom: austenitized at 1500°F., 2 minutes (100x), nital etch .....	64
31 Air-cooled structure of Republic #5054025 (IF), (AISI 1046). Top: austenitized at 2100°F., 4 hours. Bottom: austenitized at 1575°F., 4 hours (100x), nital etch .....	65
32 Charpy V-notch transition curves for quenched and tempered Youngstown #66797 (IC), AISI 1040 .....	68
33 Charpy V-notch transition curves for quenched and tempered Youngstown #95313 (IF), AISI 1040 .....	69
34 Charpy V-notch transition curves for quenched and tempered Republic #5023766 (IC), AISI 1046 .....	70
35 Charpy V-notch transition curves for quenched and tempered Republic #5054025 (IF), AISI 1046 .....	71
36 Charpy V-notch transition curves for air-cooled AISI 1040 steel	75
37 Charpy V-notch transition curves for air-cooled AISI 1046 steel	76
38 Load-time and energy-time curves for quenched and tempered specimens fractured at -196°C. Top to bottom: Youngstown #66797 (IC), AISI 1040; Youngstown #95313 (IF), AISI 1040; Republic #5023766 (IC), AISI 1046; Republic #5054025 (IF), AISI 1046. First column quenched from coarse grained austenite, and second column quenched from fine grained austenite. Vert. load scale: 500 lbs./div. Vert. energy scale: 2 ft. lbs./div. Horiz. time scale: 0.2 m-sec./div. ....	78

- 39 Load-time and energy-time curves for quenched and tempered specimens fractured at  $-128^{\circ}\text{C}$ . Top to bottom: Youngstown #66797 (IC), AISI 1040; Youngstown #95313 (IF), AISI 1040; Republic #5023766 (IC), AISI 1046; Republic #5054025 (IF), AISI 1046. First column quenched from coarse grained austenite; second column quenched from fine grained austenite. Vert. load scale: 500 lbs./div. Vert. energy scale: 5 ft. lbs./div. Horiz. time scale: 0.2 m-sec./div. .... 79
- 40 Load-time and energy-time curves for quenched and tempered specimens fractured at  $-62^{\circ}\text{C}$ . Top to bottom: Youngstown #66797 (IC), AISI 1040; Youngstown #95313 (IF), AISI 1040; Republic #5023766 (IC), AISI 1046; Republic #5054025 (IF), AISI 1046. First column quenched from coarse grained austenite; second column quenched from fine grained austenite. Vert. load scale: 500 lbs./div. Vert. energy scale: 5 ft. lbs./div. Horiz. time scale: 0.2 m-sec./div. .... 80
- 41 Load-time and energy-time curves for quenched and tempered specimens fractured at  $22^{\circ}\text{C}$ . Top to bottom: Youngstown #66797 (IC), AISI 1040; Youngstown #95313 (IF), AISI 1040; Republic #5023766 (IC), AISI 1046; Republic #5054025 (IF), AISI 1046. First column quenched from coarse grained austenite; second column quenched from fine grained austenite. Vert. load scale: 500 lbs./div. Vert. energy scale: 5 ft. lbs./div. Horiz. time scale: 0.2 m-sec./div. .... 81
- 42 Load-time and energy-time curves for air-cooled specimens fractured at  $-18^{\circ}\text{C}$ . Top to bottom: Youngstown #66797 (IC), AISI 1040; Youngstown #95313 (IF), AISI 1040; Republic #5023766 (IC), AISI 1046; Republic #5054025 (IF), AISI 1046. First column air-cooled from coarse grained austenite; second column air-cooled from fine grained austenite. Vert. load scale: 500 lbs./div. Vert. energy scale: 5 ft. lbs./div. Horiz. time scale: 0.2 m-sec./div. .... 83
- 43 Fractures of quenched and tempered specimens of Youngstown #66797 (IC), AISI 1040. Top row: austenitized  $1500^{\circ}\text{F}$ ., 2 min. Bottom row: austenitized  $2000^{\circ}\text{F}$ ., 4 hrs. From left to right: fractured at  $22^{\circ}\text{C}$ .,  $-62^{\circ}\text{C}$ .,  $-114^{\circ}\text{C}$ . and  $-196^{\circ}\text{C}$ . 84
- 44 Fractures of quenched and tempered specimens of Youngstown 95313 (IF), AISI 1040. Top row: austenitized  $1500^{\circ}\text{F}$ ., 5 min. Bottom row: austenitized  $2100^{\circ}\text{F}$ ., 4 hrs. From left to right: fractured at  $22^{\circ}\text{C}$ .,  $-62^{\circ}\text{C}$ .,  $-114^{\circ}\text{C}$ ., and  $-196^{\circ}\text{C}$ . ... 85
- 45 Fractures of quenched and tempered specimens of Republic #5023766 (IC), AISI 1046. Top row: austenitized  $1500^{\circ}\text{F}$ ., 2 min. Bottom row: austenitized  $2100^{\circ}\text{F}$ ., 4 hrs. From left to right: fractured at  $22^{\circ}\text{C}$ .,  $-62^{\circ}\text{C}$ .,  $-114^{\circ}\text{C}$ ., and  $-196^{\circ}\text{C}$ . ... 86

Number	Page
46 Fractures of quenched and tempered specimens of Republic #5054025 (IF), AISI 1046. Top row: austenitized 1500°F., 5 min. Bottom row: austenitized 2100°F., 4 hrs. From left to right: fractured at 22°C., -62°C., -114°C., and -196°C. ...	87
47 Fractures of air-cooled specimens tested at 22°C. Top row: air-cooled from fine grained austenite. Bottom row: air-cooled from coarse grained austenite. From left to right: Youngstown #66797 (IC), AISI 1040; Youngstown #95313 (IF), AISI 1040; Republic #5023766 (IC), AISI 1046; Republic #5054025 (IF), AISI 1046. ....	89
48 SEM fractographs of quenched and tempered specimens, quenched from coarse grained austenite. Top: Fracture at 22°C. shows microvoid coalescence. Bottom: Fracture at -196°C. shows cleavage and quasi-cleavage. (2000x) .....	90
49 SEM fractographs of quenched and tempered specimens, quenched from fine grained austenite. Top: Fracture at 22°C. shows microvoid coalescence. Bottom: Fracture at -196°C. shows cleavage and quasi-cleavage. (2000x) .....	91
50 SEM Fractographs of air-cooled specimens at 22°C. Top: air-cooled from coarse grained austenite shows fracture by cleavage. Bottom: air-cooled from fine grained austenite shows fracture by cleavage and quasi-cleavage. (2000x) .....	93
51 SEM fractographs of air-cooled specimens at 22°C. Top: Center of specimen shows a cleavage fracture. Bottom: Edge away from the notch shows a substantial microvoid coalescence. (2000x) .	94
52 Optical photomicrograph of inclusions apparently located in prior austenite grain boundaries of aluminum killed steel. Austenitized at 2100°F., 4 hrs. (1000x), unetched .....	96
53 X-ray spectrum (top) of inclusion protruding from fractured surface of SEM fractograph (Bottom). Inclusion is identified as a manganese sulfide. ....	97
54 Top: Three inclusions identified with microprobe analyzer: (triangle) high silicon; (oval) manganese sulfide; (elongated) high aluminum. Bottom: (long stringer) high aluminum; (round) manganese sulfide. Specimens were austenitized at 2100°F., 4 hrs. (2000x) .....	98
55 X-ray spectrum (top) of complex inclusion (bottom) showing peaks for aluminum, sulfur, manganese, and iron. (10000x) .....	100
56 Schematic representation of the influence of aluminum content and prior austenite grain size on the yield point of specimens tested in the quenched and tempered condition. ....	102

Number	Page
57 Classical yield point behavior in annealed low carbon steel ...	120

## INTRODUCTION

In 1938, Cross and Lowther<sup>(1)</sup> investigated the effect of austenite grain size on impact properties of air-cooled steels. They reported that inherently fine grain steels have Izod impact values 400% greater than inherently coarse grain steels, even though the actual austenite grain size was identical. They concluded that inherently fine grain steels are vastly superior in impact, and as austenite grain size increases, the impact properties of these steels decrease only moderately. The mystery of these results concerning inherently coarse grain steels was summarized by their statement, "Apparently coming events cast their shadows before." The apparent superiority of inherently fine grain steels regardless of the actual grain size, cannot be explained by present theories. The results of these experiments are summarized in Table 1.

Table 1

Effect of Inherent and Actual Grain Size on Impact Properties

<u>STEEL</u>	<u>AUSTENITIZING TREATMENT</u>	<u>ASTM GRAIN SIZE NO.</u>	<u>IZOD IMPACT FT. LBS.</u>
Inherently Coarse Grain Steel	1650°F., air cool	2-4	4
Inherently Fine Grain Steel	1800°F., air cool	2-4	16-18
Inherently Fine Grain Steel	1550°F., air cool	6-8	23-27

An inherently coarse grain steel is one in which the austenite grains coarsen to ASTM No. 4<sup>(2)</sup> or larger when austenitized at 1700°F. An inherently fine grain steel is one in which the austenite grains remain fine, ASTM No. 5 or finer, when austenitized at 1700°F. The methods for controlling and determining this grain size will be discussed later.

The effect of finer grain size resulting in vastly improved impact properties is well known and can generally be applied to all metals<sup>(3)</sup>. The situation in steel is more complicated since a phase transformation occurs during most heat treatments. One must contend with prior austenite grain size, as well as grain size after transformation. Steel subjected to impact type loading is often used in the quenched and tempered condition. Prior austenite grain size is shown to have a remarkable effect on impact properties at a relatively high hardness level (Figure 1)<sup>(4)</sup>. The steel quenched from fine grained austenite has 400% superior impact properties compared to the steel quenched from coarse grained austenite.

When using steel in impact type applications, it is important to consider impact properties over a range of temperatures. Most metals and alloys having a body-centered-cubic or hexagonal-close-packed structure show a rapid decrease in impact properties with decreasing temperature. The temperature at which the fracture changes from ductile to brittle, and impact energy shows a sharp decrease, is known as the "transition temperature". Metals which have a face-centered-cubic structure do not have a transition temperature<sup>(3)</sup>. Since steel is often used at temperatures as low as -40°C., the transition temperature is an important consideration. Brittle fractures of ships, low temperature storage vessels, bridges, and pipelines have occurred without warning and often under conditions of low stress<sup>(5)</sup>.

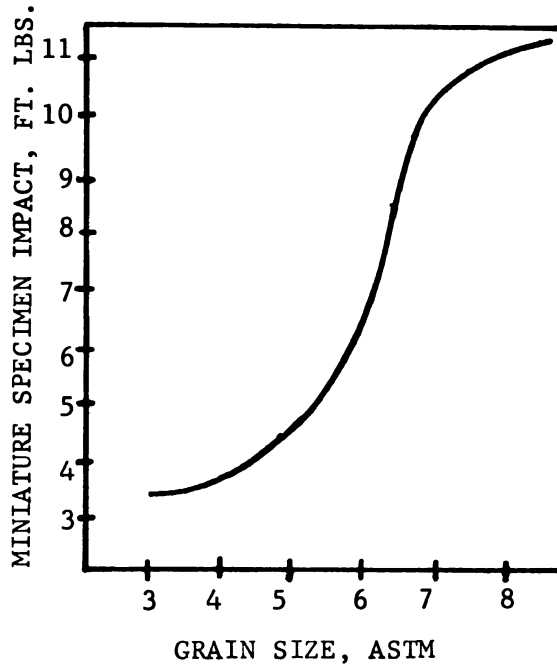


Fig. 1. Relation of Austenite Grain Size to Toughness at 50 R<sub>c</sub>

### 1.1 Economic Considerations

When selecting a grade of steel for a particular application, a critical balance usually exists between the properties required and the cost of steel. One cannot afford the insurance of using a high cost alloy steel where a carbon steel would suffice. These cost considerations extend to steelmaking practice and the use of deoxidizers. Steel is usually deoxidized by making additions of silicon, manganese, aluminum, vanadium, columbium, zirconium or titanium to the the ladle<sup>(6)</sup>. Silicon and aluminum are the least expensive and the presence of 0.02-0.06% aluminum serves to make the steel inherently fine grain. This practice is used for a majority of all structural steels.

There are many applications in which fine grain steel is not desirable since coarse grain steels have increased hardenability, better

machinability, and superior high temperature creep properties. In modern steelmaking, many problems are encountered with the use of aluminum in continuous casting operations. Aluminum oxide clogs the mold feed nozzle and abrades the mold walls. When aluminum is used for deoxidizing in continuous casting operations, an inert gas is used to shroud the ladle, or an aluminum wire is inserted into the stream above the mold. If aluminum is not used and inherently fine grain steel is made by using elements such as vanadium or columbium, approximately 3% is added to the cost of the steel. To insure fine grained austenite, hot forgings are often normalized prior to quenching and tempering. Industry spends millions of dollars annually on deoxidizers and special heat treatments to produce fine grained steel.

In our research, we are studying the effect of deoxidation practice, which largely controls grain size, on impact properties of steel in the heat treated condition. With increasing substitution of medium carbon or water quenching grades of steel as a result of economic conditions or the availability of alloying elements, a thorough knowledge of the properties of these steels becomes more important. Conditions under which less expensive grades of steel may be used or expensive heat treatments eliminated must be carefully identified.

## 1.2 Historical Summary

In 1922, the classic work of McQuaid and Ehn<sup>(7)</sup> showed that each heat of steel has its own characteristic grain growth behavior. The inherent or McQuaid-Ehn grain size was determined by carburizing a sample for eight hours at 1700°F., followed by slow cooling to allow a network of carbides to outline the prior austenite grains. Completely deoxidized

steel (killed) in which aluminum was used for final deoxidation was found to be inherently fine grain. Steel deoxidized with silicon and manganese, was found to be inherently coarse grain. Steels partially deoxidized (semi-killed), or steels not deoxidized (rimmed) were found to be inherently coarse grain. It was determined later that other elements were also capable of rendering steel inherently fine grain. The work of McQuaid and Ehn was a major breakthrough because prior to that time, the effect of aluminum in controlling grain size was not completely understood. Aluminum was often secretly added without the knowledge of higher level management in the steel mill in order to subside gas evolution and produce a sound ingot<sup>(8)</sup>. As late as 1930, German steel specifications forbid the use of aluminum in making rail steel<sup>(9)</sup>.

In the 1930's, Bain<sup>(10)</sup> (Figure 2) and Scott<sup>(11)</sup> (Figure 3) demonstrated that steel quenched from fine grained austenite had up to 400% superior impact properties over steel quenched from coarse austenite. Other investigators, such as Shane<sup>(12)</sup>, showed a 500-1000% improvement in impact properties for fine grained austenite; McQuaid<sup>(8)</sup> showed a 300-500% improvement.

Other work by Rosenberg and Gagnon<sup>(13)</sup>, and Gillett<sup>(14)</sup> showed that fine grained austenite has little or no effect on impact properties in the quenched and tempered condition. At a hardness level of 27 R<sub>c</sub>, Jaffee and Wallace<sup>(15)</sup> (Figure 4) showed that maximum impact values as well as the transition temperature are adversely affected by coarse austenite grains. More recent investigations by Parker and co-workers<sup>(16,17)</sup> showed that medium and high alloy steels have improved fracture toughness when quenched from a coarse austenitic grain size. While the work of Jolley and Kottcamp<sup>(18)</sup> showed that fine grained steels have superior

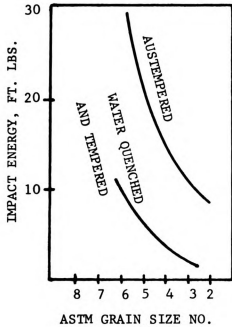


Fig. 2. Impact properties v.s. grain size at 50  $R_c$

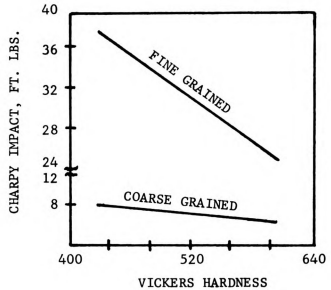


Fig. 3. Impact properties v.s. hardness for coarse and fine grain steels

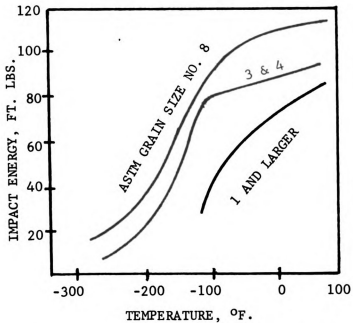


Fig. 4. Effect of austenite grain size on toughness and transition temperature at 27  $R_c$

impact properties, they noted that fine grained steels have fewer sub-grain boundaries, but were unable to relate this effectively to actual fracture mechanisms.

Over a period of fifty years, much work has been published on the effect of chemical composition and prior austenite grain size on impact properties. The magnitude of improvement in impact properties by use of fine grained steels is not clear since much of the earlier work is contradicting. This was pointed out by Bullens<sup>(19)</sup>, who discussed the role of some inherent factor within each heat of steel which controls the impact properties. The effect of prior austenite grain boundaries, and the relationship between these boundaries and ferrite grain size in tempered martensite is not well established. Results gained from properly controlled experiments, using selected heats of steel, would help to clarify the true effect of these variables.

### 1.3 Grain Size Control

Many early investigators, including McQuaid himself<sup>(8)</sup>, felt that the presence of aluminum in solid solution was effective in controlling grain growth. It was later demonstrated that as much as 0.20% of aluminum in solid solution was not effective in controlling grain size unless in the presence of oxygen<sup>(20)</sup> or air<sup>(21)</sup>. Throughout the thirties and forties, it was generally accepted that a dispersion of aluminum oxides or some other unknown constituent was responsible for restricting austenite grain growth. It was felt that these substances set up a "barrier" and advancing grain boundaries were not able to move across. Other theories suggested the degree of deoxidation was the controlling factor<sup>(22)</sup>, or the solution and re-precipitation of a grain growth

controlling substance in austenite grain boundaries precisely at the moment of transformation<sup>(23)</sup>.

In 1949, Beeghly<sup>(24)</sup> developed a dependable method for determining the aluminum combined as aluminum nitride (AlN) in steel. His results (Figure 5) showed that on heating, aluminum nitride begins to precipitate at an increased rate near the transformation temperature, and then begins to redissolve above 1800°F. A substantial amount of aluminum nitride still remains undissolved at 2000°F., which is the temperature at which most fine grain steels coarsen appreciably. Other work showed that the amount of aluminum nitride which precipitates on cooling, depends on the cooling rate<sup>(25,26)</sup>. Samples air-cooled from 2100°F. have very little aluminum as aluminum nitride at room temperature. When the sample is reheated, aluminum nitride will precipitate from solid solution indicating that thermal history is extremely important.

In 1951, Darken, Smith and Eiler<sup>(27)</sup> determined the solubility product of aluminum in austenite. They reported that solubility increased with increasing temperature in a linear relationship to the reciprocal of the absolute temperature. This is in general agreement with the work of Beeghly.

Grain boundaries are high energy areas and grains grow to effectively reduce the grain boundary area. The generally accepted modern theories on the role of aluminum in controlling austenite grain growth involve precipitation of aluminum nitride in the austenite grain boundaries. This precipitate may effectively lower the grain boundary energy. A dispersion of aluminum nitrides of microscopic or sub-microscopic size may be effective in inhibiting grain boundary movement, thereby controlling grain growth. As the temperature increases, precipitates begin to

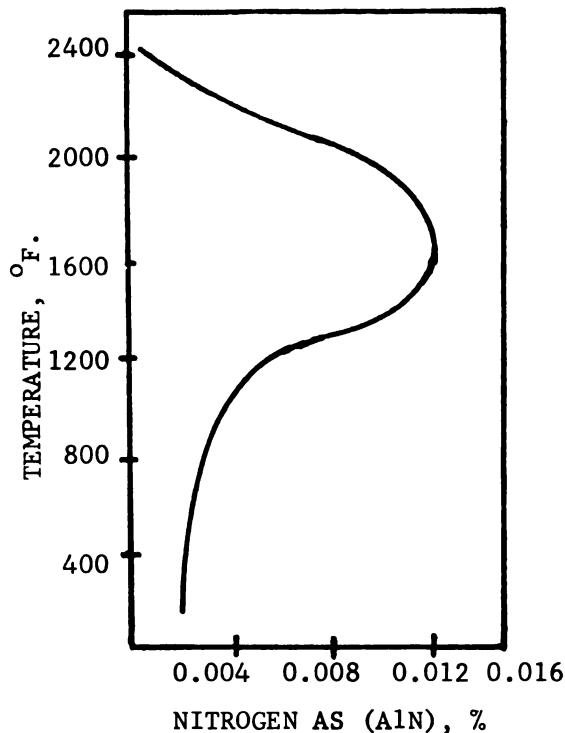


Fig. 5. Aluminum nitride v.s. temperature for steel heated one hour and quenched from the temperature indicated

coarsen, which reduces their effectiveness. At higher temperatures, aluminum nitride goes into solution and the restrictions for grain boundary movement are removed. For this reason, inherently coarse grain steels coarsen gradually over a range of temperature; while inherently fine grain steels resist coarsening at lower temperatures and then coarsen rapidly at temperatures in the range of 1900–2100°F.<sup>(4)</sup>

The aluminum nitride theory answers many of the questions concerning austenite grain growth; however, some controversy still exists. It has been shown that inherently coarse grain steel deoxidized with silicon and manganese begins to coarsen within seconds after being heated above

the transformation temperature<sup>(28,29)</sup>. Since inherently fine grain steels do not show this same behavior, one would assume that a microscopic dispersion of aluminum nitride precipitates almost instantaneously at the newly formed grain boundaries, thereby inhibiting grain boundary movement. If sufficient aluminum nitrides were present prior to transformation, this behavior could be explained; however, the results of Beeghly<sup>(24)</sup> showed very little aluminum nitrides to be present below this temperature. Since steels air-cooled from a high temperature pre-treatment have very little aluminum nitride present at room temperature, grain growth must be controlled by precipitation in the newly formed grain boundaries. The availability of aluminum for this precipitation is questionable since it is substitutional in iron and has a relatively low diffusion rate<sup>(30)</sup>. Precipitates of aluminum nitride and aluminum oxide may restrict grain boundary movement and lower grain boundary free energy, thereby decreasing the driving force for grain growth.

Other grain refining elements used in steelmaking, such as vanadium or columbium, are strong carbide formers<sup>(4)</sup> and tend to form complex carbides which resist solution in austenite. A dispersion of these carbides is present in the structure prior to transformation and are available to restrict grain boundary movement. This situation is a different one from that of steel deoxidized with aluminum where substantial nitrides may not be present prior to transformation.

#### 1.4 Transition Temperature

The transition temperature may be determined by tensile testing; however, impact testing is an effective and inexpensive alternate method. For any given material, the transition temperature varies considerably

depending on the specimen geometry and testing method<sup>(31,32)</sup>. When using notched bar impact testing, two criteria are commonly employed to determine the transition temperature. They are the fracture appearance transition which is usually taken as the temperature where the fracture is 50% ductile and 50% brittle; and the impact energy transition which is usually taken as the inflection point of the impact energy-temperature curve. The latter method of determination was used in our research.

The impact energy transition temperature is influenced by several mechanical and metallurgical variables. Typical mechanical variables are notch effect, rate of straining, and specimen size and geometry<sup>(32)</sup>. Typical metallurgical variables are chemical composition, and microstructural factors such as grain size and secondary phases as influenced by heat treatments<sup>(3)</sup>.

#### 1.4.1. Notch Effect

The presence of a notch increases the transition temperature<sup>(31)</sup>. The notch results in a stress concentration which can be extremely high as the radius of the notch decreases. When plastic deformation occurs, the stress concentration decreases; however, the surrounding metal which has only been elastically deformed, resists contraction in the notch area. When the bulk of the metal resists contraction, a complicated set of transverse and radial stresses (triaxial stresses) are located just below the notch. The triaxial stresses may result in an increase in the yield strength by a factor of three. This increases the flow curve relative to the fracture curves, resulting in less plastic deformation prior to fracture and increasing a tendency for brittle fracture.

1. 2. 3. 4. 5. 6. 7. 8. 9. 10. 11. 12. 13. 14. 15. 16. 17. 18. 19. 20. 21. 22. 23. 24. 25. 26. 27. 28. 29. 30. 31. 32. 33. 34. 35. 36. 37. 38. 39. 40. 41. 42. 43. 44. 45. 46. 47. 48. 49. 50. 51. 52. 53. 54. 55. 56. 57. 58. 59. 60. 61. 62. 63. 64. 65. 66. 67. 68. 69. 70. 71. 72. 73. 74. 75. 76. 77. 78. 79. 80. 81. 82. 83. 84. 85. 86. 87. 88. 89. 90. 91. 92. 93. 94. 95. 96. 97. 98. 99. 100.

#### 1.4.2. Specimen Size

As the size of the specimen increases, the transition temperature increases<sup>(32)</sup>. The maximum constraint factor for triaxial stresses is a function of the bulk of the specimen. Most investigators have agreed that the standard Charpy V-notch specimen is not large enough for maximum constraint; however, recent work shows the effect on the transition temperature is minimal when double-width specimens are used<sup>(33)</sup>.

#### 1.4.3. Strain Rate

Increasing the strain rate increases the transition temperature. A linear relationship between the logarithm of the strain rate and the reciprocal of the transition temperature has been demonstrated<sup>(32)</sup>. As the rate of straining is increased from  $9.5 \times 10^{-7} \text{ sec.}^{-1}$  to  $300 \text{ sec.}^{-1}$ , the ratio of the yield strength to ultimate tensile strength is increased from 0.5 to nearly 1.0 for structural steel<sup>(5)</sup>. The tendency for brittle fracture is greatly increased.

#### 1.4.4. Chemical Composition

Increasing amounts of carbon, phosphorous and oxygen generally increase the transition temperature<sup>(3)</sup>. Even a few parts per million of interstitial elements have a detrimental effect on the transition temperature. This has been demonstrated by experiments with ultra-pure zone refined iron which showed substantial ductility at temperatures as low as  $4^\circ\text{K}$ <sup>(34)</sup>. Moderate amounts of manganese, controlled additions of aluminum, as well as nickel in all quantities decrease the transition temperature. The effects of many alloying elements are extremely complicated since they often improve the degree of carbide dispersion through increased hardenability while at the same time promote detrimental effects such as temper brittleness<sup>(3)</sup>.

#### 1.4.5. Microstructure

For applications requiring maximum impact energy, it has been demonstrated that tempered martensite is superior to all other structures<sup>(35,36)</sup>. At high hardness levels a lower bainitic structure may have superior impact properties in some instances<sup>(37,38,39)</sup>; however, bainite mixed with tempered martensite is definitely detrimental (Figure 6)<sup>(36)</sup>. The effect of quenching and tempering serves to change the distribution of carbon from a lamellar arrangement to a fine dispersion in tempered martensite. There are many cases where heat treatment to achieve tempered martensite is not possible because of chemical composition limitations or other manufacturing process restrictions as in the case of structural steels. In these cases, the transition temperature decreases with decreasing ferrite grain size. Ferrite grain size is controlled to some extent by prior austenite grain size, so the use of fine grain steels is important in these cases. Although not investigated to the same extent but equally important is the effect of ferrite grain size in tempered martensite. A fine ferrite grain size and a fine carbide dispersion contribute to maximum toughness<sup>(40)</sup>. The carbide dispersion may deviate microcracks from one atomic plane to the next, thereby absorbing energy and decreasing the tendency for crack propagation.

The presence of second phases such as a brittle carbide network, increases the tendency for brittle fracture and increases the transition temperature. There is evidence that even a soft and ductile network of ferrite is detrimental to impact properties<sup>(3)</sup>. Temper embrittlement has a marked effect on increasing the transition temperature.

The presence of inclusions is generally detrimental to impact properties. This is especially true of inclusions which have low surface

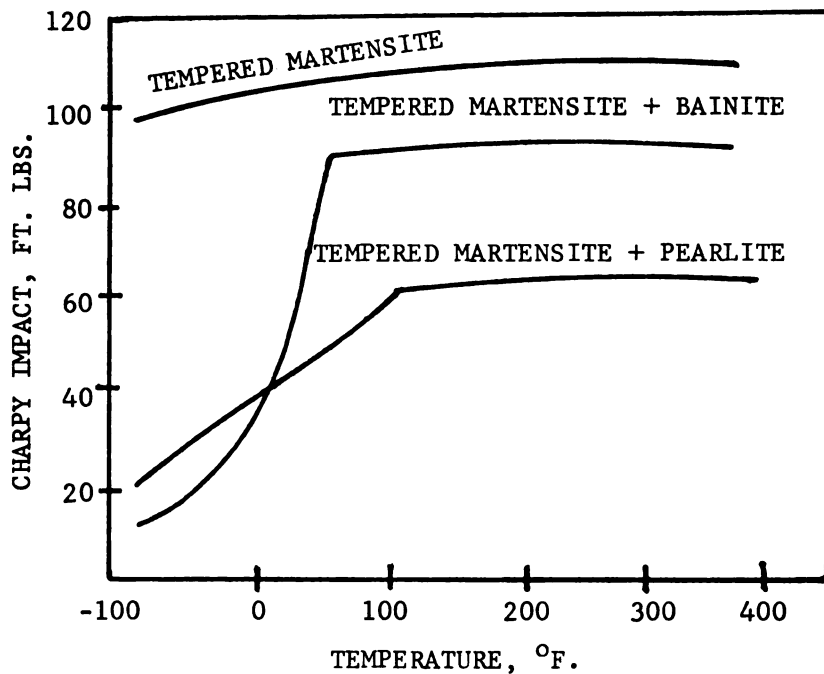


Fig. 6. Effect of microstructure on impact properties

tension and form elongated networks in grain boundaries. Small spheroidal inclusions which are uniformly dispersed throughout the structure have little effect on impact properties.

### 1.5. Fracture

The original concept of Ludwick<sup>(41)</sup>, who suggested only one type of fracture, may be modified to show that fracture will occur when the flow stress curve intersects the cleavage fracture curve or the shear fracture curve (Figure 7)<sup>(5)</sup>. Failure will occur by shear or cleavage depending on the relative position of the curves. As a typical case for steel, yield strength increases rapidly as the testing temperature is decreased. The fracture strength also increases but not as rapidly. The effect of these two curves is shown in connection with the change in percent

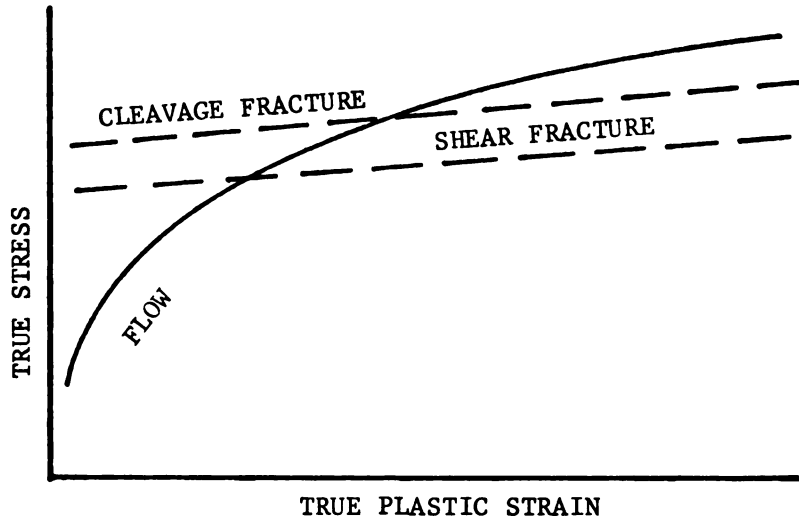


Fig. 7. Schematic representation of a flow curve intersecting cleavage and fracture curves

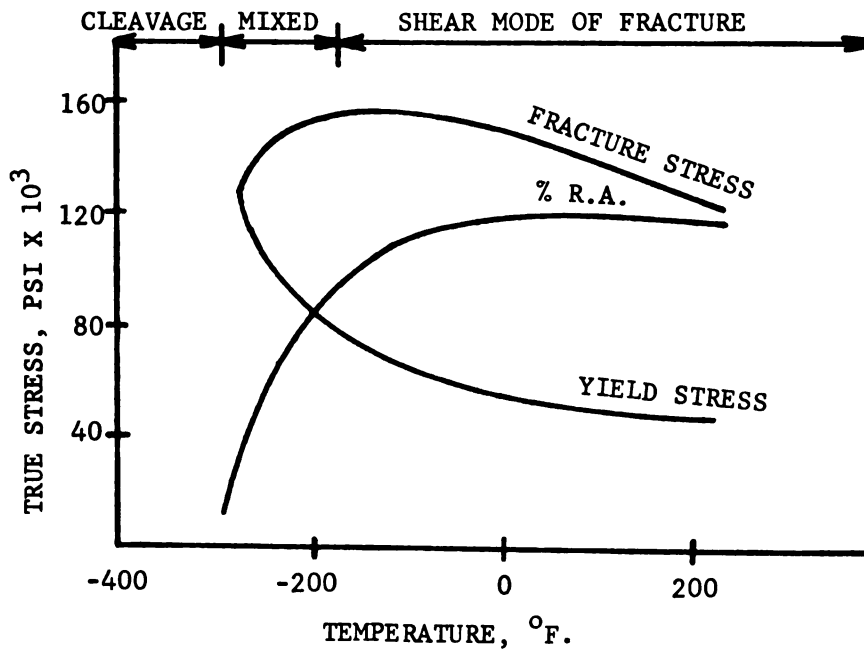


Fig. 8. The effect of testing temperature on the fracture strength, yield strength, and ductility of steel

reduction in area and mode of fracture (Figure 8)<sup>(5)</sup>. Decreasing the testing temperature results in a change in the mode of fracture, as well as a sharp decrease in ductility in the region of the transition temperature. The position of the curves in Figures 7-8 are influenced by many mechanical and metallurgical variables which have been described in Section 1.4.

### 1.6. Description of Fractures

Ductile fractures are those in which appreciable plastic deformation occurs prior to fracture. Brittle fractures are not associated with substantial plastic deformation; however, results show that all metallic brittle fractures have a slight amount of plastic deformation on the fracture surface<sup>(42)</sup>. Fractures in polycrystalline metals may be described by their path, being either transgranular or intergranular. Fractures may also be described by their mode, being either cleavage or shear. Fractures may be described by their appearance, either fibrous or granular. Many of these descriptions are interrelated and most fractures do not proceed by any one mechanism. In steel, brittle fractures usually propagate by transgranular cleavage on the (110) planes<sup>(43)</sup>. In the presence of embrittling grain boundary networks, brittle fractures may propagate in an intergranular fashion. Ductile fractures are always associated with appreciable plastic deformation and have a fibrous appearance. A fracture may be initiated in a ductile manner and as the crack grows, it may suddenly propagate catastrophically by cleavage.

### 1.7. Brittle Fracture

Brittle fractures are those which have little plastic deformation associated with the crack. The crack propagates rapidly and may approach

0.4 to 0.5 times the speed of sound<sup>(42)</sup>. Theories of brittle fracture differ as to whether crack nucleation or crack propagation is the controlling factor. The early work of Griffith<sup>(44)</sup> postulated that in order for a brittle crack to grow the energy supplied must be greater than the surface energy created by the crack extension. This theory assumes a pre-existing microcrack and a totally brittle fracture. It cannot be applied directly to metals since some plastic deformation is always associated with the fracture. One of the many modifications of the Griffith theory was developed by Orowan<sup>(45)</sup>, who assumed a layer of plastic deformation 0.5 mm thick adjacent to the crack. This made the plastic work term at least 1000 times greater than the surface energy term. This approach brings the size of the necessary pre-existing flaw to a reasonable value; however, since the amount of plastic deformation varies for each situation, this type of calculation is of little value in actual practice.

Several dislocation models have been proposed to account for the nucleation of cracks. Zener<sup>(46)</sup> and Stroh<sup>(47,48)</sup> have proposed mechanisms which advance the idea that high stresses caused by dislocation pile-ups can nucleate a cleavage crack. In these cases, one must assume that crack nucleation rather than propagation is the controlling factor.

Since microcracks are often seen in specimens which do not have macrocracks, Cottrell<sup>(49)</sup> and Petch<sup>(50)</sup> have suggested that crack propagation is the controlling factor. If the yield stress of a metal is greater than the stress required to propagate the crack, a brittle fracture will occur.

In commercial grade steels there are many factors such as the presence of brittle phases, grain boundary films, or inclusions which play a more important role in brittle fracture than do the dislocation

mechanisms. There is experimental evidence for pure metals which indicates that even a few parts per million of interstitial elements can drastically affect the mode of fracture<sup>(34)</sup>. Dislocation mechanisms such as locked dislocations being torn from their solute atmospheres resulting in a sudden avalanche of dislocation movement may be extremely important.

### 1.8. Ductile Fracture

Ductile fractures are those which have a substantial amount of plastic deformation associated with the crack<sup>(31)</sup>. The crack propagates very slowly by means of microvoid coalescence. Voids tend to form at inclusions or grain boundaries, coalesce by elongating and form "void sheets" which spread the crack across the cross-section. Microvoid coalescence may be observed on the fractured surface with a scanning electron microscope. In practice, cracks often nucleate in a ductile manner, and upon reaching a critical size, propagate in a brittle fashion.

### 1.9. Use of SEM in Fractography

The scanning electron microscope is a tool which has been used only recently for fracture surface examination. The SEM was first used in 1961 for this application, and the first commercial microscope was on the market by 1965<sup>(51)</sup>. The SEM is extremely versatile and is often equipped with a microprobe analyzer, which may be used to identify constituents qualitatively or semi-quantitatively.

### 1.10. Objectives

The objectives of this research are:

1. To check the results of Cross and Lowther (Table 1) which indicated that air-cooled, inherently fine grain steels had superior impact

properties compared with inherently coarse grain steels, even though the austenite grain size was identical.

2. To check the results of Bain (Figure 1) which indicated quenched and tempered steels quenched from fine grained austenite had up to 400% improvement in impact properties, compared with those quenched from coarse grained austenite. The extent of this effect is to be determined at a lower hardness than the results of Bain.
3. To evaluate the transition temperature data for medium carbon steels. With increasing use of less expensive and shallow hardening steels, this data is of increased importance for quenched and tempered as well as air-cooled structures.
4. To relate ferrite grain size in the tempered martensite to the prior austenite grain size. The importance of this area has been verified through conversations with leading experts including Drs. Grange, Tata, and Kapadia of U. S. Steel Corporation.
5. To relate the micro and macro fracture examination resulting from various heat treatments. A modern research tool, the scanning electron microscope, is utilized.
6. To search for experimental evidence concerning the theories of the role of aluminum in controlling austenite grain growth.
7. To aid in the definition of conditions under which inherently coarse grain steels may be substituted for inherently fine grain; or when medium carbon steels may be substituted for alloy steels.

The inferior impact resistance of coarse grain steels, is the one factor which most often deters their use. The degree to which coarse

grain steels are inferior must be better defined for medium carbon steels. Economic considerations are important when using expensive additions of vanadium, columbium, or zirconium. The use of aluminum has created serious problems in continuous casting which is our most modern steelmaking process. For these reasons, the conditions under which coarse grain steels may be used or the consequences resulting from their substitution must be carefully determined.

Due to increasing cost and in some cases the lack of alloying elements, the future tendency will be to substitute carbon or lower alloy grades of steel. The result will be a greater percentage of mixed structures in the core of quenched and tempered sections. Investigations using air-cooled or slack quenched specimens are important because they simulate the core conditions in actual applications.

The general importance of problems involving fracture investigations can be emphasized by quoting from the Department of the Army Publication of June 1974, "Basic Research Problems of the U. S. Army"<sup>(52)</sup>,

"Fracture of structural materials continues to be a major source of difficulty in both military and civilian endeavors. Especially disturbing is the fact that, at present, little confidence can be placed in any prediction about the conditions under which a particular material will exhibit brittleness, or the degree to which it may have been embrittled. Theories and hypotheses exist, but some of these have limited application, and others lack experimental substantiation."

### 1.11. Summary

In summarizing the current understanding of the effect of grain size on impact properties, some experimental observations are without adequate explanation.

1. More information is needed regarding the effect of grain size on impact properties. This lack of information particularly applies to

the effect of both actual and inherent austenite grain size on the impact properties of quenched and tempered steel structures.

2. An explanation is required for the experimental results of Cross and Lowther who showed that inherently fine grain steels are superior in impact regardless of the actual grain size.
3. In order to analyze quenched and tempered structures, more information is required concerning the role of prior austenite grains on the size and shape of ferrite grains in tempered martensite.
4. The work of Bain and Scott showed that slightly tempered martensite quenched from fine grained austenite is vastly superior in impact. Additional work is required to investigate this effect at lower hardness levels.
5. The effect of ferrite grain size and deoxidation practice on the impact properties of structural steels should be reviewed.
6. The modern theory of grain size control by aluminum nitride is quite well accepted; however, it does not furnish an adequate explanation for some experimental results. The possibility of another mechanism such as a precipitation strengthening effect produced by precipitation of aluminum nitride on lattice defects should be investigated.
7. The effect of grain size on the impact energy transition temperature requires further explanation. To avoid brittle fracture, plastic deformation is required. Since dislocation motion is necessary for plastic deformation, further work is required to adequately explain factors such as grain size, fine precipitates, and elements in solid solution which all affect dislocation motion.

## PROCEDURE

### 2.1. Chemical Analysis

Samples of four heats of commercial grade steel were obtained for this research. Two heats were cut from 5" x 5" billets of AISI 1040, and two from 3" x 3" billets of AISI 1046 steel. One heat of each grade was made to an inherently fine grain practice by final deoxidation with aluminum, and subsequently will be identified (IF). One heat of each grade was made to an inherently coarse grain practice by final deoxidation with silicon or a small amount of aluminum, and will be identified (IC). Through cooperation with the steel mills, heats with closely matching chemistry were selected for each grade. The chemical analysis of the steels are shown in Table 2 which includes the mill analysis and our check analysis. Carbon content was measured using a Leco combustion carbon determinator, manganese and sulfur were checked using standard analytical chemistry procedures, and the balance of the elements were checked using an emission spectrometer.

Additional analyses were made for nitrogen and oxygen and are shown in Table 3. These results are reported in parts-per-million and were determined using the Leco combustion method. The combustion temperature is not high enough to dissociate aluminum oxide, so the oxygen results may be misleading because oxygen reported is only that which is not combined as aluminum oxide.

Table 2  
Chemical Analysis of Steel in Weight Percent

|                              | <u>C</u> | <u>Mn</u> | <u>P</u> | <u>S</u> | <u>Si</u> | <u>Cu</u> | <u>Ni</u> | <u>Cr</u> | <u>Mo</u> | <u>Al</u> | ASTM<br>G.S. |
|------------------------------|----------|-----------|----------|----------|-----------|-----------|-----------|-----------|-----------|-----------|--------------|
| Youngstown #66797            |          |           |          |          |           |           |           |           |           |           |              |
| AISI 1040                    | .38      | .74       | .006     | .021     | .19       | .02       | .04       | .01       | -         | -         | 1            |
| Inherently Coarse Grain (IC) | .38      | .72       | .004     | .025     | .15       | .02       | 0         | 0         | 0         | 0         | 1            |
| Youngstown #95313            |          |           |          |          |           |           |           |           |           |           |              |
| AISI 1040                    | .40      | .67       | .007     | .025     | .17       | -         | .07       | -         | -         | -         | 7/8          |
| Inherently Fine Grain (IF)   | .40      | .67       | .004     | .024     | .15       | .02       | 0         | 0         | 0         | .012      | 7/8          |
| Republic #5023766            |          |           |          |          |           |           |           |           |           |           |              |
| AISI 1046                    | .46      | .73       | .008     | .030     | .16       | .09       | .03       | .03       | -         | .013      | 3/4          |
| Inherently Coarse Grain (IC) | .48      | .73       | .013     | .034     | .20       | .09       | .07       | 0         | 0         | .008      | 3/4          |
| Republic #5054025            |          |           |          |          |           |           |           |           |           |           |              |
| AISI 1046                    | .46      | .76       | .008     | .028     | .18       | .05       | .03       | .02       | -         | .037      | 8            |
| Inherently Fine Grain (IF)   | .48      | .76       | .012     | .030     | .21       | .05       | 0         | 0         | 0         | .051      | 8            |

Table 3

Nitrogen and oxygen analysis in parts per million

|                                     | <u>Nitrogen</u> | <u>Oxygen</u> |
|-------------------------------------|-----------------|---------------|
| Youngstown #66797 (IC)<br>AISI 1040 | 43              | 560           |
| Youngstown #95313 (IF)<br>AISI 1040 | 46              | 48            |
| Republic #5023766 (IC)<br>AISI 1046 | 35              | 540           |
| Republic #5054025 (IF)<br>AISI 1046 | 47              | 24            |

## 2.2. Grain Coarsening Characteristics

The steel mill chemistry report, the check analysis, and the reported McQuaid-Ehn grain size all indicated that one heat of each grade of steel was inherently fine grain and the other inherently coarse grain. Since the McQuaid-Ehn Test only determines grain size at 1700°F., a comprehensive study was completed to determine the grain coarsening characteristics of each heat of steel over a range of temperature. Samples of each heat were austenitized four hours at 100°F. intervals between 1600-2200°F. The samples were cooled below the upper critical temperature to allow a network of ferrite to precipitate in austenite grain boundaries, then they were quenched in a brine solution. Microscopic examination after polishing and etching clearly revealed the prior austenite grain size. A complete summary of these grain size results is shown in Table 4. Average grain diameter was determined by using the linear intercept method<sup>(2)</sup> and the ASTM grain size number<sup>(2)</sup> was determined by counting the number of grains/in<sup>2</sup> at 100x. The data from Table 4 is shown graphically in Figure 9. This data demonstrates that each heat of steel has

its own inherent resistance to grain coarsening at lower temperatures, but at higher temperatures grain coarsening proceeds rapidly.

The work of Grange<sup>(28)</sup> showed that inherently coarse grain steel was extremely time-sensitive to coarsening at low austenitizing temperatures. Steel may transform initially into a fine grained asutenite but coarsening begins almost immediately. The time-sensitive nature of the four heats of steel was demonstrated by results shown in Table 5. These data indicated that both inherently fine and inherently coarse grain steels are time-sensitive to coarsening at 1500°F.

Grain size results in Table 5 were obtained from samples austenitized by immersion in molten salt for the time prescribed, followed by quenching in iced brine. The samples were tempered at 510°C. for 16 hours and furnace cooled. Repeated etching with a boiling solution of picric acid in water was used to reveal the prior austenite grain size. This method proved to be dependable for revealing prior austenite grains since check pieces using the ferrite grain boundary precipitation method yielded identical results.

Photomicrographs illustrating grain coarsening characteristics of the four heats of steel are shown in Figures 10-13. In these photographs, prior austenite grains are outlined with a network of ferrite. The austenitizing time at 1500°F. was 5 minutes and at all other temperatures the time was 4 hours.

Table 4

## Grain Coarsening Characteristics

| <u>Temperature</u>  | Youngstown<br>#66797 (IC) |            | Youngstown<br>#95313 (IF) |            | Republic<br>#5023766 (IC) |            | Republic<br>#5054025 (IF) |            |
|---------------------|---------------------------|------------|---------------------------|------------|---------------------------|------------|---------------------------|------------|
|                     | <u>Dia.</u><br><u>mm.</u> | <u>No.</u> | <u>Dia.</u><br><u>mm.</u> | <u>No.</u> | <u>Dia.</u><br><u>mm.</u> | <u>No.</u> | <u>Dia.</u><br><u>mm.</u> | <u>No.</u> |
| 1600 °F. (871 °C.)  | 0.188                     | 2          | 0.029                     | 7          | 0.114                     | 3          | 0.022                     | 8          |
| 1700 °F. (927 °C.)  | 0.250                     | 1          | 0.033                     | 7          | 0.175                     | 2          | 0.028                     | 7          |
| 1800 °F. (982 °C.)  | 0.270                     | 1          | 0.050                     | 6          | 0.227                     | 1          | 0.033                     | 7          |
| 1900 °F. (1038 °C.) | 0.286                     | 1          | 0.081                     | 4          | 0.264                     | 1          | 0.067                     | 5          |
| 2000 °F. (1093 °C.) | 0.455                     | 0          | 0.185                     | 2          | 0.279                     | 1          | 0.167                     | 2          |
| 2100 °F. (1149 °C.) | 1.000                     | -3         | 0.357                     | 0          | 0.323                     | 0          | 0.357                     | 0          |
| 2200 °F. (1204 °C.) | 1.250                     | -4         | 0.555                     | -1         | 0.435                     | -1         | 0.667                     | -2         |

26

Table 5

## Time-Sensitive Grain Coarsening

| <u>Temperature</u>              | Youngstown<br>#66797 (IC) |            | Youngstown<br>#95313 (IF) |            | Republic<br>#5023766 (IC) |            | Republic<br>#5054025 (IF) |            |
|---------------------------------|---------------------------|------------|---------------------------|------------|---------------------------|------------|---------------------------|------------|
|                                 | <u>Dia.</u><br><u>mm.</u> | <u>No.</u> | <u>Dia.</u><br><u>mm.</u> | <u>No.</u> | <u>Dia.</u><br><u>mm.</u> | <u>No.</u> | <u>Dia.</u><br><u>mm.</u> | <u>No.</u> |
| 1500 °F. (816 °C.)<br>2 Minutes | 0.035                     | 7          | 0.008                     | 11         | 0.021                     | 8          | 0.007                     | 11         |
| 1500 °F. (816 °C.)<br>5 Minutes | 0.065                     | 5          | 0.013                     | 9          | 0.045                     | 6          | 0.012                     | 10         |

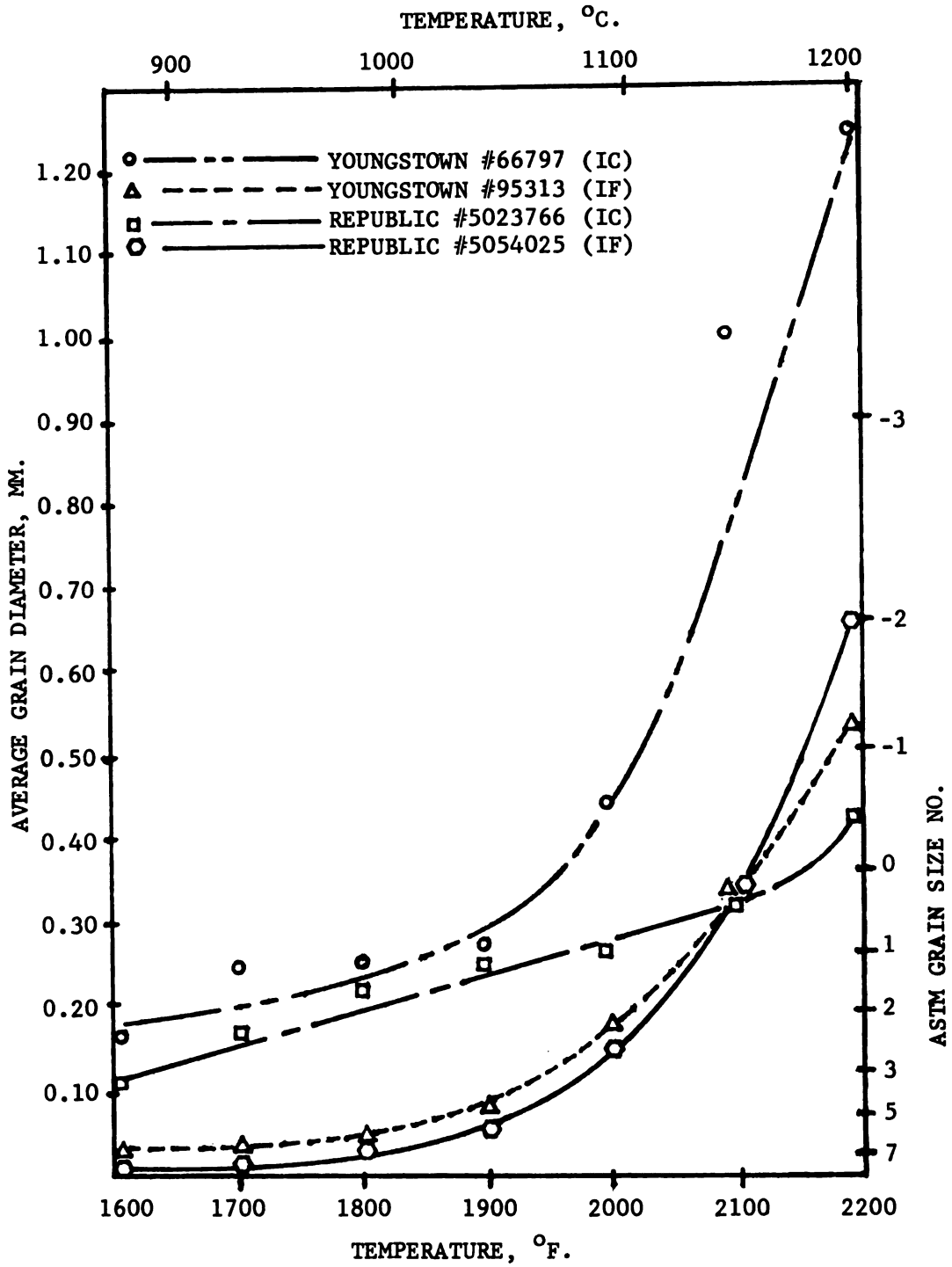


Fig. 9. Grain Coarsening Characteristics

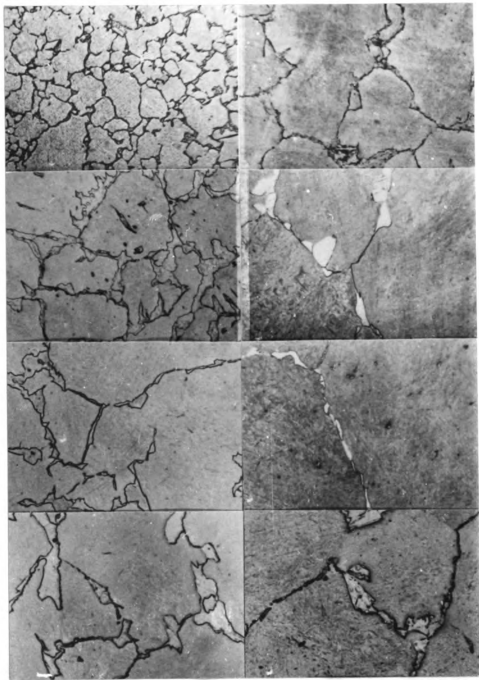


Fig. 10. Grain coarsening characteristics of Youngstown #66797 (IC). First column top to bottom: austenitized at 1500, 1600, 1700 and 1800°F. Second column top to bottom: austenitized at 1900, 2000, 2100 and 2200°F. (100x)

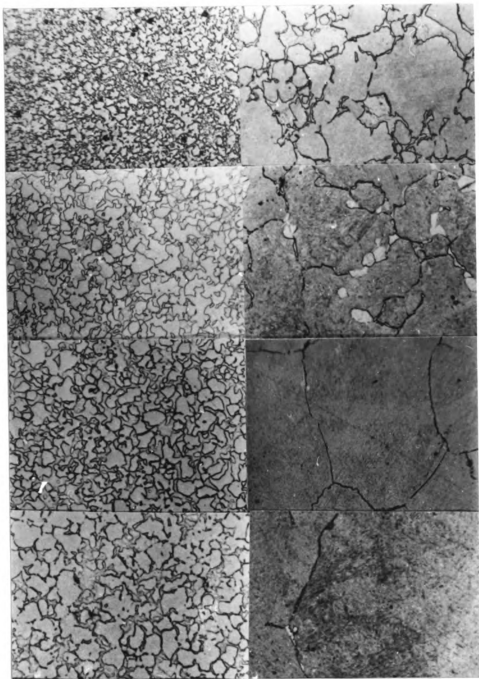


Fig. 11. Grain coarsening characteristics of Youngstown #95313 (IF). First column top to bottom: austenitized at 1500, 1600, 1700 and 1800°F. Second column top to bottom: austenitized at 1900, 2000, 2100 and 2200°F. (100x)

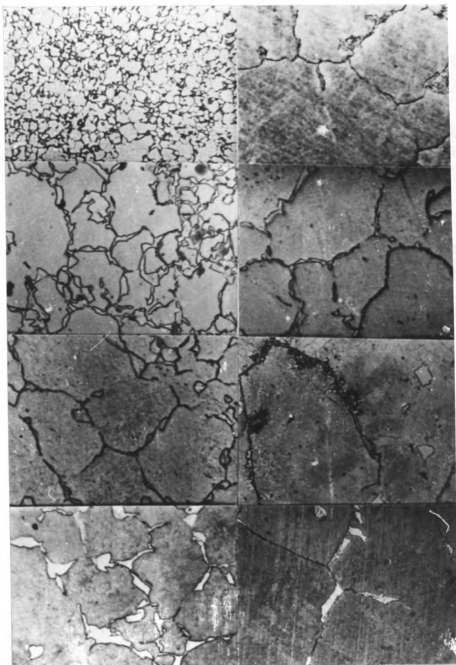


Fig. 12. Grain coarsening characteristics of Republic #5023766 (IC). First column top to bottom: austenitized at 1500, 1600, 1700 and 1800°F. Second column top to bottom: austenitized at 1900, 2000, 2100 and 2200°F. (100x)

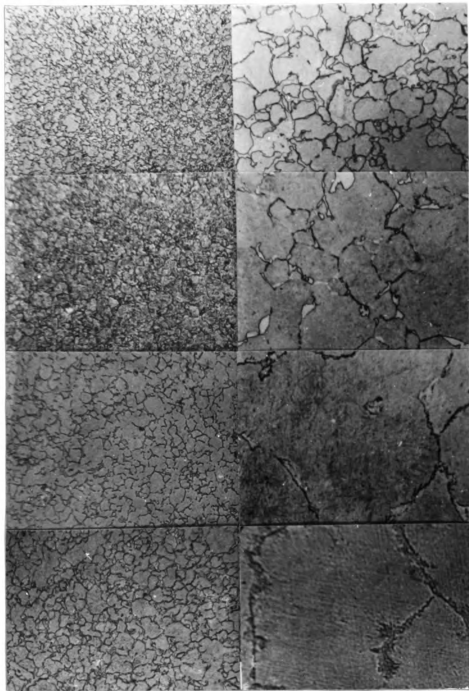


Fig. 13. Grain coarsening characteristics of Republic #5054025 (IF). First column top to bottom: austenitized at 1500, 1600, 1700 and 1800°F. Second column top to bottom: austenitized at 1900, 2000, 2100 and 2200°F. (100x)

### 2.3. Selection of Austenitizing Temperatures

Grain coarsening studies were performed so the austenite grain size would be known over a range of temperatures. One of our objectives was to relate prior austenite grain size to ferrite grain size in tempered martensite. Austenitizing temperatures were selected to yield closely matching austenite grain sizes for both inherently fine and coarse grain steels. Tests were conducted for each steel using specimens having coarse, intermediate, and fine prior austenite grain size. The average grain sizes for the austenitizing temperatures selected are shown in Table 6.

Table 6

Average Grain Size for Austenitizing Treatments Selected

| <u>Steel</u>                        | <u>Austenitizing Treatment</u> | <u>Ave. Grain<br/>Dia., mm.</u> | <u>ASTM No.</u> |
|-------------------------------------|--------------------------------|---------------------------------|-----------------|
| Youngstown #66797<br>AISI 1040 (IC) | 1500 °F. (816 °C.), 2 Min.     | 0.035                           | 7               |
|                                     | 1500 °F. (816 °C.), 5 Min.     | 0.065                           | 5               |
|                                     | 2000 °F. (1093 °C.), 4 Hrs.    | 0.455                           | 0               |
| Youngstown #95313<br>AISI 1040 (IF) | 1500 °F. (816 °C.), 5 Min.     | 0.013                           | 10              |
|                                     | 1725 °F. (941 °C.), 4 Hrs.     | 0.038                           | 6-7             |
|                                     | 2100 °F. (1149 °C.), 4 Hrs.    | 0.357                           | 0               |
| Republic #5023766<br>AISI 1046 (IC) | 1500 °F. (816 °C.), 2 Min.     | 0.021                           | 8               |
|                                     | 1500 °F. (816 °C.), 5 Min.     | 0.045                           | 6               |
|                                     | 2100 °F. (1149 °C.), 4 Hrs.    | 0.323                           | 0               |
| Republic #5054025<br>AISI 1046 (IF) | 1500 °F. (816 °C.), 5 Min.     | 0.012                           | 10              |
|                                     | 1575 °F. (857 °C.), 4 Hrs.     | 0.020                           | 8               |
|                                     | 2100 °F. (1149 °C.), 4 Hrs.    | 0.357                           | 0               |

#### 2.4. Heat Treating

The billets were all austenitized at 1700°F., 4 hours and air-cooled. The specimens heated to 1500°F. for 2 minutes in molten salt and then quenched in iced-brine were pretreated using the same 1500°F.-quench cycle. Repeated rapid heating and cooling cycles have been reported by Grange<sup>(28)</sup> to yield finer austenite grains; however, these cycles also increase the tendency for quench cracking. This treatment was used for inherently coarse grain steels where retaining fine grained austenite is difficult.

Specimens heated to 1500°F. for 5 minutes in molten salt and quenched in iced-brine were pretreated using a 1500°F.-air cool cycle. This treatment was used for all steels and produced a fine to intermediate grain size.

Specimens austenitized at 1575°F., 1725°F., 2000°F., and 2100°F. were sealed in quartz tubes to protect the surface from scaling and decarburization. Six to ten specimens were sealed in each tube at  $10^{-4}$  mm. Hg pressure and pretested by heating to 1500°F. and air cooling. The pretreatment served to check the seal and refine the grain structure. The specimens were heated to the designated austenitizing temperature, held 4 hours and furnace cooled to 1575-1600°F. After stabilizing for 1 hour, the quartz tubes were broken on the furnace hearth and the specimens were quenched in iced-brine.

All quenched specimens were tempered to the same hardness range. The hardness selected was much lower than that of Bain or Scott (Figures 1-3) since we tested in the region of maximum impact properties. The two heats of AISI 1040 steel, Youngstown #66797 and Youngstown #95313, were both tempered at 960°F. for 2 hours. The two heats of AISI 1046 steel,

Republic #5023766 and Republic #5054025, were both tempered at 1060°F. for 2 hours. Specimens were air-cooled from the tempering temperature to more closely duplicate commercial practice; however, a few check specimens were quenched to investigate the possibility of temper embrittlement. These steels would not usually be considered susceptible to temper embrittlement and quenching from the tempering temperature did not alter the properties.

Measuring ferrite grain size in tempered martensite which has been tempered at relatively low temperatures is extremely difficult. The structure has a fine dispersion of carbides and etchants do not reveal ferrite grain boundaries in a sharp and consistent manner. Transmission electron microscopy has been used to make some measurements on thin foil specimens, however, this method is tedious and does not produce sharply defined grain boundaries. A set of specimens was tempered at 1300°F. for 24 hours to coalesce the carbides and make microscopic examination of ferrite grain size possible. This examination was performed to study the size and shape of ferrite grains as influenced by prior structure.

One of the objectives of our research was to check the results of Cross and Lowther (Table 1) concerning the effect of prior structure on impact properties of air-cooled specimens. To investigate this behavior, one set of specimens was air-cooled from the austenitizing temperature. All specimens were pretreated in molten salt at 1500°F. for 2 minutes followed by air-cooling. The specimens austenitized at 1500°F. were air-cooled from molten salt. The specimens austenitized at 1575°F., 1725°F., 2000°F. and 2100°F. were protected by painting a "No-Carb" sealant on the surface. This protected the surface from scaling and decarburization during the austenitizing treatment. The specimens were

furnace-cooled to 1575-1600°F. prior to air-cooling. Air-cooling small specimens closely duplicates the core cooling rate in heavy sections which are oil or water quenched. Also, this type of structure is often present in the core area of induction hardened parts.

### 2.5. Hardness

One sample from each lot of 6-10 specimens was sectioned for hardness testing and microstructure examination. Hardness testing is a rapid and inexpensive quality control method to determine the effectiveness of the quench. The hardness of martensite is related to carbon content and appreciable amounts of other phases is reflected in lower hardness readings. The as-quenched hardness range for an essentially complete martensitic structure is 55-58  $R_c$  for AISI 1040 and 58-61  $R_c$  for AISI 1046 steel.

Maximum impact properties are achieved by tempering the as-quenched martensitic structure. The specimens were tempered and one specimen from each lot was sectioned for hardness testing and microstructure examination. The tempering temperature was adjusted for each grade of steel to achieve a hardness of 26-28  $R_c$  for tempered martensite.

Hardness variations from surface to core within each specimen can readily be determined by microhardness testing. The microhardness was checked on three specimens from each quenching and tempering treatment. All microhardness testing was performed using a Tukon microhardness tester with a 500 gram load. Hardness values were obtained at 0.040" intervals across the section.

Hardness of the air-cooled specimens was more difficult to control within a narrow range. The protective paint on the high temperature

specimens acted as an insulator and decreased the cooling rate. Specimens austenitized in molten salt did not have protective paint and were cooled in warm air to decrease their cooling rate. The hardness range for air-cooled specimens was 84-92  $R_b$  for AISI 1040 and 90-98  $R_b$  for AISI 1046 steel.

## 2.6. Microstructure

Since mixed structures or the presence of second phases in grain boundaries are known to be detrimental to impact properties<sup>(3,36)</sup>, a careful examination of the microstructure was necessary. To avoid unnecessary tempering from the heat in the mounting press, all as-quenched specimens were cold mounted. All tempered and air-cooled specimens were hot mounted in bakelite. The specimens were ground, polished and etched using 2% nital prior to examination at 100x and 1000x. Photographs were taken at 100x, as well as 1000x using a Bausch & Lomb Research Metallograph equipped with an oil immersion objective lens. Exposures were made using Kodak Orthochromatic metallographic plates to achieve maximum detail.

Examinations in the unetched condition were also made at various magnifications to observe the size and distribution of inclusions. Inclusion ratings concerning size, density and distribution were based on ASTM Specification E45<sup>(53)</sup>. Some lower magnification photomicrographs were taken using a 35 mm. camera attachment on the eyepiece of a Bausch & Lomb Dyna-Zoom Metallograph.

## 2.7. Specimen Preparation

The steels used have low hardenability, and, to insure the core was fully quenched, half-width Charpy specimens were used. Blanks were

machined 0.030" oversize to allow for stock removal after heat treating. All specimens were cut in a longitudinal direction of the billet. After heat treating, blanks were returned to the machine shop for surface stock removal and V-notching. The notch and specimen geometry were in accordance with ASTM Specification E23-66<sup>(54)</sup>. The specimens were notched using a special V-notch cutting tool which produces constant notch dimensions. The dimensions are not altered when the tool is sharpened. Representative notched specimens were checked for accuracy using an optical comparator and found to be well within specification.

Tensile properties of the steel in the quenched and tempered condition were also investigated. Tensile specimens were specially designed to be gripped and tested using an Instron Model Testing Machine. The tensile specimens were 0.190" and the gage length was one inch. After heat treating, the specimens were cleaned by vapor blasting prior to testing.

## 2.8. Impact Testing

The half-width Charpy V-notch specimens were fractured using a 240 Ft.-Lb. Satec Tester equipped with a Dynatup instrumented package<sup>(55)</sup>. The Dynatup instrumentation was pre-calibrated to yield load-time and energy-time curves for the specimen being fractured. All testing procedures were in accordance with ASTM Specification E23-66<sup>(54)</sup>. Other handbooks<sup>(56,57)</sup> were consulted for supplementary information on impact testing procedures.

In Charpy V-notch impact testing, the specimen is centered horizontally on a supporting anvil and fractured with a striking hammer mounted on a swinging pendulum. The energy absorbed in fracturing the specimen

is measured by a decrease in follow-through of the swinging pendulum. The test assumes no loss of energy due to mechanical factors. This assumption is not entirely true since strain and vibrational energy is transmitted to the striking hammer, the pendulum arm, and the supporting anvil of the impact tester. If the impact tester is properly maintained, these mechanical losses will be negligible. Extensive analysis has been made regarding factors which lead to erroneous results in impact testing<sup>(58)</sup>. The geometry of the notch and alignment of the specimen on the supporting anvil are especially critical. When using a properly maintained tester and correct testing methods, scatter within  $\pm 5\%$  can be expected; however, a poorly organized approach may lead to substantial experimental error.

When testing at temperatures other than room temperature, care must be taken to use correct procedures for cooling the specimens and transferring from the cooling medium to the supporting anvil. Specimens fractured at  $-18^{\circ}\text{C}$ . and  $-40^{\circ}\text{C}$ . were air-cooled for a minimum of one hour in a specially designed refrigerator. In the temperature range between  $-40^{\circ}\text{C}$ . and  $-114^{\circ}\text{C}$ ., specimens were cooled for a minimum of 15 minutes in methyl or ethyl alcohol cooled with additions of liquid nitrogen. At  $-196^{\circ}\text{C}$ ., specimens were cooled a minimum of 15 minutes in liquid nitrogen. In the temperature range between  $-114^{\circ}\text{C}$ . and  $-196^{\circ}\text{C}$ ., specimens were air-cooled for a minimum of one hour in a specially constructed refrigerator consisting of a copper coil wound around an insulated stainless steel flask. Liquid nitrogen was fed through the coil by means of an elevated holding tank and regulating valve. The specimens were placed on an insulating block and the temperature was monitored with two thermometers, one embedded in a heavy piece of steel located in the center of

the flask, and the other located in open air halfway between center and flask surface. When readings of the two thermometers approached each other, uniform conditions were assumed to exist. Temperatures as low as  $-180^{\circ}\text{C}$ . were achieved using this system.

When transferring the specimen from the cooling medium to the supporting anvil, transferring tongs must be cooled to the same temperature as the specimen. Rapid transfer of the specimen is a critical process and must be accomplished within 5 seconds to insure consistent results. The critical nature of this transfer is shown in Figure 14<sup>(59)</sup> for single-width charpy specimens at  $-40^{\circ}\text{F}$ .

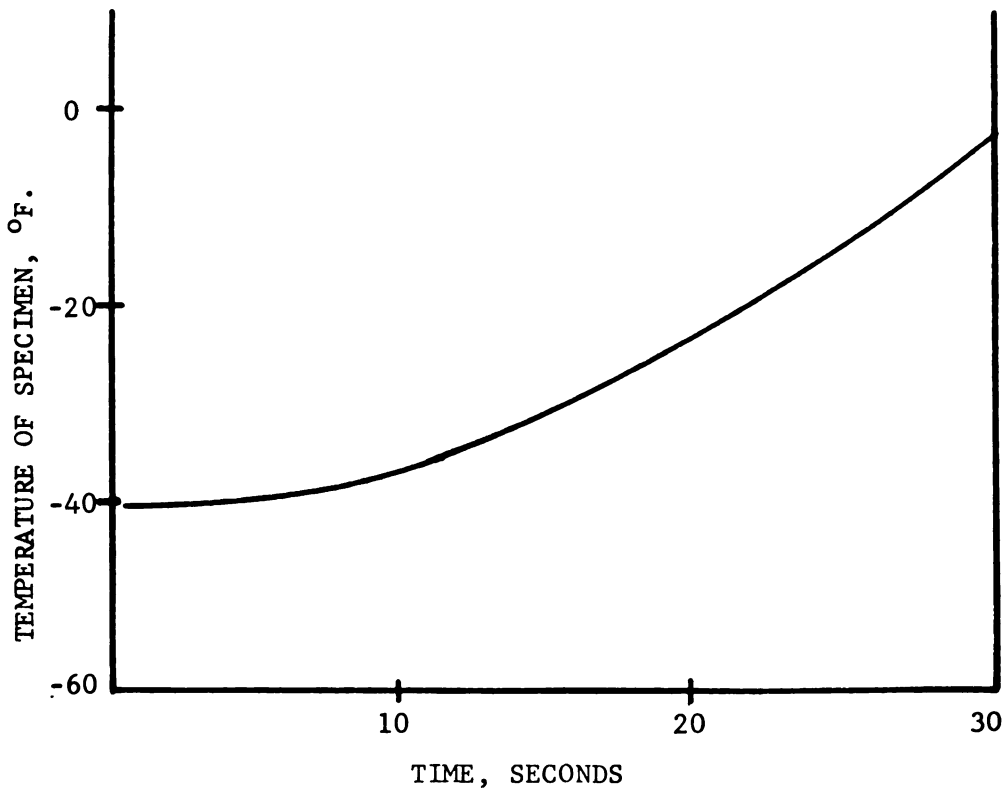


Fig. 14. Effect of transfer time from cooling medium to fracturing a standard charpy V-notch specimen

### 2.9. Instrumented Impact Testing

The Charpy V-notch impact test is rapid and inexpensive; however, the energy results do not relate well to design applications. For this reason, in recent years experimentalists have been motivated to gain additional information concerning fracture characteristics by instrumenting the test. A commercial instrumented impact tester, "Dynatup"<sup>(55)</sup> was used in our research. The instrumented system consists of three major components: a dynamic response module, a velocimeter, and an instrumented striking hammer. The dynamic response module includes an oscilloscope with storage capacity. The velocimeter triggers the oscilloscope sweep by means of a series of grids mounted on the pendulum which interrupt a light source to a photo cell. The striking hammer, or tup, is instrumented with semi-conductor strain gages mounted on or embedded in the hammer head. From one to four strain gages may be used to measure the strain-pulse. Tardif and Marquis<sup>(60,61)</sup>, who did much of the pioneer work on instrumented impact testing, used B-L-H Type C-7 strain gages in their instrumentation.

Instrumented impact testers are calibrated either statically or dynamically. The response from the wheatstone bridge circuit yields a load-time trace on the oscilloscope. The response from the grid interrupting light to the photo cell, yields a deflection-time curve. In the Dynatup system, the response module integrates the resulting load-deflection curve and produces an energy-time curve on the oscilloscope screen. Typical load-time and energy-time curves are shown in Figure 15<sup>(62)</sup>.

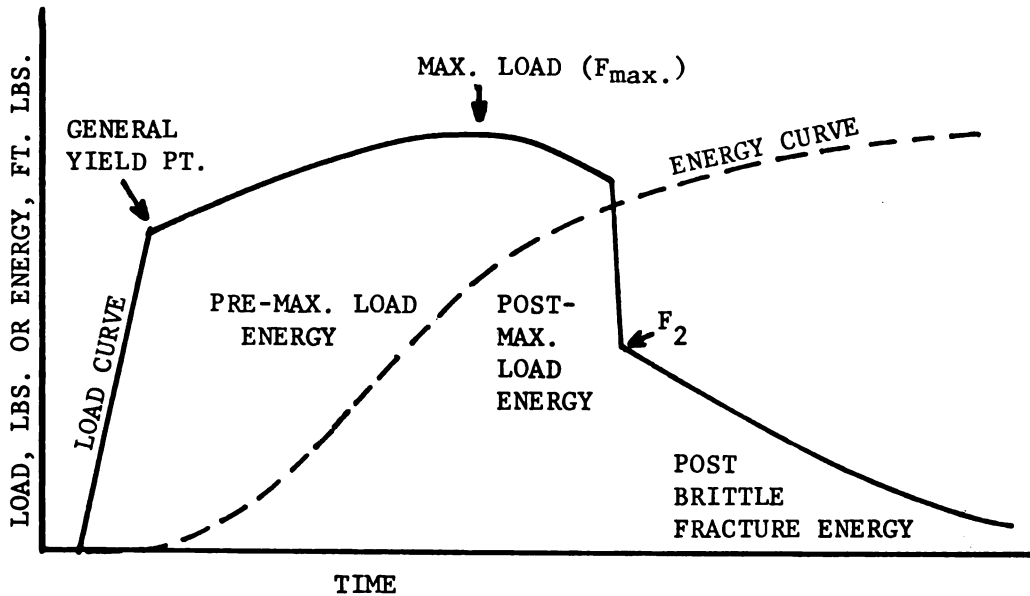


Fig. 15. Typical load-time and energy-time curves from instrumented impact testing

The maximum value of the energy-time curve corresponds to the value of energy determined by the follow-through of the pendulum arm. This serves as an excellent check on the mechanically determined energy value since errors may occur in the system. Various points on the load-time curve have been analyzed regarding fracture behavior. The general yield point is the point where the specimen begins to plastically deform. The maximum load is the load necessary to initiate fracture. The brittle fracture load is not present in ductile fractures where the curves slope gradually downward. The premaximum load energy is the energy required to initiate fracture. The post-maximum load energy is the energy required to propagate fracture. The post-brittle fracture energy is the energy

associated with formation of a shear lip. Although the load-time curve does not yield energy units, it may be used for comparison purposes since the shape of the load-deflection curve is similar.

Fracture appearance is used in some cases to determine the transition temperature. For some structures an accurate estimate of the percent ductile fracture is difficult. The percent ductile fracture can be determined from the load-time curve by using the following relationship:

$$\text{Percent ductile fracture} = F_2/F_{\text{max.}} \times 100$$

This is valuable when determining the 50% ductile-50% brittle transition temperature and correlates well to actual visual examinations.

With use of pre-cracked specimens<sup>(60,61)</sup>, attempts have been made to determine the dynamic  $K_{ID}$ , which is the plane strain, stress intensity factor at the onset of unstable crack growth. This area is currently being heavily researched and some results to date show the dynamic stress intensity factor to be greater than the static stress intensity factor determined by slow-bend tests<sup>(60)</sup>.

### 2.10. Tensile Testing

Tensile properties were investigated to determine the effect of prior structure on strength and ductility of tempered martensite. All tensile testing was performed using an Instron Model Testing Machine with a 5000 Kg. load cell. The specimens were clamp gripped and the crosshead speed was 0.1 cm./min. for all tests. Special care was taken to align the specimen in the grips since alignment is known to affect results such as the observation of a sharp yield point<sup>(42)</sup>. Three or four specimens were tested from each heat treatment cycle. All tests

were performed at room temperature and the following data were recorded: yield strength, ultimate tensile strength, percent elongation, and percent reduction in area.

### 2.11. Examination of Fractures

The fractures were examined visually and selected specimens were photographed at approximately 3x for comparison purposes. One fracture tested at room temperature and one tested at  $-196^{\circ}\text{C}$ . were examined with a scanning electron microscope. An American Metals Research Model 1000 SEM was used for these examinations. The microstop preservative was removed from the fracture surface with acetone and specimens were ultrasonically cleaned in ethyl alcohol. After securing to the pedestal, silver conductor paint was applied to the junction between the specimen and pedestal. Fractured surfaces were first scanned at low magnification and then increased to examine specific areas. Photographs were usually taken at 200x and 2000x on each specimen.

Several inclusions on the fractured surface were analyzed using an EDAX microprobe analyzer. This analysis is generally qualitative and the equipment did not have the capability to analyze elements of atomic number lower than sodium due to X-ray absorption by a beryllium window. Polished specimens were also analyzed with the microprobe, with special emphasis on inclusions which appeared to occupy the area of prior austenite grain boundaries.

## EXPERIMENTAL RESULTS

### 3.1. Quenched Hardness

The Rockwell "C" hardness readings for the specimens in the quenched condition are shown for each austenitizing temperature in Table 7. The results represent the total range of core hardness for three specimens sectioned and tested from each heat treatment. Since hardness is a reliable quality control for quenched structures of this type, the results

Table 7

Rockwell "C" hardness of specimens quenched  
from the austenitizing temperature shown

| <u>Austenitizing Treatment</u>  | <u>Youngstown #66797 (IC)</u><br><u>AISI 1040</u> | <u>Youngstown #95313 (IF)</u><br><u>AISI 1040</u> | <u>Republic #5023766 (IC)</u><br><u>AISI 1046</u> | <u>Republic #5054025 (IF)</u><br><u>AISI 1046</u> |
|---------------------------------|---|---|---|---|
| 1500 °F. (816 °C.)<br>2 Minutes | 54-56 R <sub>C</sub>                              |   | 59-61 R <sub>C</sub>                              |   |
| 1500 °F. (816 °C.)<br>5 Minutes | 54-55 R <sub>C</sub>                              | 54-56 R <sub>C</sub>                              | 59-60 R <sub>C</sub>                              | 58-59 R <sub>C</sub>                              |
| 1575 °F. (857 °C.)<br>4 Hours   |   |   |   | 58-60 R <sub>C</sub>                              |
| 1725 °F. (941 °C.)<br>4 Hours   |   | 54-55 R <sub>C</sub>                              |   |   |
| 2000 °F. (1093 °C.)<br>4 Hours  | 55-56 R <sub>C</sub>                              |   |   |   |
| 2100 °F. (1149 °C.)<br>4 Hours  |   | 54-56 R <sub>C</sub>                              | 58-60 R <sub>C</sub>                              | 59-60 R <sub>C</sub>                              |

indicate that our specimens were essentially martensitic throughout the cross-section.

Microhardness testing is an excellent method to detect small variations in hardness from one location to another. Starting at 0.010" below the surface, microhardness readings were taken at 0.040" intervals across the section. The results expressed as Knoop Hardness Number (KHN) were obtained using a 500 gram load and are shown in Table 8. The results represent the total range of readings from eighteen tests on three specimens from each heat treatment. These results indicate excellent uniformity since a 30 point variation in KHN is only 1.5 points  $R_c$  at this hardness level.

### 3.2. Tempered Hardness

The same testing procedure used for quenched specimens was used for the tempered specimens. The Rockwell "C" hardness results are shown in Table 9, and the microhardness results are shown in Table 10. These results demonstrate that our objective of tempering all specimens to the same hardness level was achieved.

### 3.3. Hardness of Air-Cooled Specimens

The effect of actual and inherent austenite grain size on impact properties was investigated for air-cooled specimens. One specimen from each heat treatment was sectioned for hardness testing and Rockwell "B" hardness results are shown in Table 11. The hardness of specimens heat treated in this manner is more difficult to accurately control. Variations in grain size, carbon content, and residual alloying elements will all affect the air-cooled hardness. The hardness results indicate that a comparison of impact properties may be made for each grade of steel,

Table 8

Knoop hardness number of specimens quenched  
from the austenitizing temperature shown

| <u>Austenitizing<br/>Treatment</u> | <u>Youngstown<br/>#66797 (IC)<br/>AISI 1040</u> | <u>Youngstown<br/>#95313 (IF)<br/>AISI 1040</u> | <u>Republic<br/>#5023766 (IC)<br/>AISI 1046</u> | <u>Republic<br/>#5054025 (IF)<br/>AISI 1046</u> |
|------------------------------------|---|---|---|---|
| 1500 °F. (816 °C.)<br>2 Minutes    | 660-704   |   | 786-810   |   |
| 1500 °F. (816 °C.)<br>5 Minutes    | 682-700   | 670-710   | 780-810   | 798-812   |
| 1575 °F. (857 °C.)<br>4 Hours      |   |   |   | 785-800   |
| 1725 °F. (941 °C.)<br>4 Hours.     |   | 660-699   |   |   |
| 2000 °F. (1093 °C.)<br>4 Hours     | 685-710   |   |   |   |
| 2100 °F. (1149 °C.)<br>4 Hours     |   | 660-695   | 770-800   | 775-800   |

Table 9

Rockwell "C" hardness after quenching and tempering.  
Specimens were quenched from the austenitizing temperature shown.

| <u>Austenitizing<br/>Treatment</u> | <u>Youngstown<br/>#66797 (IC)<br/>AISI 1040</u> | <u>Youngstown<br/>#95313 (IF)<br/>AISI 1040</u> | <u>Republic<br/>#5023766 (IC)<br/>AISI 1046</u> | <u>Republic<br/>#5054025 (IF)<br/>AISI 1046</u> |
|------------------------------------|---|---|---|---|
| 1500 °F. (816 °C.)<br>2 Minutes    | 27-28 R <sub>C</sub>                            |   | 27-28 R <sub>C</sub>                            |   |
| 1500 °F. (816 °C.)<br>5 Minutes    | 26-28 R <sub>C</sub>                            | 27-28 R <sub>C</sub>                            | 27-28 R <sub>C</sub>                            | 27-28 R <sub>C</sub>                            |
| 1575 °F. (857 °C.)<br>4 Hours      |   |   |   | 26-28 R <sub>C</sub>                            |
| 1725 °F. (941 °C.)<br>4 Hours      |   | 26-28 R <sub>C</sub>                            |   |   |
| 2000 °F. (1093 °C.)<br>4 Hours     | 27-28 R <sub>C</sub>                            |   |   |   |
| 2100 °F. (1149 °C.)<br>4 Hours     |   | 27-28 R <sub>C</sub>                            | 27-28 R <sub>C</sub>                            | 27-28 R <sub>C</sub>                            |

Table 10

Knoop hardness number after quenching and tempering.  
Specimens were quenched from the austenitizing temperature shown.

| <u>Austenitizing Treatment</u>  | <u>Youngstown #66797 (IC) AISI 1040</u> | <u>Youngstown #95313 (IF) AISI 1040</u> | <u>Republic #5023766 (IC) AISI 1046</u> | <u>Republic #5054025 (IF) AISI 1046</u> |
|---------------------------------|---|---|---|---|
| 1500 °F. (816 °C.)<br>2 Minutes | 315-320                                 |   | 308-315                                 |   |
| 1500 °F. (816 °C.)<br>5 Minutes | 314-320                                 | 310-314                                 | 308-315                                 | 305-318                                 |
| 1575 °F. (857 °C.)<br>4 Hours   |   |   |   | 308-312                                 |
| 1725 °F. (941 °C.)<br>4 Hours   |   | 312-316                                 |   |   |
| 2000 °F. (1093 °C.)<br>4 Hours  | 308-322                                 |   |   |   |
| 2100 °F. (1149 °C.)<br>4 Hours  |   | 313-320                                 | 314-320                                 | 311-314                                 |

Table 11

Rockwell "B" hardness of specimens air-cooled  
from the austenitizing temperature shown

| <u>Austenitizing Treatment</u>  | <u>Youngstown #66797 (IC) AISI 1040</u> | <u>Youngstown #95313 (IF) AISI 1040</u> | <u>Republic #5023766 (IC) AISI 1046</u> | <u>Republic #5054025 (IF) AISI 1046</u> |
|---------------------------------|---|---|---|---|
| 1500 °F. (816 °C.)<br>2 Minutes | 87-88 R <sub>b</sub>                    |   | 95-97 R <sub>b</sub>                    |   |
| 1575 °F. (857 °C.)<br>4 Hours   |   |   |   | 91-94 R <sub>b</sub>                    |
| 1725 °F. (941 °C.)<br>4 Hours   |   | 84-85 R <sub>b</sub>                    |   |   |
| 2000 °F. (1093 °C.)<br>4 Hours  | 90-91 R <sub>b</sub>                    |   |   |   |
| 2100 °F. (1149 °C.)<br>4 Hours  |   | 88-89 R <sub>b</sub>                    | 94-96 R <sub>b</sub>                    | 97-98 R <sub>b</sub>                    |

but the range of hardness of AISI 1046 steel was too high to be compared with AISI 1040 steel.

#### 3.4. Microstructure of Quenched Specimens

The hardness testing results must be supplemented by actual examination of the microstructure. Small quantities of a second phase may be located in the grain boundaries and may not be revealed by hardness testing, but could have a serious detrimental effect on impact properties. The microstructure of quenched specimens was examined at 100x and 1000x. Representative areas in the core of the specimens were photographed at 1000x and are shown in Figures 16-19. These photographs represent the quenched structure in specimens quenched from the coarsest and the finest austenite grain size. Although there is a remarkable difference in martensite needle length depending on the prior austenite grain size, only isolated areas of bainite were found in the structure. One of the more important observations was the presence of continuous or semi-continuous inclusion networks located in prior austenite grain boundaries of steels quenched from coarse grained austenite. These inclusions were found only in the three heats of steel which contained aluminum and are shown in the top photograph in Figures 17-19.

#### 3.5. Microstructure of Quenched and Tempered Specimens

The microstructure after tempering was examined and representative photographs at 1000x are shown in Figures 20-23. In this condition a fine dispersion of carbides in the structure contributes to the difficulty of revealing the ferrite grain size by etching or measuring grain size by other methods. Photographs do reveal that the pattern of original martensite needles is still present, and that prior austenite grain boundaries can still be located in some cases.

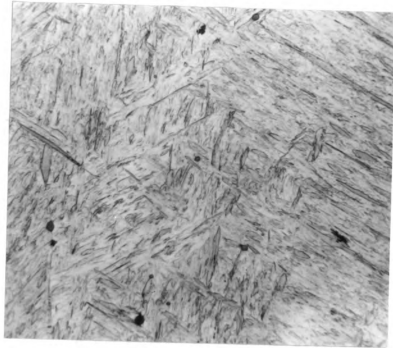


Fig. 16. As-quenched martensite structure for Youngstown #66797 (IC) (AISI 1040) Top: austenitized at 2000°F., 4 hours. Bottom: austenitized at 1500°F., 2 minutes (1000x), nital etch

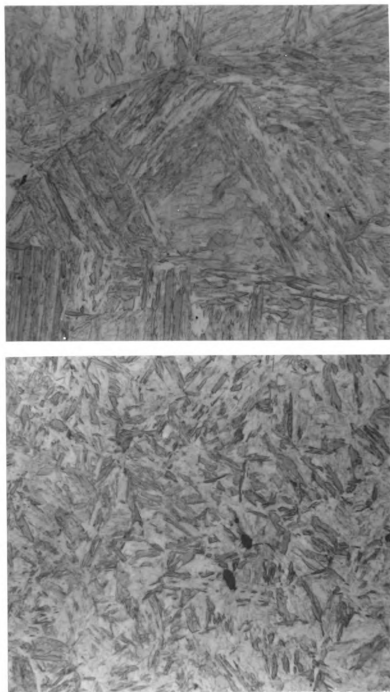


Fig. 17. As-quenched martensite structure for Youngstown #95313 (IF) (AISI 1040) Top: austenitized at 2100°F., 4 hours. Bottom: austenitized at 1500°F., 5 minutes (1000x), nital etch

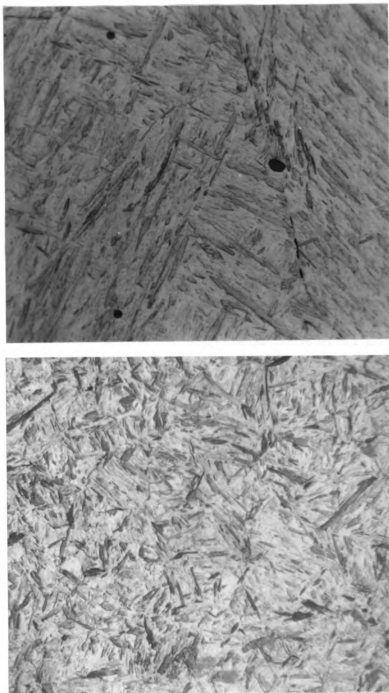


Fig. 18. As-quenched martensite structure for Republic #5023766 (IC) (AISI 1046) Top: austenitized at 2100°F., 4 hours. Bottom: austenitized at 1500°F., 2 minutes (1000x), nital etch

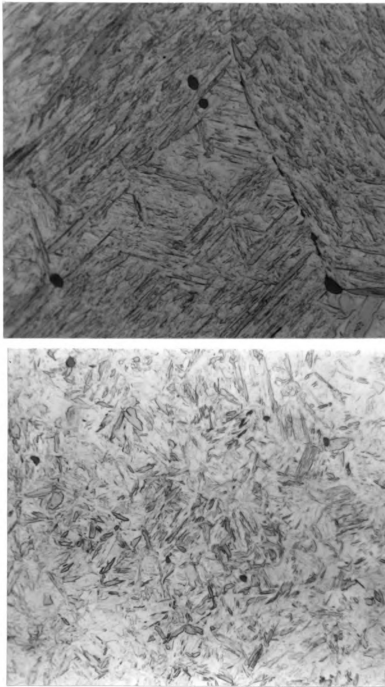


Fig. 19. As-quenched martensite structure for Republic #5054025 (IF) (AISI 1046) Top: austenitized at 2100°F., 4 hours. Bottom: austenitized at 1500°F., 5 minutes (1000x), nital etch

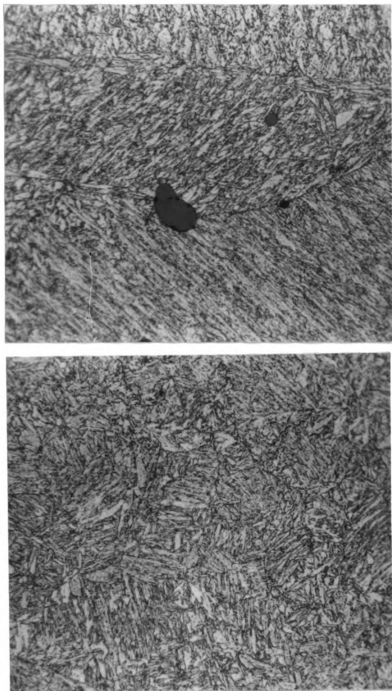


Fig. 20. Quenched and tempered structure for Youngstown #66797 (IC) (AISI 1040) Top: austenitized at 2000°F., 4 hours. Bottom: austenitized at 1500°F., 2 minutes (1000x), nital etch

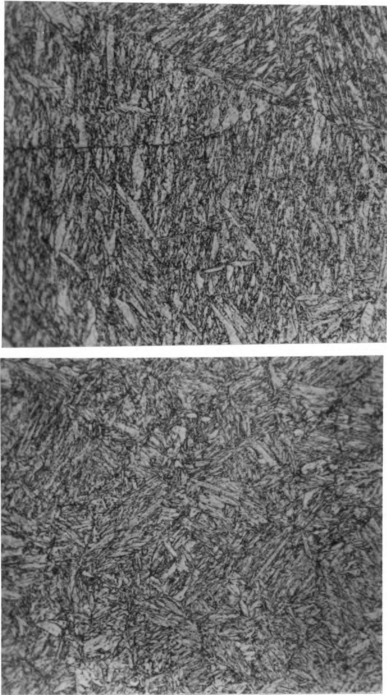
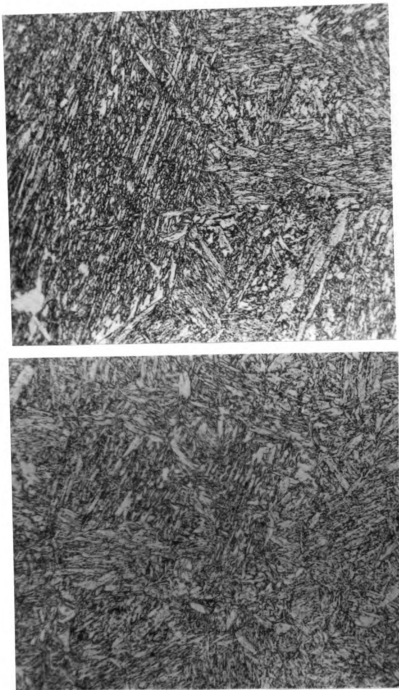


Fig. 21. Quenched and tempered structure for Youngstown #95313 (IF) (AISI 1040) Top: austenitized at 2100°F., 4 hours. Bottom: austenitized at 1500°F., 5 minutes (1000x), nital etch



**Fig. 22.** Quenched and tempered structure for Republic #5023766 (IC) (AISI 1046) Top: austenitized at 2100°F., 4 hours. Bottom: austenitized at 1500°F., 2 minutes (1000x), nital etch

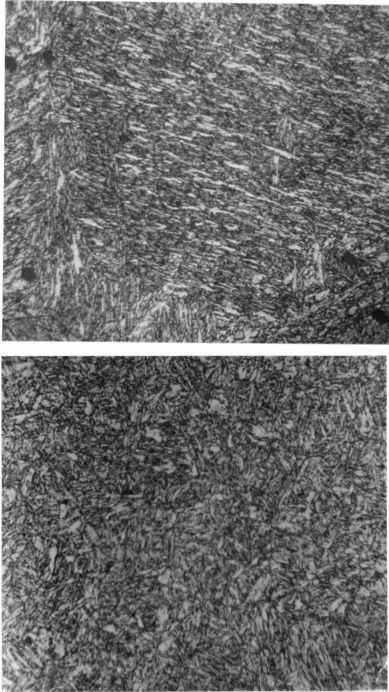


Fig. 23. Quenched and tempered structure for Republic #5054025 (IF) (AISI 1046) Top: austenitized at 2100°F., 4 hours. Bottom: austenitized at 1500°F., 5 minutes (1000x), nital etch

In order to investigate the size and shape of ferrite grains in tempered martensite as affected by prior structure, specimens were tempered at 1300°F. for 24 hours. This tempering treatment served to coalesce the carbides and increase the grain size. This made possible the examination of ferrite grains by using standard etching techniques. These photographs at 1000x are shown in Figures 24-27 for steel quenched from the coarsest and finest austenite grain sizes. The photographs indicate that prior austenite grain size has little or no effect on ferrite grain size. The most significant effect is the shape of ferrite grains and the distribution of carbides. Even after this lengthy tempering treatment, ferrite grain shape reflects the shape of the martensite plates, and carbides tend to be distributed parallel to this direction.

### 3.6. Microstructure of Air-Cooled Specimens

Air-cooled specimens were sectioned and examined at 100x. Representative photographs of the microstructure are shown in Figures 28-31 for specimens cooled from coarse and fine grained austenite. For specimens cooled from fine grained austenite, we observed a uniform structure of pearlite and ferrite. Specimens cooled from coarse grained austenite have a continuous network of ferrite surrounding the pearlite. One heat of steel, Youngstown #95313 (IF), (Figure 29) has a substantial amount of ferrite precipitated as Widmanstätten plates. This type of precipitate was observed even though the cooling rate was identical to other steels. The Widmanstätten precipitate apparently enhanced impact properties and this will be discussed in more detail in a later section.

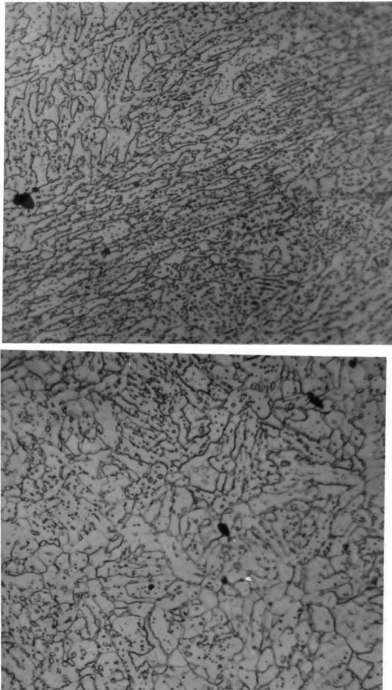


Fig. 24. Quenched and tempered structure for Youngstown #66797 (IC) (AISI 1040) Tempered at 1300°F., 24 hours. Top: austenitized at 2000°F., 4 hours. Bottom: austenitized at 1500°F., 2 minutes (1000x), nital etch

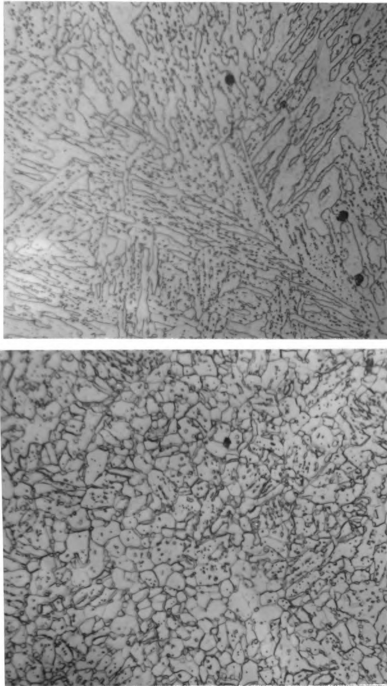


Fig. 25. Quenched and tempered structure for Youngstown #95313 (IF) (AISI 1040) Tempered at 1300°F., 24 hours. Top: austenitized at 2100°F., 4 hours. Bottom: austenitized at 1500°F., 5 minutes (1000x), nital etch

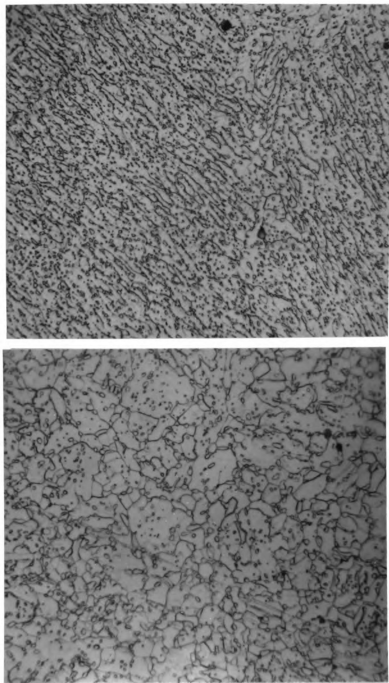


Fig. 26. Quenched and tempered structure for Republic #5023766 (IC) (AISI 1046) Tempered at 1300°F., 24 hours. Top: austenitized at 2100°F., 4 hours. Bottom: austenitized at 1500°F., 2 minutes (1000x), nital etch

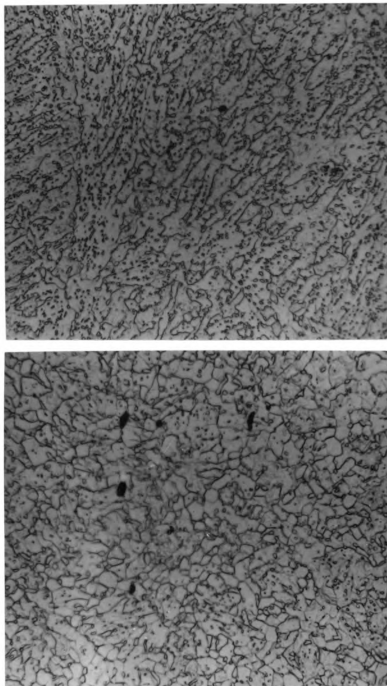


Fig. 27. Quenched and tempered structure for Republic #5054025 (IF) (AISI 1046) Tempered at 1300°F., 24 hours. Top: austenitized at 2100°F., 4 hours. Bottom: austenitized at 1500°F., 5 minutes (1000x), nital etch

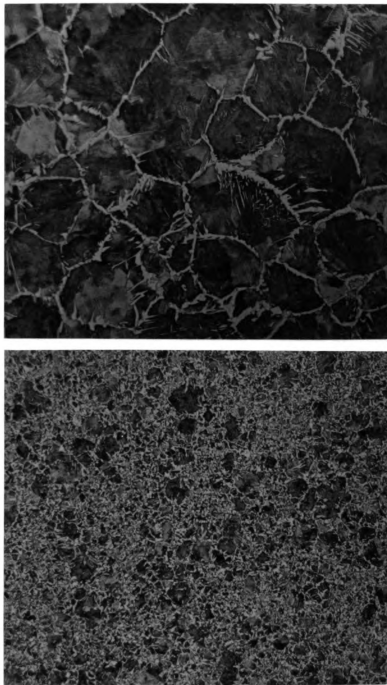


Fig. 28. Air-cooled structure of Youngstown #66797 (IC), (AISI 1040).  
Top: austenitized at 2000°F., 4 hours. Bottom: austenitized  
at 1500°F., 2 minutes (100x), nital etch

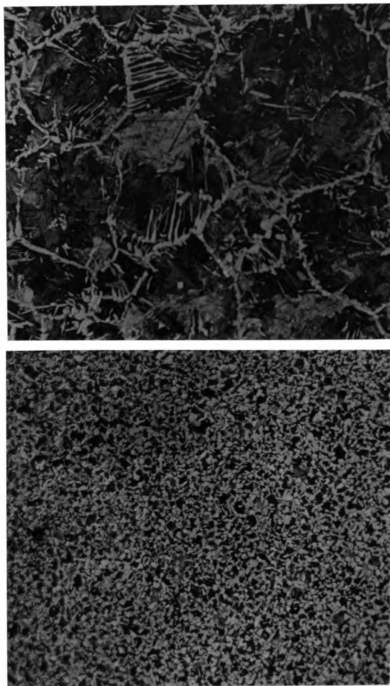


Fig. 29. Air-cooled structure of Youngstown #95313 (IF), (AISI 1040).  
Top: austenitized at 2100°F., 4 hours. Bottom: austenitized  
at 1725°F., 4 hours (100x), nital etch

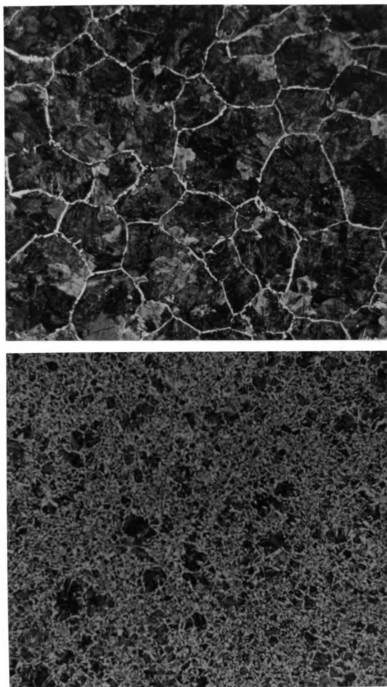


Fig. 30. Air-cooled structure of Republic #5023766 (IC), (AISI 1046).  
Top: austenitized at 2100°F., 4 hours. Bottom: austenitized  
at 1500°F., 2 minutes (100x), nital etch

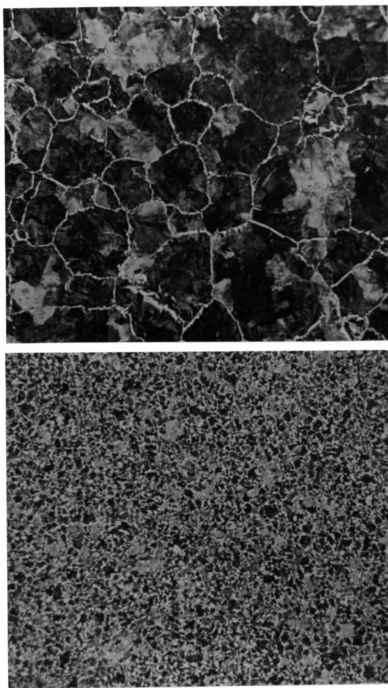


Fig. 31. Air-cooled structure of Republic #5054025 (IF), (AISI 1046).  
Top: austenitized at 2100°F., 4 hours. Bottom: austenitized  
at 1575°F., 4 hours (100x), nital etch

### 3.7. Impact Testing

In order to determine a transition curve, impact energy was determined at several temperatures for each heat treatment. These results for quenched and tempered specimens are shown in Tables 12 and 13. The results are energy absorbed by fracturing the specimen as measured by pendulum follow-through. The scale could be read to the nearest 0.5 ft. lb.

Results from Table 12 and Table 13 are shown graphically in Figures 32-35. In each of these Figures, three curves are plotted. Each curve represents impact energy for specimens quenched from fine, intermediate, and coarse austenite grains. The transition temperature is taken as the inflection point of the impact energy-temperature curve and these results are summarized in Table 14. For each of the four heats of steel, there is no consistency with respect to the effect of austenite grain size on the transition temperature. In one case the specimens quenched from a coarse austenite grain size had the lowest transition temperature, in two cases the intermediate grain size was the lowest, and in one case the finest grain size was lowest. When comparing inherently fine grain steel to inherently coarse grain, generally the fine grain steel has lower transition temperatures. For equivalent prior austenite grain sizes this value is 7-22°C. for AISI 1040 steel, and 7-47°C. for AISI 1046 steel.

An additional consideration when examining the transition curves is upper shelf energy or impact energy at room temperature. For three heats of steel, upper shelf impact energy is improved by approximately 10% by quenching from fine grained austenite, but for the other heat (Figure 35) impact energy is improved 100%. When comparing the upper energy shelf

Table 12

Charpy V-notch impact energy in ft. lbs. for quenched  
and tempered AISI 1040 steel

| Testing<br>Temp., °C. | Youngstown #66797 (IC) |                    |                    | Youngstown #95313 (IF) |                    |                    |
|-----------------------|------------------------|--------------------|--------------------|------------------------|--------------------|--------------------|
|                       | 1500 °F.<br>2 min.     | 1500 °F.<br>5 min. | 2000 °F.<br>4 hrs. | 1500 °F.<br>5 min.     | 1725 °F.<br>4 hrs. | 2100 °F.<br>4 hrs. |
| 22                    | 31.5                   | 31.5, 34.0         | 30.0               | 35.5                   | 36.0, 35.5         | 31.5               |
| -18                   | 29.0                   | 32.5               | 27.5               | 34.5                   | 36.5               | 30.0               |
| -40                   | 31.5                   | 32.5               | 27.5               | 34.0                   | 32.5               | 32.5               |
| -62                   | 31.0                   | 28.0               | 24.5               | 31.0                   | 33.0               | 27.0               |
| -70                   | -                      | 29.0               | -                  | -                      | -                  | -                  |
| -79                   | 28.5                   | 28.0               | 23.5               | 32.0                   | 30.0               | 25.0               |
| -85                   | -                      | 15.0               | 23.5               | -                      | -                  | 23.5               |
| -97                   | 24.5                   | 14.0               | 10.5               | 35.0                   | 31.0               | 16.5               |
| -100                  | -                      | -                  | -                  | 29.5                   | -                  | -                  |
| -114                  | 11.0                   | 8.5                | 11.5               | 27.0                   | 29.0, 29.5         | 13.5               |
| -128                  | 9.5                    | 8.0                | 7.0                | 11.5                   | 22.5               | 10.0               |
| -150                  | 8.0                    | 8.0                | 5.0                | -                      | 11.0               | 4.0                |
| -196                  | 4.0                    | 5.0, 7.5           | 3.0                | 11.0, 10.0             | 6.0                | 4.5                |

Table 13

Charpy V-notch impact energy in ft. lbs. for quenched  
and tempered AISI 1046 steel

| Testing<br>Temp., °C. | Republic #5023766 (IC) |                    |                    | Republic #5054025 (IF) |                    |                    |
|-----------------------|------------------------|--------------------|--------------------|------------------------|--------------------|--------------------|
|                       | 1500 °F.<br>2 min.     | 1500 °F.<br>5 min. | 2100 °F.<br>4 hrs. | 1500 °F.<br>5 min.     | 1575 °F.<br>4 hrs. | 2100 °F.<br>4 hrs. |
| 22                    | 29.5                   | 27.5               | 24.0, 24.5         | 42.5, 43.5             | 35.5, 41.0         | 21.5               |
| -18                   | 26.5                   | 26.5               | 24.0               | 32.5                   | 35.5               | 22.5               |
| -40                   | 25.5                   | 26.0               | 22.0               | 30.5                   | 34.0               | 21.5               |
| -62                   | 15.0, 23.0             | 22.5               | 19.0               | 29.0, 37.0             | 30.5               | 20.5, 22.0         |
| -70                   | -                      | 14.0               | -                  | -                      | -                  | 20.5               |
| 79                    | 14.5                   | 13.0               | 16.5               | 34.0                   | 29.0               | 22.0               |
| -85                   | -                      | -                  | -                  | -                      | 33.0               | 13.0               |
| -97                   | 10.0                   | 10.0               | 10.5               | 26.0                   | 29.5               | 12.5               |
| -114                  | 8.5                    | 9.0                | 7.5                | 13.5                   | 25.5               | 7.0                |
| -128                  | 8.0                    | 6.5                | 6.5                | 8.0                    | 9.5                | 6.5                |
| -150                  | 8.0                    | -                  | 4.0                | -                      | 8.0                | -                  |
| -196                  | 5.0, 5.5               | 6.0, 6.0           | 3.5                | 8.0                    | 8.0, 7.5           | 2.5                |

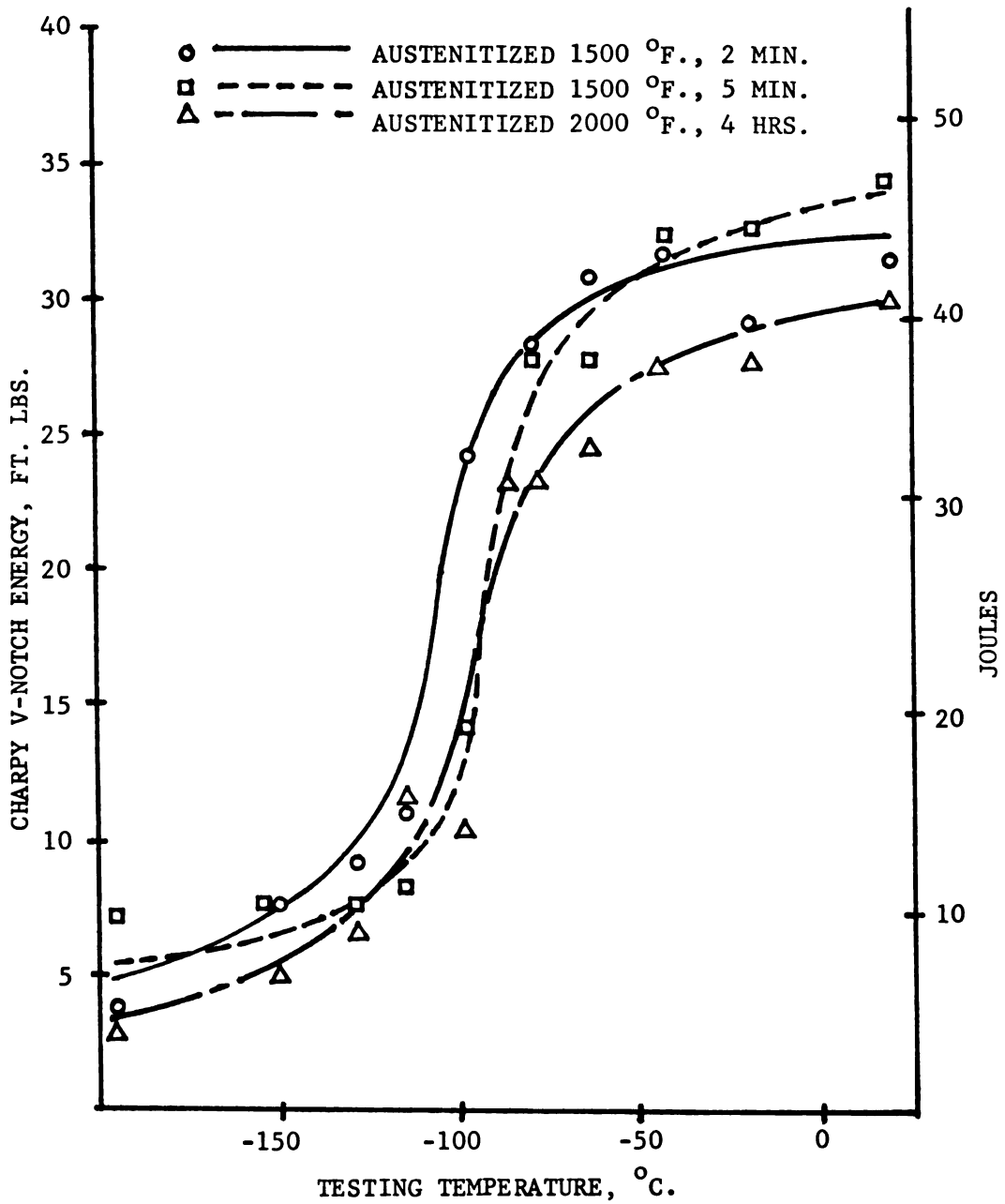


Fig. 32. Charpy V-notch transition curves for quenched and tempered Youngstown #66797 (IC), AISI 1040

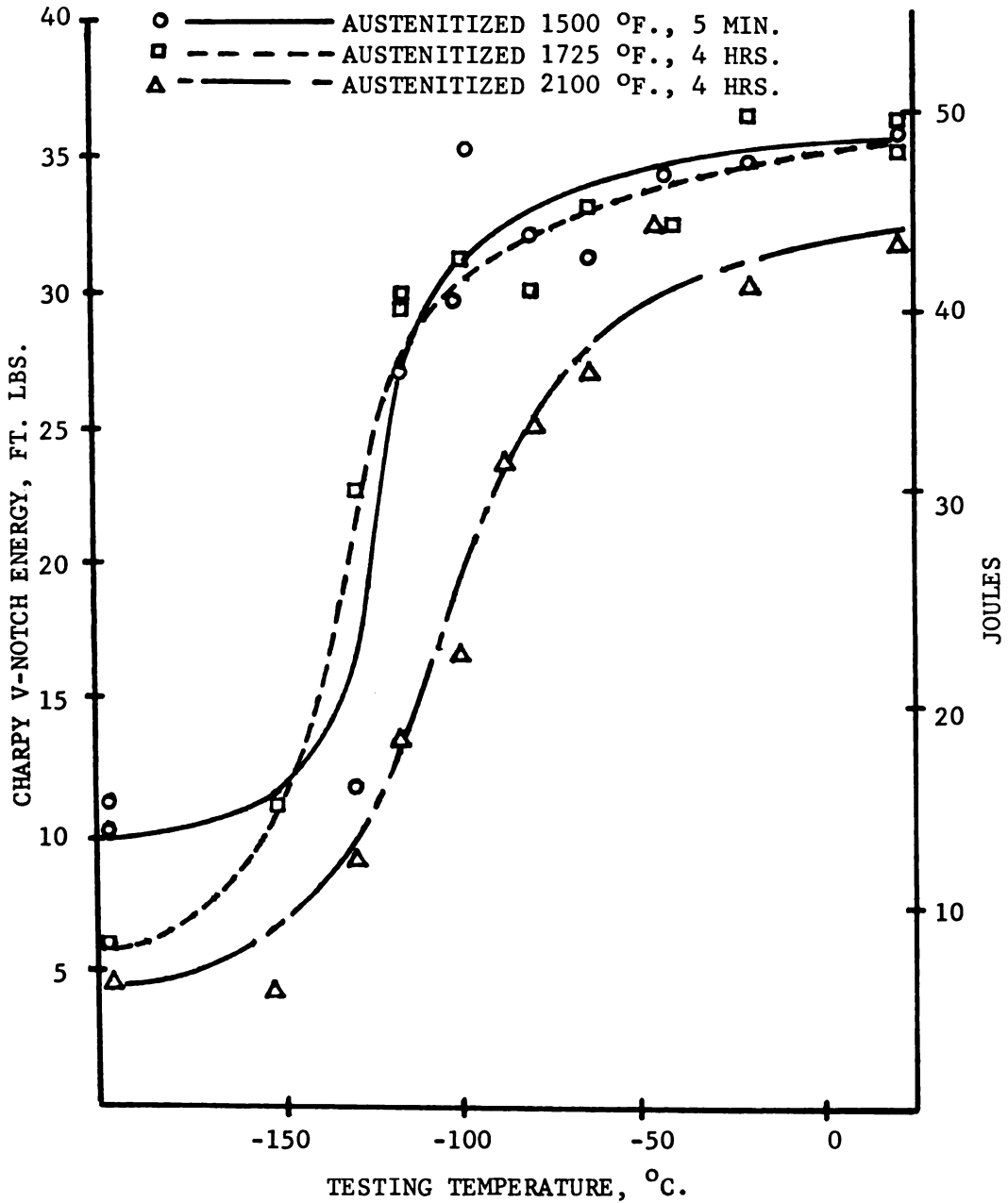


Fig. 33. Charpy V-notch transition curves for quenched and tempered Youngstown #95313 (IF), AISI 1040

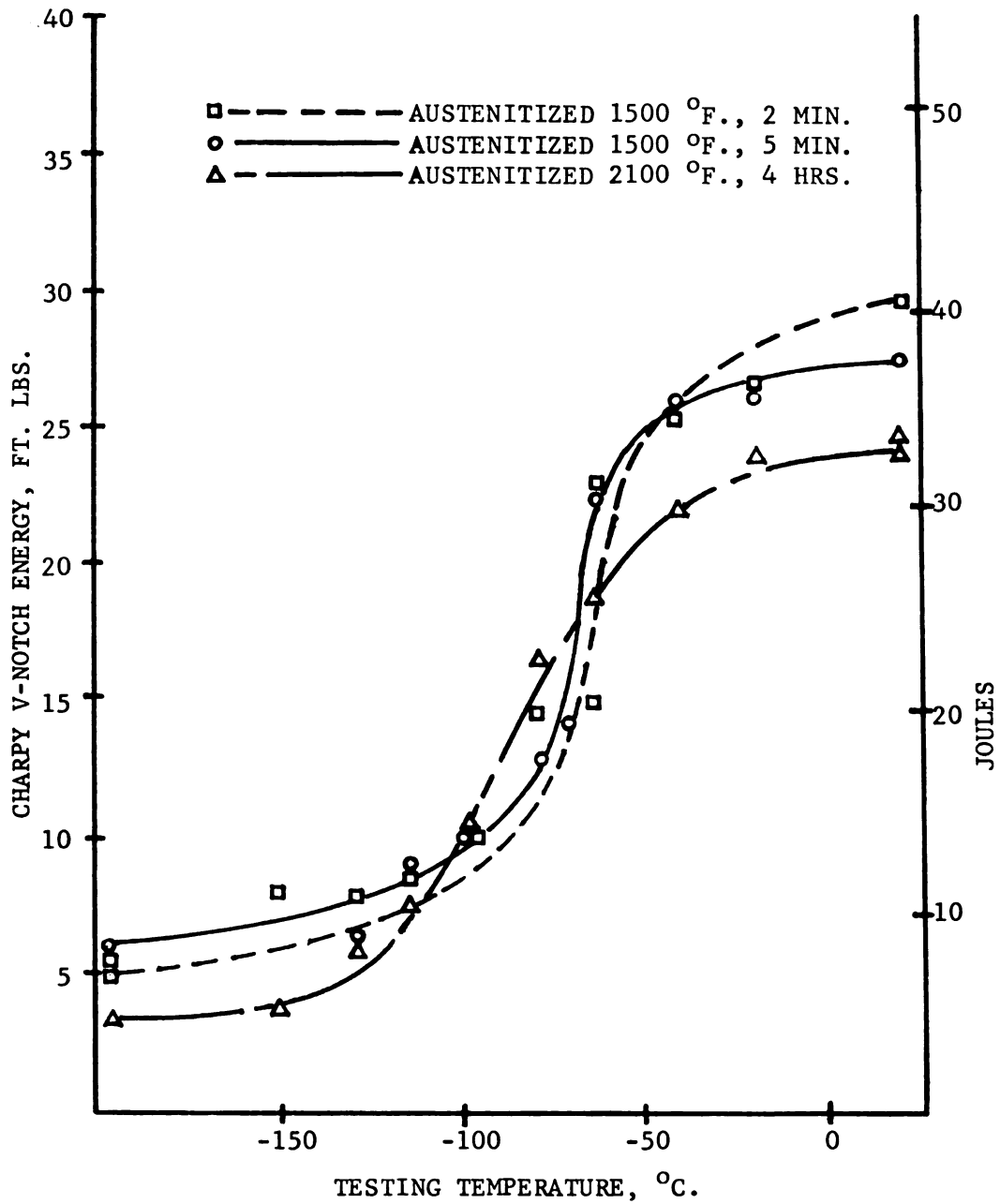


Fig. 34. Charpy V-notch transition curves for quenched and tempered Republic #5023766 (IC), AISI 1046

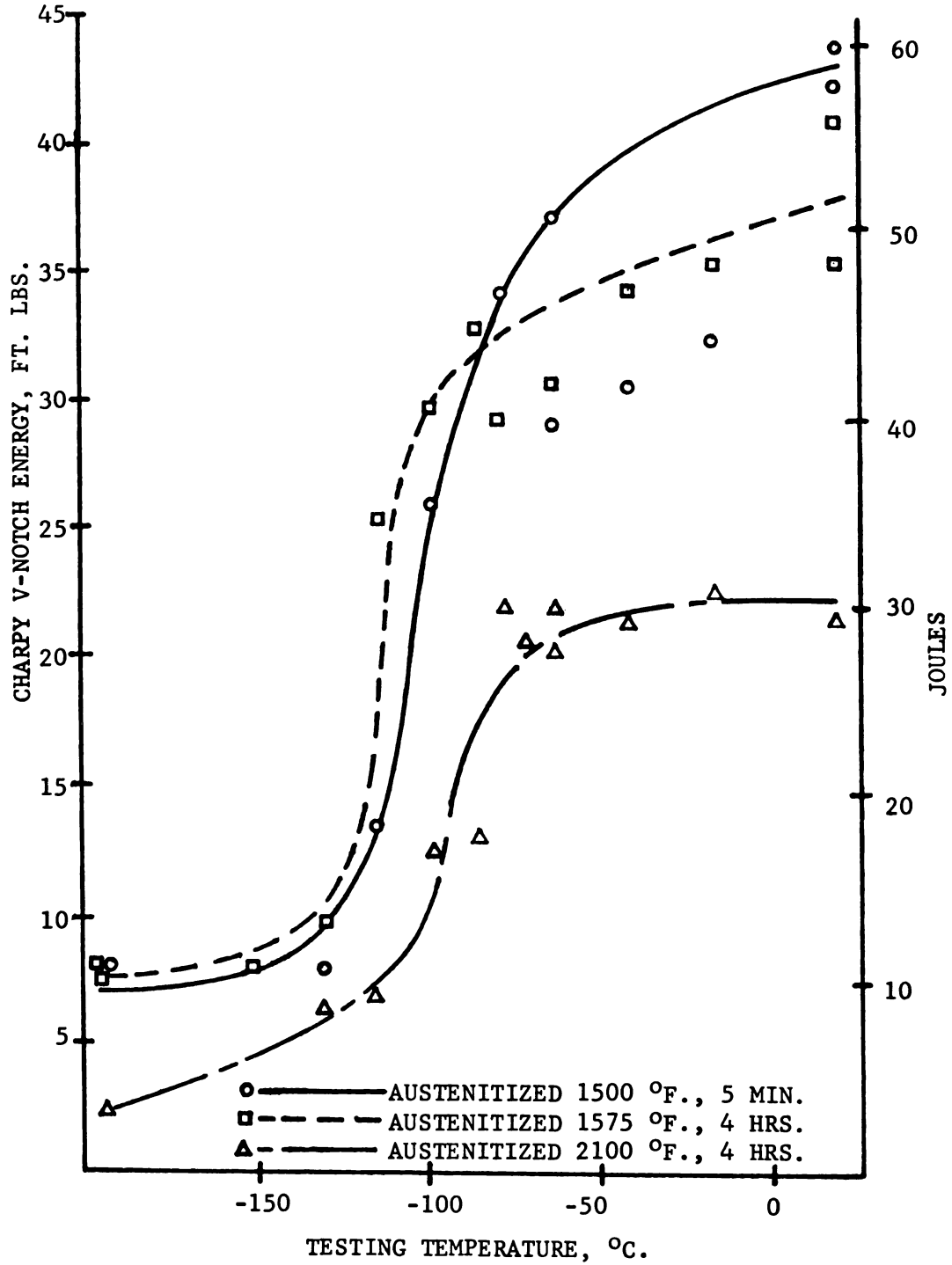


Fig. 35. Charpy V-notch transition curves for quenched and tempered Republic #5054025 (IF), AISI 1046

Table 14

Inflection point transition temperature for half-width,  
quenched and tempered Charpy V-notch specimens

| <u>Heat</u>                          | <u>Austenitizing<br/>Treatment</u> | <u>Transition<br/>Temperature, °C.</u> |
|--------------------------------------|------------------------------------|--|
| Youngstown #66797<br>(IC), AISI 1040 | 1500°F., 2 min.                    | -108                                   |
|                                      | 1500°F., 5 min.                    | -92                                    |
|                                      | 2000°F., 4 hrs.                    | -95                                    |
| Youngstown #95313<br>(IF), AISI 1040 | 1500°F., 5 min.                    | -125                                   |
|                                      | 1725°F., 4 hrs.                    | -130                                   |
|                                      | 2100°F., 4 hrs.                    | -102                                   |
| Republic #5023766<br>(IC), AISI 1046 | 1500°F., 2 min.                    | -65                                    |
|                                      | 1500°F., 5 min.                    | -68                                    |
|                                      | 2100°F., 4 hrs.                    | -85                                    |
| Republic #5054025<br>(IF), AISI 1046 | 1500°F., 5 min.                    | -102                                   |
|                                      | 1575°F., 4 hrs.                    | -112                                   |
|                                      | 2100°F., 4 hrs.                    | -92                                    |

for inherently coarse and fine grain, quenched from a fine grained condition, fine grain steel is superior by 10% for AISI 1040 and 50% for AISI 1046. However, when both inherently coarse and fine grain steels are quenched from coarse austenite grains, there is little or no advantage for fine grain steels.

When comparing transition temperature and upper shelf energy, inherently fine grain steels are equal or superior to inherently coarse grain steels. The same general relationship holds for steel quenched from a structure of fine austenite grains compared to the same steel quenched from coarse austenite grains. All steels tested in the quenched and tempered condition showed excellent impact properties and in general, low transition temperatures. This observation is true even though the transition temperature for half-width specimens is lower than full-width specimens prepared in an identical manner.

Transition curves were also determined for air-cooled specimens. Results of impact energy at various testing temperatures are shown in Table 15. The data from Table 15 are shown graphically in Figures 36-37. For these structures, prior austenite grain size was a significant variable, since steel cooled from coarse austenite grains showed a higher transition temperature and lower upper shelf energy. The only exception was Youngstown #95313 (IF) which showed improved upper shelf energy over other steels cooled from coarse grained austenite. The transition temperatures for steels in this condition (Table 16), are generally near or substantially above the temperature range to which parts or structures are subjected. This is especially significant when considering that full-width specimens would yield a higher transition temperature. The results indicate that air-cooling from fine grained austenite is of utmost importance, and generally an inherently fine grain steel is superior to an inherently coarse grain steel when coarsened to an identical austenite grain size.

### 3.8. Load-Time and Energy-Time Curves

Load-time and energy-time curves were obtained from Dynatup instrumentation used on the impact tester. As indicated earlier, these curves may be used to provide additional information about fracture characteristics of the specimen being tested. The load-time curve yields fracture information such as dynamic yield point, load to initiate fracture, and load to propagate fracture. The energy-time curve serves as a valuable double check on the energy value obtained from pendulum follow-through.

In addition to the energy transition temperature, another criterion often used in fracture studies is the fracture appearance transition

Table 15

Charpy V-notch impact energy in ft. lbs. for air-cooled specimens

| Testing<br>Temp., °C. | Youngstown #66797 (IC) |                    | Youngstown #95313 (IF) |                    |
|-----------------------|------------------------|--------------------|------------------------|--------------------|
|                       | 1500 °F.<br>2 min.     | 2000 °F.<br>4 hrs. | 1725 °F.<br>4 hrs.     | 2100 °F.<br>4 hrs. |
| 100                   | -                      | 11.0               | -                      | 24.0, 18.0         |
| 66                    | -                      | 11.5               | -                      | 13.5               |
| 22                    | 24.0, 20.0             | 8.5, 7.0           | 22.5, 26.0             | 10.0, 9.0          |
| -18                   | 9.5, 12.0              | 2.5                | 19.0                   | 1.5                |
| -40                   | 8.0                    | -                  | 11.5                   | -                  |
| -62                   | 3.0                    | -                  | 2.0                    | -                  |
| -70                   | -                      | -                  | 3.0                    | -                  |

|     | Republic #5023766 (IC) |                    | Republic #5054025 (IF) |                    |
|-----|------------------------|--------------------|------------------------|--------------------|
|     | 1500 °F.<br>2 min.     | 2100 °F.<br>4 hrs. | 1575 °F.<br>4 hrs.     | 2100 °F.<br>4 hrs. |
| 100 | -                      | 7.0, 10.0          | -                      | 12.0               |
| 66  | 24.0                   | 6.0, 6.0           | 21.0                   | 8.0                |
| 22  | 15.0                   | 3.0                | 13.5                   | 6.0, 7.5           |
| -18 | 9.5                    | 2.5                | 9.5                    | -                  |
| -40 | 7.5                    | -                  | 7.0                    | 3.0                |
| -62 | 7.0                    | -                  | 5.0                    | -                  |
| -87 | 5.5                    | -                  | 4.0                    | -                  |

Table 16

Inflection point transition temperature for half-width,  
air-cooled Charpy V-notch specimens

| <u>Heat</u>                          | <u>Austenitizing<br/>Treatment</u> | <u>Transition<br/>Temperature, °C.</u> |
|--------------------------------------|------------------------------------|--|
| Youngstown #66797<br>(IC), AISI 1040 | 1500 °F., 2 min.                   | -25                                    |
|                                      | 2000 °F., 4 hrs.                   | 25                                     |
| Youngstown #95313<br>(IF), AISI 1040 | 1725 °F., 4 hrs.                   | -35                                    |
|                                      | 2100 °F., 4 hrs.                   | 30                                     |
| Republic #5023766<br>(IC), AISI 1046 | 1500 °F., 4 hrs.                   | 15                                     |
|                                      | 2100 °F., 4 hrs.                   | 45                                     |
| Republic #5054025<br>(IF), AISI 1046 | 1575 °F., 4 hrs.                   | 15                                     |
|                                      | 2100 °F., 4 hrs.                   | 25                                     |

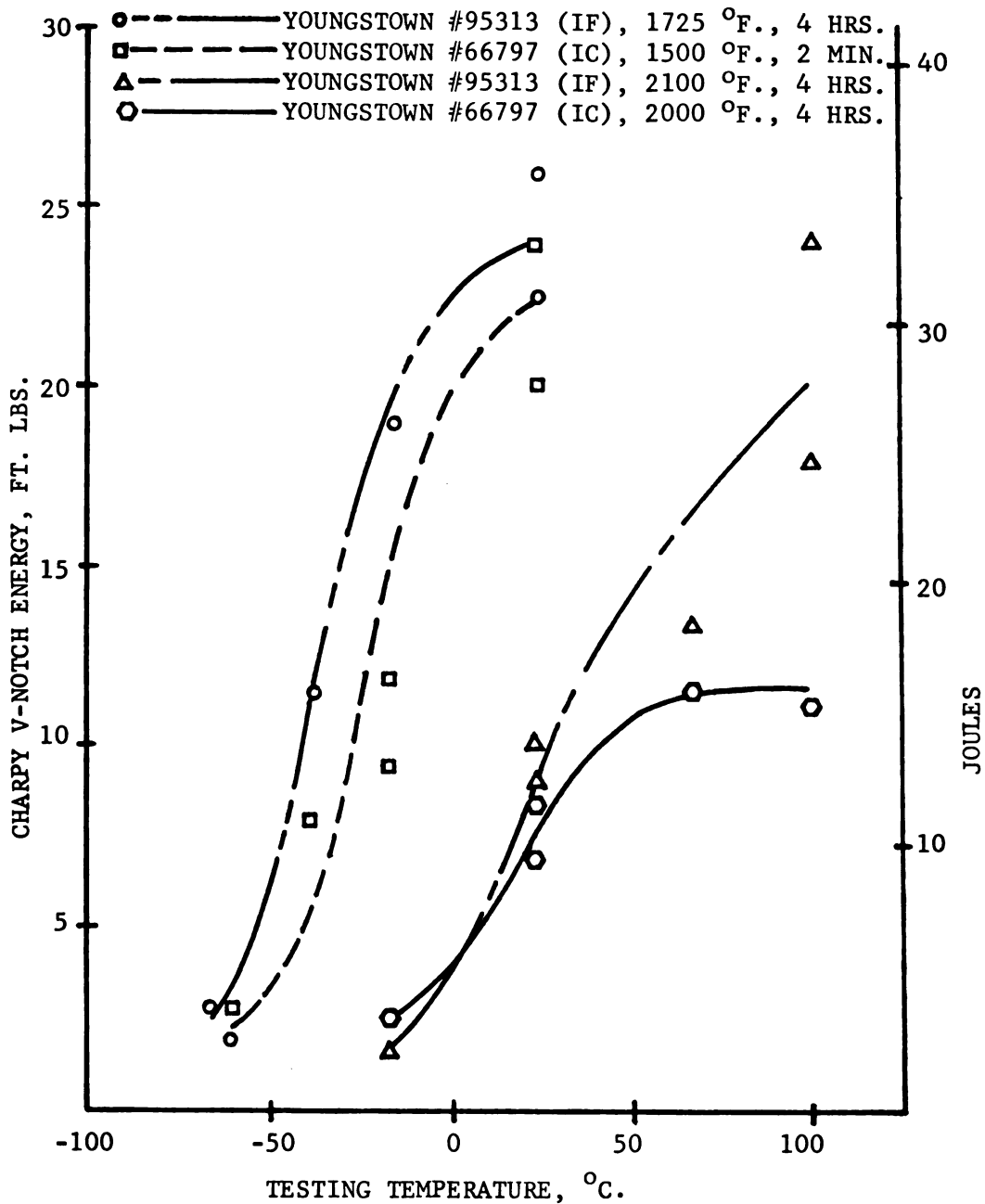


Fig. 36. Charpy V-notch transition curves for air-cooled AISI 1040 steel

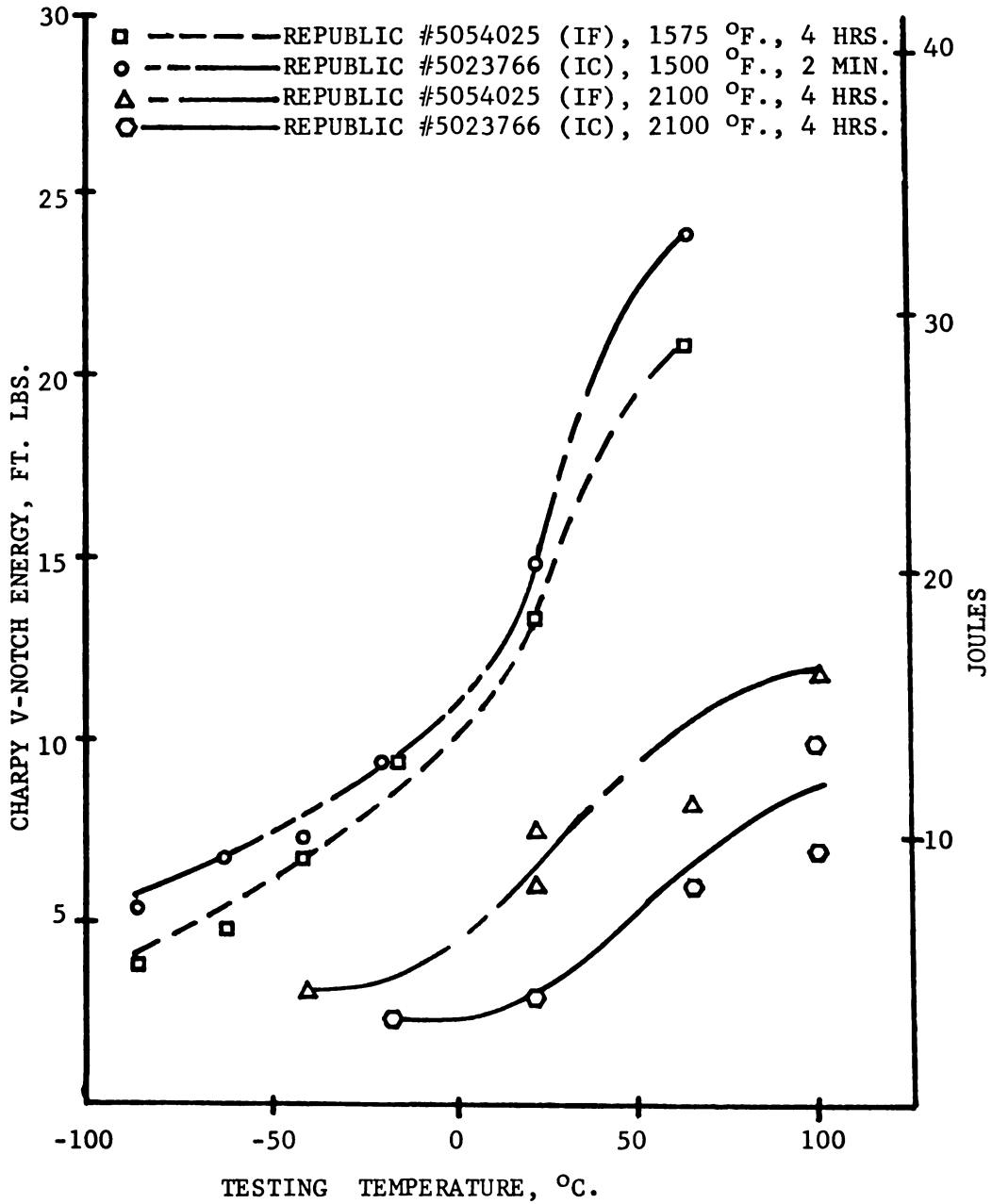


Fig. 37. Charpy V-notch transition curves for air-cooled AISI 1046 steel

temperature. The point of transition is usually considered to be the temperature at which the fracture is 50% fibrous and 50% brittle. This determination is often by visual examination or measurements on the fracture surface; however, in many cases where a sharp demarcation between the two regions does not exist, determination is difficult to perform in an accurate manner. The instrumented impact test may be used to determine percent brittle fracture in the area of the transition temperature. Energy-time and load-time curves for quenched and tempered specimens tested at  $-196^{\circ}\text{C.}$ ,  $-128^{\circ}\text{C.}$ ,  $-62^{\circ}\text{C.}$ , and  $22^{\circ}\text{C.}$  are shown in Figures 38-41. In the region of the transition temperature, percent brittle fracture may be compared for steels at each heat treatment. Results for each steel quenched from coarse and fine grained austenite are shown in Table 17. These results show that the specimen with the lowest percent brittle fracture at  $-128^{\circ}\text{C.}$  (Youngstown #95313, IF), is

Table 17

Percent brittle fracture for quenched and tempered specimens

| <u>Heat</u>                          | <u>Austenitizing Treatment</u>    | <u><math>-196^{\circ}\text{C.}</math></u> | <u><math>-128^{\circ}\text{C.}</math></u> |
|--------------------------------------|-----------------------------------|---|---|
| Youngstown #66797<br>(IC), AISI 1040 | 1500 $^{\circ}\text{F.}$ , 2 min. | 87%                                       | 84%                                       |
|                                      | 2000 $^{\circ}\text{F.}$ , 4 hrs. | 89%                                       | 84%                                       |
| Youngstown #95313<br>(IF), AISI 1040 | 1500 $^{\circ}\text{F.}$ , 5 min. | 85%                                       | 72%                                       |
|                                      | 2100 $^{\circ}\text{F.}$ , 4 hrs. | 87%                                       | 86%                                       |
| Republic #5023766<br>(IC), AISI 1046 | 1500 $^{\circ}\text{F.}$ , 2 min. | 84%                                       | 82%                                       |
|                                      | 2100 $^{\circ}\text{F.}$ , 4 hrs. | 88%                                       | 83%                                       |
| Republic #5054025<br>(IF), AISI 1046 | 1500 $^{\circ}\text{F.}$ , 5 min. | 83%                                       | 83%                                       |
|                                      | 2100 $^{\circ}\text{F.}$ , 4 hrs. | 89%                                       | 83%                                       |

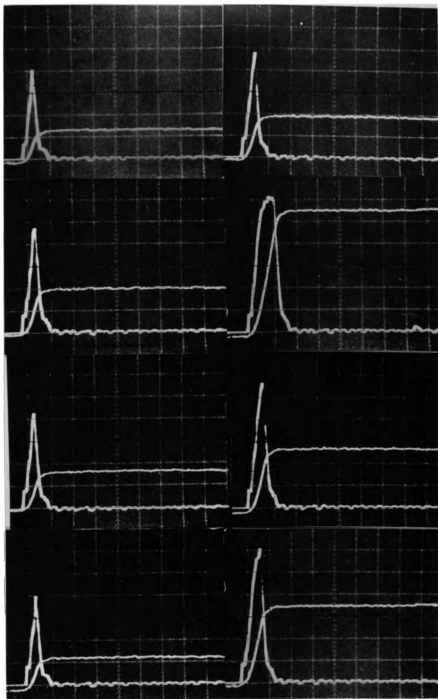


Fig. 38. Load-time and energy-time curves for quenched and tempered specimens fractured at  $-196^{\circ}\text{C}$ . Top to bottom: Youngstown #66797 (IC), AISI 1040; Youngstown #95313 (IF), AISI 1040; Republic #5023766 (IC), AISI 1046; Republic #5054025 (IF), AISI 1046. First column quenched from coarse grained austenite, and second column quenched from fine grained austenite. Vert. load scale: 500 lbs./div. Vert. energy scale: 2 ft. lbs./div. Horiz. time scale: 0.2m-sec./div.

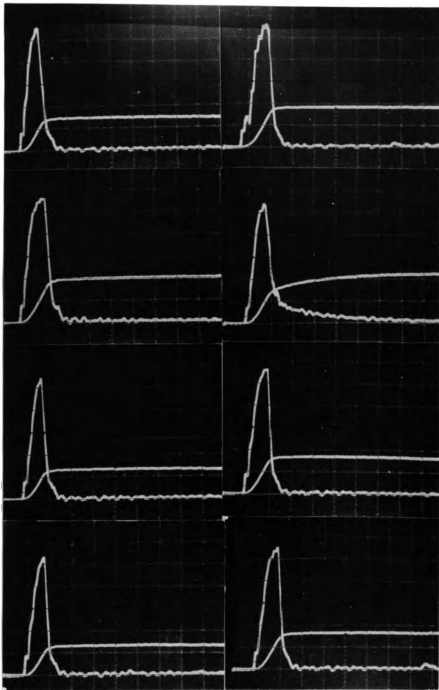


Fig. 39. Load-time and energy-time curves for quenched and tempered specimens fractured at  $-128^{\circ}\text{C}$ . Top to bottom: Youngstown #66797 (IC), AISI 1040; Youngstown #95313 (IF), AISI 1040; Republic #5023766 (IC), AISI 1046; Republic #5054025 (IF), AISI 1046. First column quenched from coarse grained austenite; second column quenched from fine grained austenite. Vert. load scale: 500 lbs./div. Vert. energy scale: 5 ft. lbs./div. Horiz. time scale: 0.2 m-sec./div.

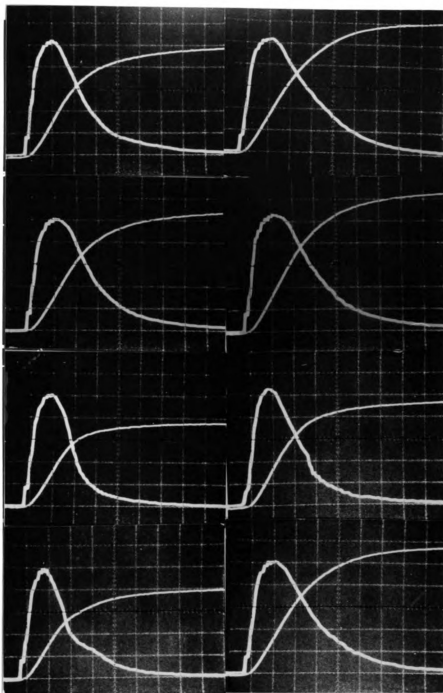


Fig. 40. Load-time and energy-time curves for quenched and tempered specimens fractured at  $-62^{\circ}\text{C}$ . Top to bottom: Youngstown #66797 (IC), AISI 1040; Youngstown #95313 (IF), AISI 1040; Republic #5023766 (IC), AISI 1046; Republic #5054025 (IF), AISI 1046. First column quenched from coarse grained austenite; second column quenched from fine grained austenite. Vert. load scale: 500 lbs./div. Vert. energy scale: 5 ft. lbs./div. Horiz. time scale: 0.2 m-sec./div.

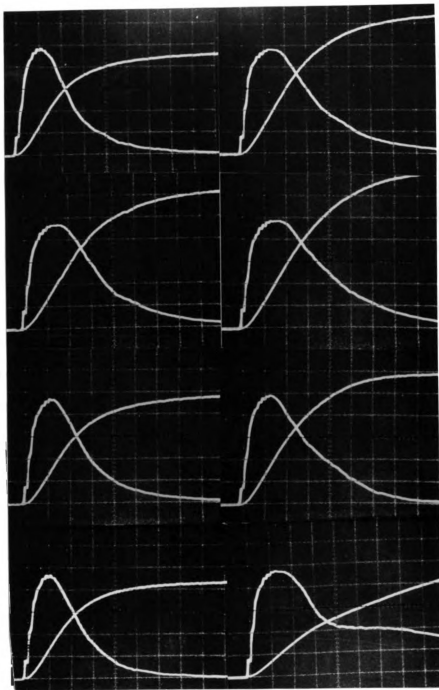


Fig. 41. Load-time and energy-time curves for quenched and tempered specimens fractured at 22°C. Top to bottom: Youngstown #66797 (IC), AISI 1040; Youngstown #95313 (IF), AISI 1040; Republic #5023766 (IC), AISI 1046; Republic #5054025 (IF), AISI 1046. First column quenched from coarse grained austenite; second column quenched from fine grained austenite. Vert. load scale: 500 lbs./div. Vert. energy scale: 5 ft. lbs./div. Horiz. time scale: 0.2 m-sec./div.

of the same heat and heat treatment as the specimens which yielded the lowest energy transition temperature. When ductile fracture is predominant, as in the fractures at  $-62^{\circ}\text{C}$ . and  $22^{\circ}\text{C}$ ., fracture appearance characteristics cannot be determined from the load-time curves.

It has been reported that a gradual slope at the trailing end of the load-time curve is associated with energy to form a shear lip<sup>(62)</sup>. An excellent correlation between the shape of the load-time curves and the fracture appearance was observed. As an example, the load-time curve for Republic #5054025 (IF), austenitized at  $1500^{\circ}\text{F}$ . for 5 minutes, is shown in Figure 41. This curve shows an extremely long and gradual slope on the trailing end, and the fracture was observed to have a large shear lip.

Energy-time and load-time curves at  $-18^{\circ}\text{C}$ . are shown for air-cooled specimens in Figure 42. For these specimens there are large differences in the energy-time curves, and the energy to initiate fracture is far greater for specimens cooled from fine grained austenite.

### 3.9. Macroscopic Examination of Fractures

The Charpy V-notch impact fractures were examined visually and photographed at approximately 3x. Photographs for the quenched and tempered specimens fractured at  $-196^{\circ}\text{C}$ .,  $-114^{\circ}\text{C}$ .,  $-62^{\circ}\text{C}$ ., and  $22^{\circ}\text{C}$ . are shown in Figures 43-46. These photographs show that the top rows, which represent specimens quenched from fine grained austenite, have a finer appearance than specimens in the bottom row, which were quenched from coarse grained austenite. The difference in fracture appearance is accentuated at lower temperatures (left to right in the photographs).

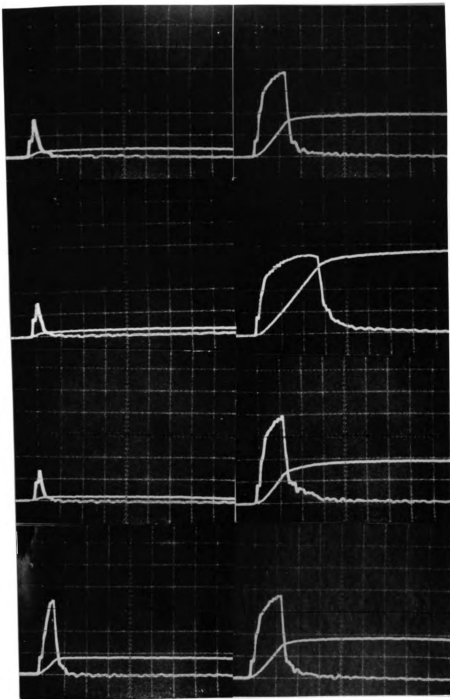


Fig. 42. Load-time and energy-time curves for air-cooled specimens fractured at  $-18^{\circ}\text{C}$ . Top to bottom: Youngstown #66797 (IC), AISI 1040; Youngstown #95313 (IF), AISI 1040; Republic #5023766 (IC), AISI 1046; Republic #5054025 (IF), AISI 1046. First column air-cooled from coarse grained austenite; second column air-cooled from fine grained austenite. Vert. load scale: 500 lbs./div. Vert. energy scale: 5 ft. lbs./div. Horiz. time scale: 0.2 m-sec./div.



Fig. 43. Fractures of quenched and tempered specimens of Youngstown #66797 (IC), AISI 1040. Top row: austenitized 1500°F., 2 min. Bottom row: austenitized 2000°F., 4 hrs. From left to right: fractured at 22°C., -62°C., -114°C. and -196°C.



Fig. 44. Fractures of quenched and tempered specimens of Youngstown #95313 (IF), AISI 1040. Top row: austenitized 1500°F., 5 min. Bottom row: austenitized 2100°F., 4 hrs. From left to right: fractured at 22°C., -62°C., -114°C., and -196°C.



Fig. 45. Fractures of quenched and tempered specimens of Republic #5023766 (IC), AISI 1046. Top row: austenitized 1500°F., 2 min. Bottom row: austenitized 2100°F., 4 hrs. From left to right: fractured at 22°C., -62°C., -114°C., and -196°C.



Fig. 46. Fractures of quenched and tempered specimens of Republic #5054025 (IF), AISI 1046. Top row: austenitized 1500°F., 5 min. Bottom row: austenitized 2100°F., 4 hrs. From left to right: fractured at 22°C., -62°C., -114°C., and -196°C.

This indicates that as percent brittle fracture increases, prior austenite grain size has an increasing influence on fracture appearance.

Photographs of air-cooled specimen fractures at 22°C. are shown in Figure 47. In this photograph, the top row of fractures are specimens cooled from fine grained austenite, and the bottom row are specimens cooled from coarse grained austenite. There is a significant difference in fracture appearance, the top row being finer and having some degree of shear lip. The top row also shows a mixture of fibrous and granular fracture, while the bottom row is completely granular. In these fractures, appearance is greatly affected by prior austenite grain size at all temperatures.

### 3.10. Microscopic Examination of Fractures

The scanning electron microscope (SEM) was used for microscopic examination of the fractured surfaces. This examination was necessary to investigate the relationship between macroscopic and microscopic fracture appearance. A SEM examination was made of all quenched and tempered specimens fractured at 22°C. and -196°C. There was great similarity between the fractographs regardless of the heat of steel tested. For example, the fractographs of all steel quenched from coarse grained austenite and tested at -196°C., were nearly identical. Representative fractographs for specimens quenched from coarse grained austenite and fractured at 22°C. and -196°C. are shown in Figure 48; and representative fractographs for specimens quenched from fine grained austenite and fractured at 22°C. and -196°C. are shown in Figure 49. In comparing these figures, specimens fractured at 22°C. show that fracture occurred by microvoid coalescence in both cases. Specimens fractured at -196°C. show



Fig. 47. Fractures of air-cooled specimens tested at 22°C. Top row: air-cooled from fine grained austenite. Bottom row: air-cooled from coarse grained austenite. From left to right: Youngstown #66797 (IC), AISI 1040; Youngstown #95313 (IF), AISI 1040; Republic #5023766 (IC), AISI 1046; Republic #5054025 (IF), AISI 1046.

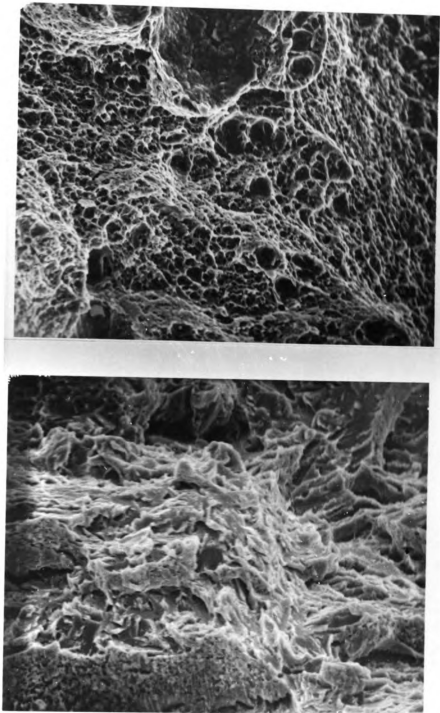


Fig. 48. SEM fractographs of quenched and tempered specimens, quenched from coarse grained austenite. Top: Fracture at 22°C. shows microvoid coalescence. Bottom: Fracture at -196°C. shows cleavage and quasi-cleavage. (2000x)

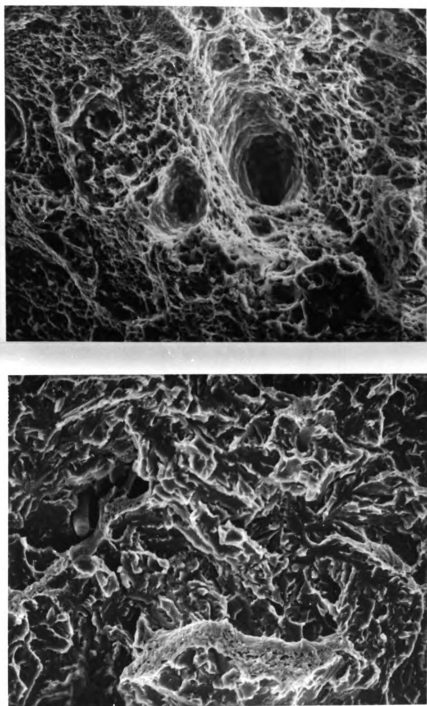


Fig. 49. SEM fractographs of quenched and tempered specimens, quenched from fine grained austenite. Top: Fracture at 22°C. shows microvoid coalescence. Bottom: Fracture at -196°C. shows cleavage and quasi-cleavage. (2000x)

that fracture occurred by cleavage and quasi-cleavage in both cases. There is essentially no difference in facet size when comparing the two brittle fractures. Results of these examinations indicate that microscopic fracture appearance is not influenced by prior austenite grain size for quenched and tempered specimens.

The SEM fractographs of specimens air-cooled from coarse and fine grained austenite and fractured at 22°C. are shown in Figure 50. The fracture of the specimen air-cooled from coarse grained austenite is almost entirely by cleavage, while the specimen cooled from fine grained austenite has fractured by cleavage and quasi-cleavage. The major difference between the two fractures is the size of cleavage facets, the fine grained specimen having much finer facets. In these cases, microscopic and macroscopic fracture appearances relate well to each other.

When examining fractures of air-cooled specimens on a macroscopic scale, it was observed that the fractured surface consisted of some areas of granular and some areas of fibrous appearance. These two areas were examined on a microscopic scale and are shown in Figure 51. A great difference can be seen in fracture appearance, with the granular area showing fracture by cleavage with large facets, and the fibrous area showing fracture by a mixture of microvoid coalescence and cleavage with smaller facets. Since this great difference in fracture mode may be observed on the same specimen, all other fractographs were taken from the area just behind the notch, which is the area most likely to show brittle fracture.

### 3.11. Microscopic Examination of Inclusions

Polished specimens of all steels were scanned at 100x with an optical microscope to determine the size and distribution of inclusions. As

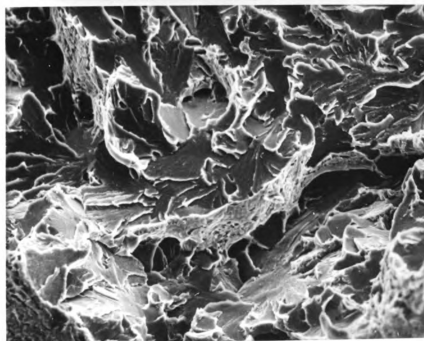
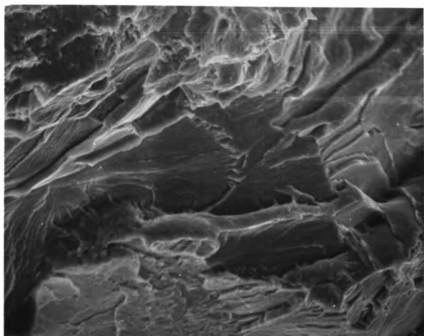


Fig. 50. SEM fractographs of air-cooled specimens at 22°C. Top: air-cooled from coarse grained austenite shows fracture by cleavage. Bottom: air-cooled from fine grained austenite shows fracture by cleavage and quasi-cleavage. (2000x)

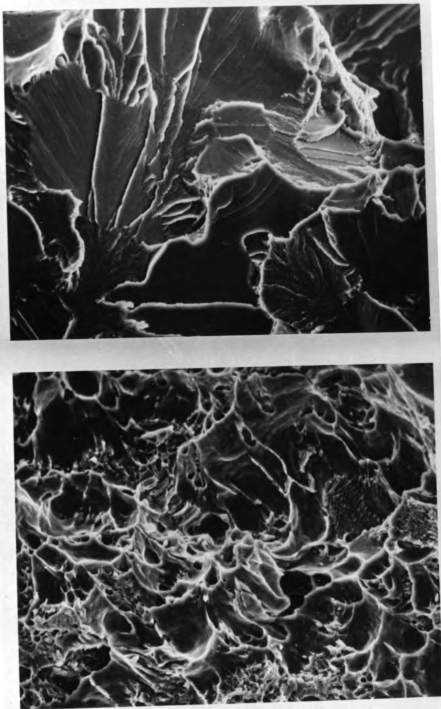


Fig. 51. SEM fractographs of air-cooled specimens at 22°C. Top: Center of specimen shows a cleavage fracture. Bottom: Edge away from the notch shows substantial microvoid coalescence. (2000x)

discussed earlier, inclusions which are small and well dispersed, would be expected to have little effect on impact properties. Stringer type inclusions or thin films in grain boundaries would be expected to be detrimental to impact properties. In general the inclusions found in all steels were small and well dispersed. The ASTM Specification E45<sup>(53)</sup> classification is mostly Type A with some areas of Type B. At higher magnification, grain boundary inclusion films were visible in steels containing aluminum, but only after they had been austenitized at high coarsening temperatures. These inclusions as shown in Figure 52, were not observed in one heat of steel which did not contain aluminum, nor were they found in any steel when low austenitizing temperatures and short times were used. The inclusion films were a result of coalescence of minute inclusions at the austenitizing temperature, or they were precipitated in austenite grain boundaries on cooling from the austenitizing temperature.

The microprobe analyzer can be used to identify inclusions on a fractured surface. An inclusion stringer protruding from the fractured surface was analyzed in such a manner as shown in Figure 53. The three peaks identified on the energy spectrum are sulfur at 2310 Ev., manganese at 5900 Ev., and iron at 6400 Ev. This inclusion was identified as a manganese sulfide. In a similar manner, the microprobe may be used to analyze inclusions on polished surfaces. Typical SEM photographs of inclusions are shown in Figure 54. In the top photograph, the triangular shaped inclusion is high in silicon, the oval inclusion is a manganese sulfide, and the thin elongated inclusion is high in aluminum. The triangular inclusion is apparently located in a junction of three grain boundaries. In the bottom photograph, the long stringer inclusion is

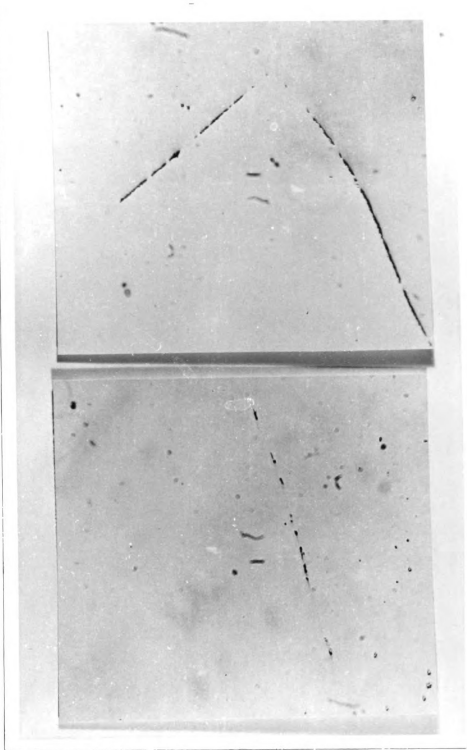


Fig. 52. Optical photomicrograph of inclusions apparently located in prior austenite grain boundaries of aluminum killed steel. Austenitized at 2100°F., 4 hrs. (1000x), unetched

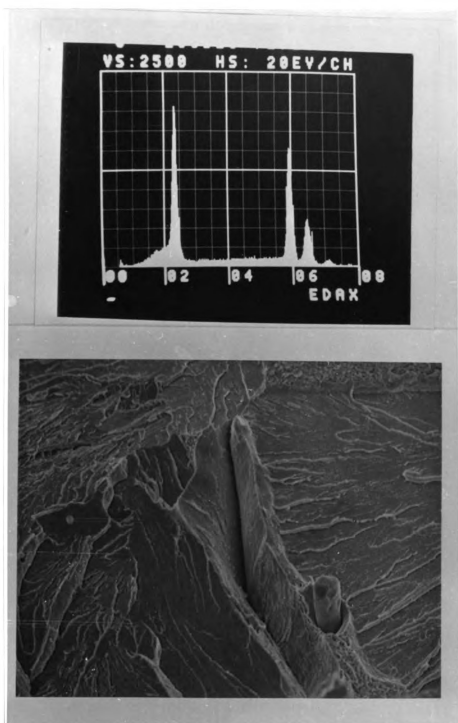


Fig. 53. X-ray spectrum (top) of inclusion protruding from fractured surface of SEM fractograph (Bottom). Inclusion is identified as a manganese sulfide.

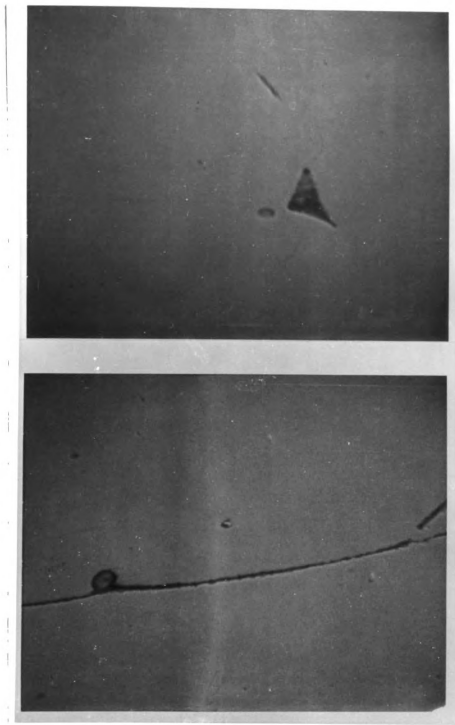


Fig. 54. Top: Three inclusions identified with microprobe analyzer: (triangle) high silicon; (oval) manganese sulfide; (elongated) high aluminum. Bottom: (long stringer) high aluminum; (round) manganese sulfide. Specimens were austenitized at 2100°F., 4 hrs. (2000x)

high in aluminum, and the circular inclusion is manganese sulfide. Most stringer type or thin film inclusions were found to be high in aluminum, indicating either aluminum oxides or aluminum nitrides.

Many inclusions (Figure 55) are of complex composition and were found to be composed of aluminum, sulfur, manganese and iron. Positive identification was not possible in these cases.

### 3.12. Sharp Yield Point

In order to investigate the possibility of other mechanical tests reflecting differences in impact properties, the general tensile properties of the steels were determined. Tensile properties were determined for quenched and tempered specimens which had been quenched from coarse grained and fine grained austenite. Results of these tests are shown in Table 18. The tests were performed at room temperature (22°C.) and the percent reduction in area shows some correlation with room temperature impact properties. This is especially true of Republic #5054025 (IF) in which specimens quenched from coarse grained austenite had only 50% as much reduction in area as those quenched from fine grained austenite. This ratio is nearly identical to that found in impact testing results, where specimens quenched from fine grained austenite had twice the impact energy at room temperature as those quenched from coarse grained austenite.

The other significant observation made in tensile testing was the presence of a sharp yield point in some cases. The presence or absence of a sharp yield point was found to be related to the austenitizing treatment used prior to quenching and tempering. A sharp yield point was observed when testing those specimens austenitized for short times at low temperatures. The sharp yield point behavior was not observed

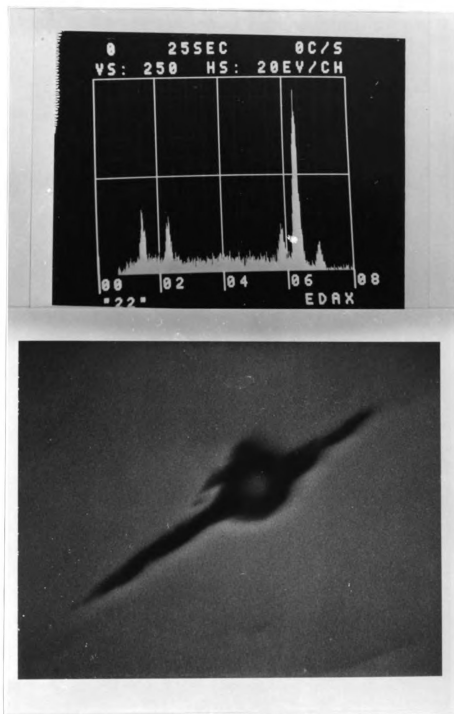


Fig. 55. X-ray spectrum (top) of complex inclusion (bottom) showing peaks for aluminum, sulfur, manganese, and iron. (10000x)

Table 18

Average tensile properties for quenched and tempered specimens.  
Crosshead speed: 0.1 cm./min.

| <u>Heat</u>               | <u>Austenitizing Treatment</u> | <u>U.T.S. (psi)</u> | <u>Y.S. (psi)</u> | <u>% E</u> | <u>% R.A.</u> | <u>No. of Tests</u> |
|---------------------------|--------------------------------|---------------------|-------------------|------------|---------------|---------------------|
| Youngstown<br>#66797 (IC) | 1500 °F., 5 min.               | 126,478             | 113,929           | 15.5       | 60.3          | 4                   |
| AISI 1040                 | 2000 °F., 4 hrs.               | 127,226             | 113,598*          | 12.1       | 44.0          | 4                   |
| Youngstown<br>#95313 (IF) | 1500 °F., 5 min.               | 123,723             | 116,919           | 16.0       | 60.8          | 4                   |
| AISI 1040                 | 2100 °F., 4 hrs.               | 124,052             | 109,079*          | 16.0       | 58.4          | 4                   |
| Republic<br>#5023766 (IC) | 1500 °F., 5 min.               | 126,992             | 115,185           | 16.5       | 57.6          | 4                   |
| AISI 1046                 | 2100 °F., 4 hrs.               | 124,934             | 108,460*          | 16.0       | 43.7          | 4                   |
| Republic<br>#5054025 (IF) | 1500 °F., 5 min.               | 123,177             | 114,168           | 15.8       | 60.0          | 3                   |
| AISI 1046                 | 2100 °F., 4 hrs.               | 125,223             | 108,376*          | 14.3       | 30.1          | 3                   |

\* 0.2% offset yield strength

when testing those specimens austenitized at 2000°F. or 2100°F. for four hours, and in those cases a 0.2% offset yield strength was determined.

When the yield point was observed, the degree of yielding was found to be related to aluminum content. Aluminum content also controlled austenite grain size. The effect of aluminum content and prior austenite grain size on the degree of yielding is shown schematically in Figure 56. Since fine grain size and presence of nitrogen in solid solution are known to increase the tendency for sharp yield point behavior<sup>(42)</sup>, it appears that aluminum plays a dual role in these experiments. First, the presence of aluminum produces finer austenite grains which result in more equiaxed ferrite grains in tempered martensite as shown in Figures 24-27. Second, aluminum combines with nitrogen to form aluminum nitride

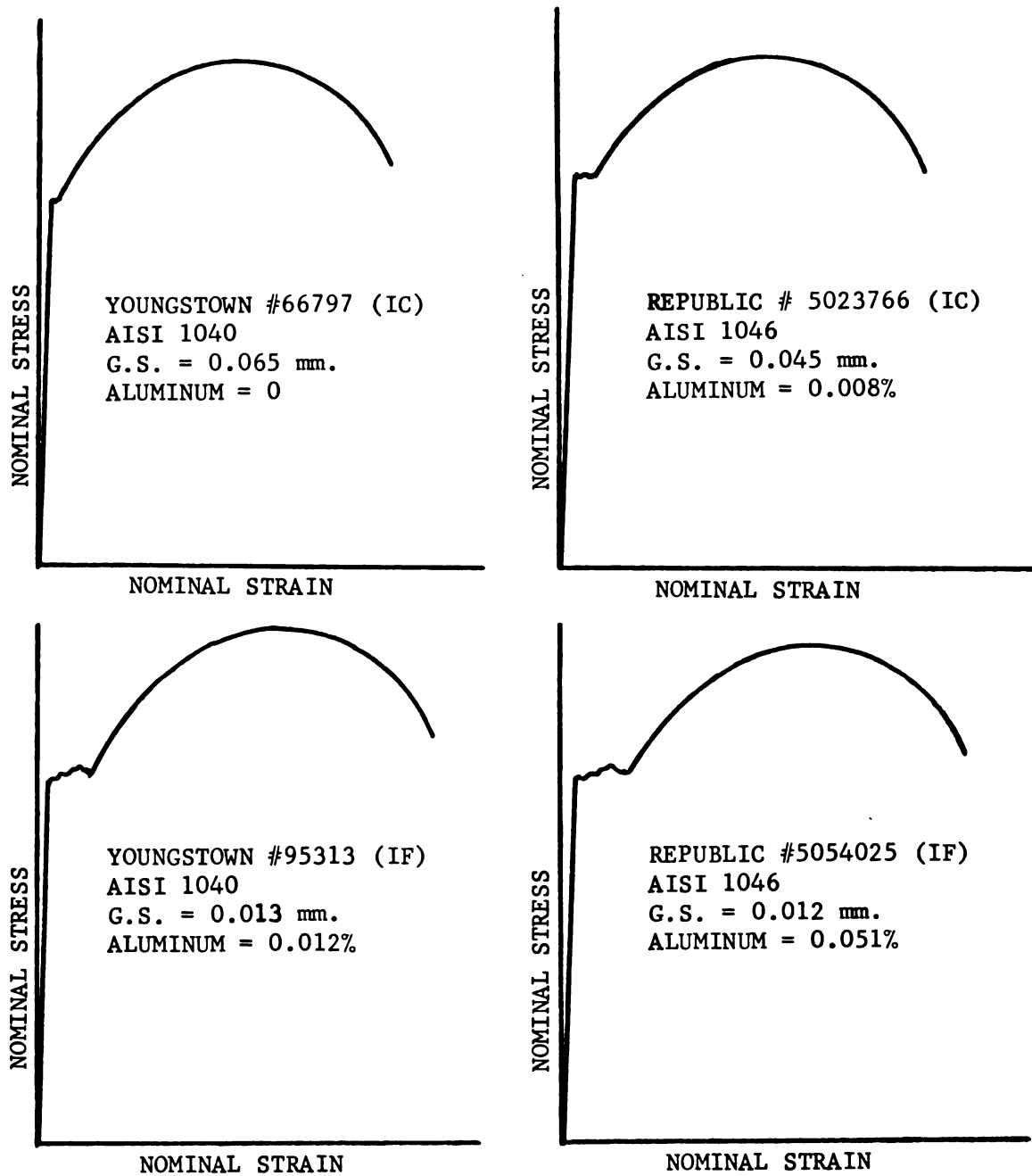


Fig. 56. Schematic representation of the influence of aluminum content and prior austenite grain size on the yield point of specimens tested in the quenched and tempered condition.

at austenitizing temperatures. By removing nitrogen from solid solution in this manner, the tendency for a sharp yield point is decreased. This accepted theory is contrary to the results we observed.

## DISCUSSION

### 4.1. Grain Growth

Grain boundaries are high energy areas within the structure. With thermal activation, grains will always tend to grow in order to reduce the total grain boundary area. The accepted theory concerning the role of aluminum in austenite grain size control, involves the precipitation of aluminum nitride in the grain boundaries. According to Beeghly<sup>(24)</sup>, this precipitation reaches a maximum at relatively low austenitizing temperatures in the range of 1400-1500°F. These precipitates act as barriers to grain boundary movement, thereby resisting grain growth. In order to be effective, these precipitates must be concentrated in the grain boundaries and be small in size. As the austenitizing temperature is increased, these precipitates coalesce, and, finally at temperatures in the range of 1900-2100°F. aluminum nitride begins to dissociate and dissolve in the austenite. This theory is supported by the work of Beeghly (Figure 5) in determining the combined and uncombined aluminum in steel after being austenitized at various temperatures. Other support<sup>(27)</sup> comes from reports of aluminum nitride precipitates being identified in or near austenite grain boundaries.

The aluminum nitride theory does have some shortcomings and is very likely an oversimplification of the actual situation. Aluminum nitrides have not been observed in other than the coalesced condition. This is not surprising since an effective barrier may consist of particles as

small as 20-200 Å in diameter. It has been shown that inherently coarse grain steels begin to coarsen within seconds of reaching the austenitizing temperature<sup>(28)</sup>. Since inherently coarse grain steels resist this type of coarsening, we assume this resistance is due to the presence of aluminum nitride in the grain boundaries. This mechanism requires instantaneous precipitation in the newly formed boundaries. The availability of aluminum for this precipitation is questionable since it is substitutional in iron and has a relatively low diffusion rate<sup>(30)</sup>. Steels having aluminum contents as low as 0.01% are inherently fine grain.

Other experimental evidence has shown that aluminum is ineffective in controlling grain size unless in the presence of air<sup>(21)</sup>. This type of experiment was also performed to show that aluminum is not effective unless in the presence of oxygen<sup>(20)</sup>. Such results support the theory that aluminum oxides play an important role in restricting grain growth.

Our grain growth studies follow the classical results. Inherently coarse grain steels begin to coarsen immediately upon reaching the austenitizing temperature, and they then show a steady increase in grain size as the temperature is increased. Inherently fine grain steels resist coarsening to a remarkable degree until the 1900-2100°F. temperature range; then coarsening proceeds rapidly until the grain size equals or surpasses the inherently coarse grain steel. This general inherently fine grain behavior was observed in one heat of steel having an aluminum content of only 0.012%.

The early theories of grain size control which were advanced in the 1930's suggest that aluminum oxide, an unknown constituent<sup>(23)</sup> or aluminum<sup>(8)</sup> itself were principally involved in restricting grain growth. It may be suggested that aluminum nitride and aluminum oxide are both

major contributors to grain growth control. Aluminum oxide is present in the structure prior to reaching the austenitizing temperature, and may aid substantially in initial grain growth control upon transformation. Aluminum oxide is stable and does not dissociate at coarsening temperatures, but it does coalesce, thereby reducing its effectiveness. Immediately upon austenitizing, minute particles of aluminum nitride may begin to precipitate in the newly formed grain boundaries. These precipitates act as a barrier to grain boundary movement along with aluminum oxides. Possibly the new precipitates lower the free energy of the grain boundary, thereby reducing the driving force for grain growth. As the temperature is increased, these particles coalesce and finally dissociate, leaving only the coalesced aluminum oxides to restrict grain growth.

This type of explanation may account for observed behavior where steels as low as 0.01% aluminum may be inherently fine grain, while steels as high as 0.02% aluminum may be inherently coarse grain. Whether a steel is inherently coarse or fine grain depends not only on the aluminum content, but on the relative concentrations of nitrogen and oxygen and the degree to which aluminum is combined as stable aluminum oxide<sup>(63)</sup>.

Further experimental evidence is required to formulate the exact grain growth controlling mechanism. Experimental observation and identification of a precipitate network in austenite grain boundaries at low austenitizing temperatures is the type of evidence required to determine the exact role of the many variables in this situation.

## 4.2. Grain Size Control During Heat Treating

It has been demonstrated that refining the grain size increases the strength and toughness of metals<sup>(64)</sup>. The situation in steel is complicated by the transformation which occurs during heat treating. The austenite grain size which exists at higher temperatures does not exist at normal testing temperatures, but it is known to have an effect on the mechanical properties. The degree of this effect is related to the heat treating method employed; specifically important is the cooling rate from the austenitizing temperature. Since our experiments involved two distinct cooling rates, these will be considered separately.

### 4.2.1. Quenching and Tempering

Quenching steel from the austenite structure to form martensite is a grain refining technique. The body-centered-tetragonal martensite plates which form are substantially smaller than the austenite grains, and hundreds of plates may form from one austenite grain. When considering large and small austenite grains, large grains produce longer plates on the average, but the plate width is essentially the same for both cases. This fact has been previously reported<sup>(65)</sup>, and it was verified by examination of our martensitic structures. Since there is little variation in plate width, the magnitude of difference between coarse and fine austenite grains is reduced considerably by the quenching operation.

As we have shown experimentally (Figures 24-27), ferrite grains in tempered martensite inherit their shape from the original martensite plates. Careful examination of Figure 25 will reveal that coarse grained austenite produces tempered martensite in which the ferrite grains are elongated in the direction of the original martensite plates. Also of

interest is the location of carbides in the tempered martensite structure. The specimen quenched from fine grained austenite has a uniform carbide dispersion; however, the specimen quenched from coarse grained austenite produced carbides which tend to precipitate in rows parallel to the original martensite plates. The size and shape of ferrite grains and the size and distribution of carbides in tempered martensite may significantly affect mechanical properties.

The effect of austenite grain size on impurities or secondary phases must be considered. Since precipitates and inclusions often segregate and tend to form in the high energy grain boundary areas, a higher concentration of impurities may be expected in the grain boundaries of coarse grained austenite. Films of embrittling impurities, which have a major detrimental effect on mechanical properties, have been shown to exist by use of Auger Spectroscopy<sup>(66,67)</sup>. Secondary phases such as bainite which tend to precipitate in prior austenite grain boundaries are known to decrease impact properties<sup>(36)</sup>. This behavior in general, is an important consideration when selecting heat treating procedures.

#### 4.2.2. Air-Cooling

When medium plain carbon steels are air-cooled in the section size employed in this research, the expected microstructure is pearlite and ferrite. This structure is not refined to the same degree as the structure produced by quenching, since ferrite tends to precipitate in the prior austenite grain boundaries and form continuous networks. These networks, even though they may consist of ductile material, are known to be detrimental to impact properties<sup>(3)</sup>. This type of behavior was observed in the experimental results where steel cooled from fine grained

austenite was superior both in upper shelf energy and transition temperature (Tables 15 and 16). Ferrite networks do not account for results which show that inherently fine grain steel has a lower transition temperature even when coarsened to the same degree as inherently coarse grain steel. The improved impact properties must be explained with respect to aluminum and oxygen which are the only major variables in composition, and to the degree in which aluminum is combined as aluminum nitride.

#### 4.3. Effect of Grain Size on Impact Properties

As previously discussed, steel cooled from fine grained austenite may have an upper shelf impact energy as much as 400% greater than that cooled from coarse austenite grains. These large differences were reported by previous investigators<sup>(8,10,11)</sup>. Higher impact energy values are always obtained from specimens which have a higher percentage of shear or plastic deformation associated with the fracture. When continuous networks are present, they are usually the controlling factor. In other cases where plastic deformation precedes fracture, the ease of dislocation movement is important since this movement is necessary for plastic deformation to occur. Since we are dealing with two distinct grain size effects (the effect of actual grain size and the effect of inherent grain size), the two areas will be considered separately. In the next two sections, we consider the ease of dislocation movement and the degree to which a soft and ductile continuous network may initiate dislocation pile-ups.

##### 4.3.1. Effect of Actual Austenite Grain Size on Impact Properties

Even though the quenching operation is a grain refining process, it was previously reported that steel quenched from fine grained austenite

has up to 400% greater room temperature impact energy than the same steel quenched from coarse grained austenite<sup>(10,11)</sup>. These results have been reported for steel at a relatively high hardness level. Our results show this effect is reduced by tempering to a lower hardness level such as is usually employed in impact type applications. At lower hardness, quenching from fine grained austenite improves the upper shelf impact energy about 10% on the average with one extreme case of 100%. The harder tempered martensite structure is more brittle, and the prior condition of coarse austenite grains may concentrate impurities in grain boundaries. Impurities are ideal points for crack initiation. Since the structure is brittle, the cracks propagate easily once initiated. In the softer tempered martensite structure, initiation sites may still be available, but since the structure is more ductile, microcracks may be blunted and arrested by plastic deformation. In this manner the effect of concentrated impurities in prior austenite grain boundaries may be minimized. We have obtained experimental evidence (Figures 52, 54, and 55) that impurities do tend to concentrate in austenite grain boundaries during the coarsening treatment, and this is one of the contributions of our work.

We have advanced an explanation which accounts for the decrease in sensitivity to prior austenite grain size as the quenched steel is tempered to a lower hardness level. These same ideas may be discussed by examining the load-time curves produced by the Dynatup impact test instrumentation. As the testing temperature was decreased, the impact energy decreased rapidly in the area of the transition temperature. At lower testing temperatures the steel exhibits similar impact properties to steel quenched and only slightly tempered and tested at room

temperature. These similarities exist because in both cases the structure is inherently brittle. As we examine the load-time curves at lower temperatures, there is a greater difference between specimens quenched from fine grained austenite and coarse grained austenite. At the lowest temperature tested,  $-196^{\circ}\text{C}.$ , the load-time curves (Figure 38) show the greatest difference. In this condition, when the steel is extremely brittle and well below the transition temperature, load to initiate fracture is less for specimens quenched from coarse grained austenite. Post-maximum load energy, which is the energy required to propagate fracture, is less for specimens quenched from coarse grained austenite. Testing relatively hard quenched and tempered specimens at room temperature is analogous to testing softer specimens at lower temperatures. Examination of the lower energy shelf portion of our impact transition curves produces larger differences in terms of percent. Specimens quenched from fine grained austenite have up to 300% greater impact energy in this case. These values more closely relate to the previously determined results obtained from relatively hard quenched and tempered specimens.

Even though the upper and lower energy shelves are increased by quenching from fine grained austenite, the transition temperature is not appreciably affected. The transition temperature is extremely important since there may be a 2000% energy increase when moving from the lower to the upper shelf. In practice, entry into the transition range often results in catastrophic failures. For three heats of steel, the specimens quenched from fine grained austenite had transition temperatures up to  $28^{\circ}\text{C}.$  lower. One heat of steel had a transition temperature which was lower by  $20^{\circ}\text{C}.$  for the specimens quenched from coarse grained austenite. The transition temperature was low for all quenched and tempered

structures, and it appears that this temperature is a function of factors other than austenite grain size prior to quenching.

The impact properties of air-cooled specimens showed a remarkable dependency on the prior austenite grain size (Tables 15 and 16). The ferrite networks which appear in the microstructure of specimens cooled from coarse grained austenite (Figures 28-31) may be the cause of this behavior. Elongated ferrite networks have a detrimental effect on both the upper and lower energy shelves, and they also increase the transition temperature. Of the steels cooled from coarse grained austenite, one heat Youngstown #95313, had some Widmanstätten plates of ferrite within the pearlite colonies. This is shown in Figure 29 and this structure results in an improvement in impact properties. The Widmanstätten plates reduced the extent of the ferrite network since the plates in themselves are not continuous.

#### 4.3.2. Effect of Inherent Grain Size on Impact Properties

When comparing the impact properties of quenched and tempered inherently coarse and inherently fine grain steels of the same AISI grade, the inherently fine grain steel is usually considered to be equal to or superior; however, when tempered to a lower hardness level, the superiority is greatly decreased. In one case the improvement in upper shelf energy is as large as 100%, but it is more usually in the order of a 10% improvement for inherently fine grain steel. The degree of improvement varies considerably depending on the heat treatment employed with the inherently fine grain steel equal or superior in all cases.

Further comparisons may be made with respect to the transition temperatures of the quenched and tempered specimens. The inherently fine

grain steels have transition temperatures which are lower by 7-47°C. for specimens quenched from equivalent prior austenite grain sizes. All transition temperatures of the quenched and tempered specimens were below normal application levels since the highest transition temperature was -65°C.

The degree of improvement for inherently fine grain steel was less when the specimens were air-cooled from the austenitizing temperature. This result may be expected since, as previously discussed, ferrite precipitation appears to be a major controlling factor in determining the impact properties of air-cooled specimens. Inherently fine grain steel did show a 50-80% improvement in upper shelf impact energy for those specimens cooled from coarse grained austenite. This improvement is consistent with other observations<sup>(1)</sup>, which indicate inherently fine grain steel is usually superior to inherently coarse grain steel even though coarsened to an equivalent austenite grain size prior to cooling. The transition temperature does not appear to be affected significantly by the inherent grain size of the steel.

Our results and the results of previous investigators indicate that inherently fine grain steels are equal to or have superior impact properties when compared with inherently coarse grain steels. In the quenched and tempered condition, all steels had excellent impact properties.

Inherently fine grain steels have the obvious advantage of resisting austenite grain coarsening to a greater degree than inherently coarse grain steels. This fact is especially significant when the cooling rate employed is less than that required to form martensite, since diffusion controlled transformation products tend to form continuous networks in

prior austenite grain boundaries. The detrimental effect of coarse austenite grains has been shown to be reduced significantly by quenching to a nearly 100% martensitic structure, followed by tempering to a relatively low hardness level. This major contribution of our work shows that advantage may be taken of the improved machinability, better hardenability, and superior high temperature creep properties of coarse grained steels with some assurance of adequate impact properties in quenched and tempered structures.

There appears to be an additional effect of inherently fine grain steel which cannot be explained entirely by prior austenite grain size. The oxygen analysis indicates that inherently coarse grain steels have more total oxygen and more dissolved oxygen than inherently fine grain steels. This difference is expected even though both steels are considered fully deoxidized, since inherently coarse grain steels rely to a greater degree on manganese and silicon for deoxidation. Aluminum is a stronger deoxidizer than either manganese or silicon<sup>(66)</sup>. Also, more oxygen is lost as aluminum oxide when the hot cap is removed from the ingot when producing inherently fine grain steel. Aluminum killed steels have less manganese combined as oxides, and they have more manganese available as a ferrite solid solution strengthener. Increased oxygen content has previously been reported to be detrimental to impact properties<sup>(9)</sup>.

The other major difference in chemical composition between inherently fine and inherently coarse grain steels, is the aluminum content. Aluminum is combined as a compound, typically a nitride or oxide, or it may be uncombined as a substitutional solid solution element. In the case of inherently fine grain steel, substantial amounts of aluminum

exist as oxides or nitrides. Aluminum nitride characteristically forms as a fine dispersion and we suggest that a precipitation mechanism may be responsible for the generally superior impact properties demonstrated by inherently fine grain steels. During the austenitizing treatment, aluminum nitride will precipitate preferentially at grain boundaries and lattice defects. Precipitation at lattice defects will result in a uniform dispersion of aluminum nitride which is retained by the quenching process. When specimens were air-cooled, the superiority of inherently fine grain steel was greatly reduced. A dispersion strengthening effect produced by a finely dispersed precipitate may account for the slight superiority of inherently fine grain steels. The presence of a precipitate may affect the yielding characteristics of the steel. This type of strengthening is found in many alloy systems such as maraging steels where aluminum is often added to form  $\text{NiAl}$ ,  $\text{Ni}_3\text{Al}$  or  $\text{AlN}$  dispersed in the structure. This generally results in improved strength without a great loss of ductility. A similar example is the strengthening effect of  $\text{TiN}$  precipitates in sheet steels<sup>(68)</sup>.

#### 4.4. The Charpy Impact Test

The Charpy impact test is a simple and inexpensive testing method for comparing the impact properties of materials. In our experiments, we compared two steels of the same AISI grade to each other, as well as the effect of prior austenite grain size as produced by changing the heat treating procedure. One of the shortcomings of the Charpy impact test is the inability to relate the results to design criteria. For this reason, much work has been done using fracture toughness determination with pre-cracked specimens and special techniques to measure crack

width displacement. In fracture toughness studies a precracked specimen is used to determine  $K_{Ic}$ , which is the plain strain stress intensity factor at the onset of unstable crack growth. This type of experiment yields information to the designer concerning the maximum flaw size permissible in a structure.

In the last few years, much research has been done in the area of correlating the simpler and less expensive Charpy impact test to the fracture toughness stress intensity factor. The ASTM criterion<sup>(69)</sup> for minimum specimen thickness to produce valid plane strain measurements is:

$$B = 2.5 \left( \frac{K_{Id}}{y_d} \right)^2$$

where B is the minimum specimen thickness;  $K_{Id}$  is the dynamic stress intensity factor, and  $y_d$  is the dynamic yield strength of the material. Since  $K_{Id}/y_d$  must be 0.4 or less, the range of valid plane strain measurements which can be made with the standard Charpy specimen is limited. Recent work by Gross<sup>(33)</sup>, indicates the ASTM criterion may be too rigid and plane strain conditions are approached with the standard size Charpy specimen in most cases. In these experiments, quarter-width, half-width, full-width and double-width Charpy V-notch specimens of the same material were tested. The transition temperature was increased 60°F. in going from quarter-width to half-width specimens; increased 26°F. in going from half-width to full-width specimens; and increased only 2°F. in going from full-width to double-width specimens. These results indicate that a standard single-width specimen is closely approaching the maximum plastic constraint value necessary for plane strain conditions at the onset of fracture. Holloman<sup>(70)</sup> has reported similar results and Clausing<sup>(71)</sup> has reported a plane strain state of stress at fracture initiation for single-width Charpy V-notch specimens.

Since the single-width Charpy V-notch specimen approaches the conditions for plane strain at fracture initiation, it is not surprising that correlations have been made between the fracture toughness stress intensity factor and Charpy test results. Barsom and Rolfe<sup>(72)</sup> have shown a good correlation between the static stress intensity factor  $K_{Ic}$  and Charpy V-notch test results. In the region of the upper energy shelf of the transition curve, the relationship is:

$$\left(\frac{K_{Ic}}{\sigma_y}\right)^2 = 5 \left(\text{CVN} - \frac{\sigma_y}{20}\right)$$

where  $K_{Ic}$  is the static stress intensity factor, CVN is the Charpy V-notch energy, and  $\sigma_y$  is the yield strength of the metal. In the region of the transition temperature the correlation is:

$$\left(\frac{K_{Ic}}{E}\right)^2 = 2 (\text{CVN})^{3/2}$$

In other work, Barsom<sup>(73)</sup> shows a general relationship:

$$\left(\frac{K_{Ic}}{E}\right)^2 = A (\text{CVN})$$

Where  $E$  is Young's Modulus and  $A$  is a constant which incorporates specimen size and notch acuity.

From the results of recent work, one can conclude that excellent possibilities exist for future correlations of impact results with fracture toughness. It appears that no general correlation can be made, but individual correlations must be determined for each material at a particular strength level. Once the correlation is determined, the simpler

and less expensive Charpy impact test may be substituted for routine quality control.

#### 4.5. Instrumented Impact Testing

The instrumented impact test yields additional information with respect to fracture characteristics, as well as providing a double check on the energy value obtained by measuring the pendulum follow-through. This method of impact testing is still in the early developmental stage. The most valuable information obtained is the load and energy required to initiate fracture, the load and energy required to propagate fracture, and the determination of percent brittle fracture. Since the load and energy required to propagate fracture may be determined, it appears these results may be successfully correlated with fracture toughness determinations.

#### 4.6. Fracture Appearance

The fracture appearance of the quenched and tempered specimens showed remarkable differences when comparing macroscopic and microscopic fractographs. As testing temperature was decreased, the macroscopic fracture appearance for specimens quenched from coarse grained austenite became progressively coarser than specimens quenched from fine grained austenite. At low testing temperatures, where brittle fracture occurred by cleavage, the facets of the specimens quenched from coarse grained austenite were considerably larger. This observation indicates that prior austenite grain size influences the macroscopic fracture appearance of quenched and tempered specimens. Specimens quenched from coarse grained austenite produce martensite which often consists of large packets of plates all orientated in the same direction. These large packets of similar orientation

still remain in the tempered martensite. Cleavage of these large packets may result in the larger facets observed on the macroscopic scale.

On the microscopic scale, SEM fractographs do not indicate the same differences observed on the macroscopic scale. There is essentially no difference in SEM fractographs when comparing the fractures of specimens quenched from coarse and fine grained austenite. On the microscopic scale, cleavage of individual ferrite plates is observed in the brittle specimens, but the general boundary area of the packets is not distinguished.

Air-cooled specimens show a great difference in both macroscopic and microscopic appearance when comparing specimens cooled from coarse and fine grained austenite. There is an excellent correlation between prior austenite grain size and grain size after transformation. The grain size is related to cleavage facet size on both the macroscopic and microscopic scales.

#### 4.7. Sharp Yield Point

The sharp yield point is most often associated with annealed low carbon steel. The classical stress-strain curve which involves the propagation of Lüders Bands during yielding, is shown in Figure 57. This type of yielding is a major problem in low carbon steel stampings such as automobile fenders and panels where surface finish is critical. When the steel is formed, it may show a sharp yield point behavior and propagate Lüders Bands to the surface of the stamping.

Although sharp yield point behavior is primarily associated with low carbon steel, it has been observed in high carbon steels, other body-centered-cubic metals, as well as some face-centered-cubic and hexagonal

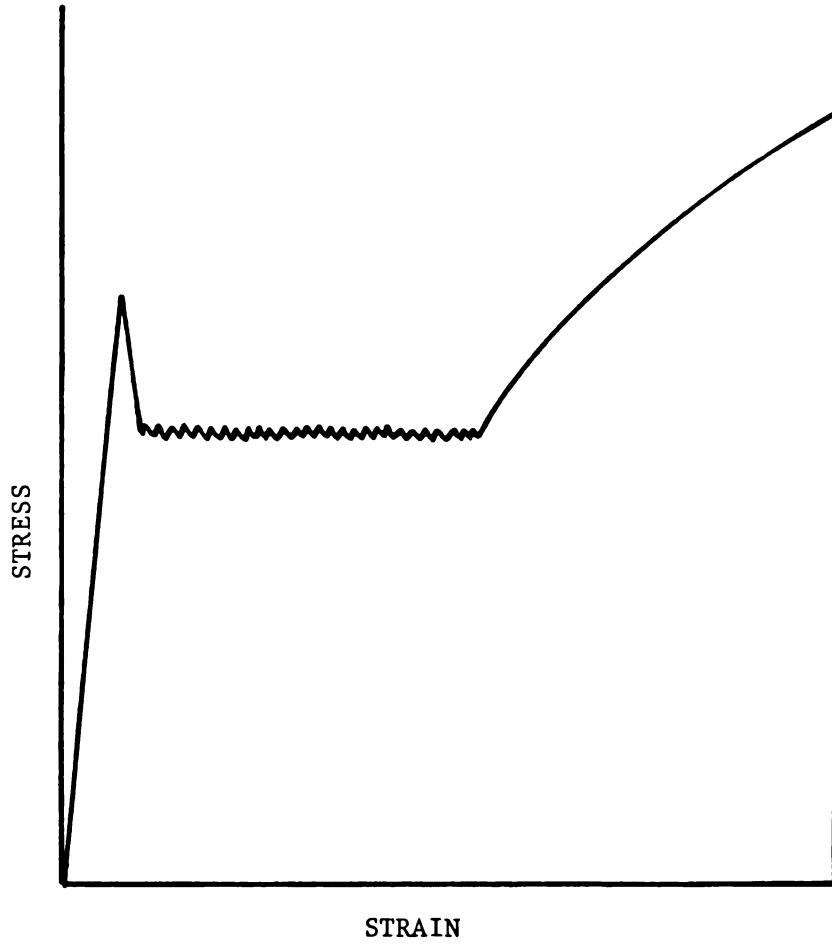


Fig. 57. Classical yield point behavior in annealed low carbon steel.

close-packed metals<sup>(42,43)</sup>. Exact specimen alignment and increased strain rates increase the tendency to observe sharp yield point behavior<sup>(43)</sup>. Specimen misalignment and variations within the structure increase the possibility that localized regions in the cross-section will pass through the upper and lower yield points before other regions reach the stress level of the upper yield point.

Most theories of sharp yield point behavior incorporate Cottrell's<sup>(43)</sup> idea of solute atoms diffusing to dislocations in order to lower the strain energy of the crystal. Solute atoms pin the dislocations and form an "atmosphere" from which the dislocations must be torn away before plastic deformation is possible. The upper yield point is the stress at which dislocations are torn from their atmospheres and may move at a lower stress level which is the lower yield point. This movement releases an avalanche of dislocations into the slip planes, thereby propagating the observed Lüders Bands. Other investigators<sup>(74)</sup> have questioned the Cottrell mechanism and suggest that the generation and multiplication of new dislocations can explain sharp yield point behavior. Present theories<sup>(42)</sup> encompass both the Cottrell "atmosphere" and the role of new dislocation multiplication and velocity into an explanation of yield point behavior. Also a strong consideration is the release of dislocation pile-ups at grain or subgrain boundaries to propagate Lüders Bands. The magnitude of each of these effects depends on the strength of dislocation locking and many factors such as impurity content which are inherent to each material.

In steels, the most prominent source of pinning solute atoms are carbon and nitrogen which occupy interstitial sites in the lattice. Large substitutional atoms such as aluminum may also have an effect on

dislocation movement since they distort the lattice; however, they are not considered to be as important as interstitials since they are not mobile enough to diffuse to and pin dislocations. Aluminum is substitutional in iron and has an atomic diameter approximately 14% larger than the iron atom.

It has been shown that nearly complete removal of carbon and nitrogen from steel will eliminate sharp yield point behavior<sup>(42)</sup>. Additions of as little as 0.001% of carbon or nitrogen will restore sharp yielding<sup>(42,43)</sup>. In higher carbon steels, a sharp yield point is not usually observed since carbides may effectively block the free moving dislocations or dislocations torn from their atmospheres. In commercial practices, Lüders Bands may be eliminated by subjecting the steel to a light skin pass or flex roll which stresses the surface beyond the upper and lower yield points. Sharp yield point behavior will return in a few days when interstitials pin the fresh dislocations created during the skin pass. Steels are often stabilized with small additions of elements such as titanium, vanadium, or calcium which combine with interstitials making them ineffective for pinning dislocations. Other methods, such as rapid heating and quenching treatments in the 800-900°F. range developed by Koistinen<sup>(76)</sup>, have been utilized to remove sharp yield point behavior. In this process, rapid heating and holding for short times of typically 6-8 seconds unpins dislocations or dissolves dislocations by the thermal stresses involved, which may account for yield point removal<sup>(77)</sup>. Removal of the sharp yield point is only temporary and will return in a few days, presumably by pinning of dislocations by nitrogen diffusion at room temperature.

In our experimental results, we observed a sharp yield point behavior for quenched and tempered specimens when they were austenitized for short times at low temperatures. At the low austenitizing temperature of 1500°F., aluminum nitride will precipitate; however, since the holding time was only five minutes, this precipitation may have been minimal. Sufficient nitrogen may have been left in solid solution to pin dislocations and promote sharp yield point behavior. None of the quenched and tempered specimens austenitized at high temperatures showed a sharp yield point behavior. At high austenitizing temperatures of 1900°F. and 2100°F., aluminum nitride dissociates and dissolves in the austenite. When the specimens are cooled to the 1600°F. quenching temperature and held one hour to stabilize, aluminum nitrides may reprecipitate and remove nitrogen from solid solution. It has been argued that reprecipitation of aluminum nitrides would reduce the tendency for sharp yield point behavior of one heat of steel (Youngstown #66797) which does not contain aluminum; however, when the yield point was observed it was extremely small and barely noticeable. Since we would expect this heat of steel to have the most nitrogen in solid solution and available to pin dislocations, this indicates a mechanism other than the Cottrell atmosphere would seem to be the major influence.

When sharp yield point behavior was observed, the degree of yielding was related to the aluminum content of the steel. Elongated yield behavior was observed over a longer range of strain for steel containing the most aluminum. Only a slight yield point was observed when testing the heat of steel which did not contain aluminum. To account for this behavior, we suggest that many dislocations may be broken from their atmospheres at stresses lower than the upper yield point. This behavior

appears likely since fresh dislocations and Lüders Bands have been observed immediately after the specimen reaches the upper yield<sup>(74)</sup>. Steel containing a higher concentration of aluminum has a more dense dispersion of aluminum nitrides present, and these precipitates interfere with dislocation motion. Aluminum nitrides may promote an extended lower yield point since higher stress is necessary for dislocation motion, and the propagation of Lüders Bands is inhibited. It has been reported that aluminum killed steels contain fewer subgrain boundaries than steel killed by other methods<sup>(18)</sup>. Fewer boundaries may result in larger dislocation pile-ups, which when released have a greater tendency to propagate into Lüders Bands.

The yield point behavior we observed appears to defy complete explanation when applying the generally accepted theory. We suggest that precipitation of a fine dispersion of aluminum nitride on lattice defects during the austenitizing treatment may result in a higher stress level for dislocation motion necessary to propagate Lüders Bands. This proposed mechanism is supported by our observations in which the steels with higher aluminum contents showed a more prolonged sharp yield point behavior. Attention is primarily focused on the detrimental effects of Lüders Bands when considering surface finish. We suggest there may be a beneficial stress relieving effect created when a sudden avalanche of dislocations propagates along the slip planes. This stress relieving may be reflected in the improvement of other mechanical properties at the expense of surface finish.

#### 4.8. General Remarks

We have supplied additional experimental evidence that the effect of prior austenite grain size on impact properties is influenced by the

microstructure produced by heat treating methods employed. For quenched and tempered structures consisting of tempered martensite at relatively low hardness levels, prior austenite grain size has little effect on impact properties. When slower cooling rates, which allow time for diffusion controlled transformation products to form in austenite grain boundaries are employed, coarse grained austenite is extremely detrimental. Our results are contrary to those reported by many of the early investigators, who found large differences when comparing impact properties of specimens quenched from fine and coarse grained austenite. An energy transition curve must be determined to obtain a true picture of impact properties. Many of the discrepancies between our results and those of earlier investigators may be explained when considering the energy transition curve. Since most of the testing was performed at room temperature, one set of specimens may have been below the transition temperature, thereby creating the large differences.

Inherently fine grain steels, in general, show a slight superiority in impact properties which cannot be explained on the basis of prior austenite grain size. This improvement may result from the precipitation of aluminum nitride on lattice defects prior to quenching. Improvement may also be gained by an increase in ferrite strengthening by manganese. Since aluminum is present, less manganese is combined as oxides and more is available for solid solution strengthening.

Strengthening effects from aluminum nitride precipitation are suggested by observations during tensile testing. Since sharp yield point behavior is increased with increasing aluminum content, it appears that a precipitation mechanism may be important in both matrix strengthening and the dislocation movement necessary to propagate Lüders Bands.

Explanations of the Koistinen process to remove sharp yield point behavior which are based on the Cottrell mechanism cannot account for the necessity to rapidly quench the steel from the 800-900°F. treatment. It appears that rapid quenching is necessary to produce fresh dislocations due to the thermal stresses produced. Dislocation atmosphere locking does not account for observations in our tensile testing, since the steel with the largest amount of uncombined nitrogen available in solid solution showed the least degree of sharp yielding.

In his 1948 Campbell Memorial Lecture, Morris Cohen<sup>(78)</sup> described the effect of prior austenitizing treatment on the percent retained austenite observed after quenching. Austenitizing at 1580°F. and quenching produced 39% retained austenite. Austenitizing at 1900°F. and quenching produced 70% retained austenite. Austenitizing at 1900°F. and cooling to 1580°F. prior to quenching produced the same 70% retained austenite. However, when the specimen was austenitized at 1900°F., cooled to 1580°F. and held four hours prior to quenching, the retained austenite was less than 39%. This result could not be explained on the basis of heat treating techniques, carbide solution, austenite grain size, or concentration gradients. In his discussion, the author attributed this effect to a change in the martensite nucleation mechanism, suggesting that high temperature treatment removed nucleation centers. We suggest that these results are added evidence that precipitation of aluminum nitride on lattice defects may occur at lower austenitizing temperatures. At the austenitizing temperature of 1900°F., aluminum nitride dissociates and dissolves; however, when cooled to 1580°F., nitrides may reprecipitate and aid in martensite nucleation. If coarse grained steels contain more retained austenite in the as-quenched condition, this constituent will

be transformed to bainite during tempering. A mixture of bainite and tempered martensite is known to have inferior impact properties when compared to a structure of tempered martensite.

The results reported by Cohen are difficult to explain and this was affirmed in his discussion. Since these results show the phenomenon is reversible and time dependent, explanations based on solution and precipitation are supported.

Any experiments which involve tempering in the 800-1100°F. range require that the possible influence of temper embrittlement be considered. Temper embrittlement in plain carbon steels is highly controversial and only rarely reported. If it does occur, the literature<sup>(80)</sup> indicates it cannot be suppressed by rapid quenching and, therefore, it is essentially unavoidable. Temper embrittlement, which is generally considered to involve an embrittling precipitate, could account for some of the differences in experimental results which in the past have been attributed to effects of prior austenite grain size.

## CONCLUSIONS

In these experiments, two heats of AISI 1040 and two heats of AISI 1046 steel were tested. One heat of each AISI grade was inherently fine grain and the other was inherently coarse grain. These steels were subjected to several austenitizing treatments which varied the prior austenite grain size from ASTM No. 0 to ASTM No. 10. After austenitizing, one group of specimens was quenched and tempered to a hardness of 26-28  $R_c$ , and another group of specimens was air-cooled. The impact energy transition curve was determined for all groups of specimens using half-width Charpy V-notch specimens and an instrumented impact tester. Tensile tests were also performed on quenched and tempered specimens using an Instron Model Testing Machine.

Based on the analysis of impact test results for quenched and tempered specimens, the following conclusions were drawn:

1. All quenched and tempered structures produced excellent impact properties with the highest energy transition temperature being  $-65^{\circ}\text{C}$ .
2. Actual austenite grain size does not significantly affect the transition temperature.
3. Inherently fine grain steel has a slightly lower transition temperature ( $7-47^{\circ}\text{C}$ .) compared with inherently coarse grain steel when quenched from an equivalent prior austenite grain size.



4. Actual fine austenite grain size increases the upper shelf impact energy by approximately 10%, but up to 100% in one case, when compared with coarse austenite grain size.
5. Inherently fine grain steel has upper shelf impact energy equal to, or in one case up to 100% greater than, inherently coarse grain steel, when quenched from an equivalent prior austenite grain size.

The differences in impact properties reported for quenched and tempered martensitic structures can be tolerated in most applications. The real danger is an elevated transition temperature since impact energy may be reduced to 1/20th of the original value after passing through the transition.

Based on the analysis of impact test results for air-cooled specimens which produced structures other than tempered martensite, the following conclusions were drawn:

1. Actual fine austenite grain size decreased the transition temperature 10-65°C. compared with actual coarse austenite grain size.
2. Inherent austenite grain size does not significantly affect the transition temperature.
3. Actual fine austenite grain size increases room temperature impact energy 100-400% compared with actual coarse austenite grain size.
4. Inherently fine grain steel has upper shelf impact energy equal to, or up to 100% greater in one case, than inherently coarse grain steel, when cooled from an equivalent prior austenite grain size.

The grain size dependency on impact properties is much greater for structures produced by air-cooling compared with the tempered martensite structures. Since inherently fine grain steels resist coarsening to a greater degree, it may be advantageous to use these steels when structures other than tempered martensite are produced; however, accurate temperature control may be utilized when austenitizing inherently coarse grain steels to minimize the degree of coarsening.

Based on the analysis of tensile test results for quenched and tempered specimens, the following conclusions were drawn:

1. The ultimate strength, yield strength, or percent elongation were not significantly affected by either actual or inherent austenite grain size.
2. Percent reduction in area was not influenced by inherent austenite grain size, but was equal to, or increased up to 100% in one case, by quenching from actual fine grained austenite.
3. Sharp yield point behavior was observed only in specimens quenched from fine grained austenite. Specimens quenched from coarse grained austenite produced a smooth curve in the yield area.
4. The degree of sharp yield point behavior was influenced by the aluminum content of the steel. The steel with the highest aluminum content produced elongated yielding over the longest range of strain.

The percent reduction in area results correlate with impact test results in general, since the specimens which showed the greatest loss

of reduction in area, produced an equivalent loss in room temperature impact energy. To the best of our knowledge, evidence demonstrating the effect of prior austenite grain size and aluminum content on sharp yield point behavior has not been reported in the literature.

Based on the analysis of fracture appearance and grain size studies, the following conclusions were drawn:

1. The actual austenite grain size is related to macroscopic fracture appearance for both quenched and tempered, and air-cooled specimens. This relationship is more pronounced for air-cooled specimens, where the facet size of brittle fractures increases with increasing prior austenite grain size.
2. The influence of actual austenite grain size is not observed in the SEM microscopic fracture appearance for quenched and tempered specimens, but is observed for air-cooled specimens, where the cleavage facet size increases with increasing actual austenite grain size.
3. Ferrite grain shape in tempered martensite reflects the shape of the original martensite plates, even after tempering at 1300°F. for 24 hours. Carbide distribution is also affected, and carbides tend to precipitate in rows which are parallel to the original martensite plates.

Since actual austenite grain size influences macroscopic fracture appearance, it influences the impact properties of the steel even though the austenite phase is no longer present at testing temperatures. The degree of this influence is reduced considerably by quenching and

tempering to produce a tempered martensitic structure. Ferrite grain shape and carbide distribution in tempered martensite are generally related to actual austenite grain size. When quenched, coarse austenite grains produce longer martensite plates. This process results in more elongated ferrite grains and rows of carbides parallel to the original martensite plates in the tempered martensite structure.

In many cases, inherently fine grain steels have improved impact properties compared with inherently coarse grain steels. This improvement cannot be explained entirely on the basis of the effects of actual austenite grain size. We suggest this improvement may result in part from precipitation of aluminum nitride on lattice defects during the austenitizing treatment. Observations of sharp yield point behavior during tensile testing cannot be adequately explained by any of the generally accepted theories. We suggest that in the presence of aluminum nitride a higher threshold stress level is required for dislocation motion necessary to propagate Lüders Bands. In this manner, sharp yield point behavior may be prolonged. In usual observations, attention is focused only on the detrimental effect to surface quality produced by Lüders Bands. The release of sudden avalanches of dislocations may have an important stress relieving effect, and result in improvement of other mechanical properties.

Earlier investigators have reported that coarse actual austenite grain size is detrimental to impact properties for all heat treatments. We have demonstrated that this effect is greatly reduced by quenching and tempering to produce a tempered martensitic structure at a relatively low hardness level. Low hardness tempered martensitic structures, produced from actual coarse grained austenite or inherently coarse grain

steels have excellent impact properties and may be successfully used in most applications.

**BIBLIOGRAPHY**

## BIBLIOGRAPHY

1. Cross, H. C. and J. G. Lowther, "The Study of the Effects of Manufacturing Variables on the Creep Resistance of Steels", Appendix V. to Committee Report, Proc. ASTM, V. 38, 1938, 149-171.
2. "Estimating the Average Grain Size of Metals", ASTM Spec. E112, V. 31, 414-427.
3. Lorig, C. H., "Influence of Metallurgical Factors", Behavior of Metals at Low Temperatures, ASM, 1953, 71-105.
4. Bain, E. C., Alloying Elements in Steel, ASM, 1952, Metals Park, Ohio.
5. Parker, Earl R., Brittle Behavior of Engineering Structures, John Wiley & Sons, Inc., New York, 1957.
6. Derge, Gerhard, Basic Open Hearth Steelmaking, AIME, 1964, New York.
7. McQuaid, H. W., and E. W. Ehn, "Effects of Quality of Steel on Case-Carburizing Results", AIME Trans., V. 67, 1922, 341-362.
8. McQuaid, H. W., "The Importance of Aluminum Additions in Modern Commercial Steels", ASM Trans., V. 23, 1935, 797-838.
9. Case, S. L. and K. R. Van Horn, Aluminum in Iron and Steel, John Wiley & Sons, Inc., New York, 1953.
10. Bain, E. C., "Factors Influencing the Inherent Hardenability of Steel", Trans. ASST, V. 20, 1932, 385-428.
11. Scott, H., "The Problems of Quenching Media for the Hardening of Steel", Trans. ASM, V. 22, 1934, 577-604.
12. Schane, P., Jr., "Effects of McQuaid-Ehn Grain-Size on the Structure and Properties of Steel", Trans. ASM, V. 22, 1934, 1038-1050.
13. Rosenberg, Samuel J. and Daniel H. Gagnon, "Effect of Grain Size and Heat Treatment Upon Impact Toughness at Low Temperatures of Medium Carbon Forging Steel", ASM Trans., V. 30, 1942, 361-375.

14. Gillett, H. W., "Impact Resistance and Tensile Properties of Metals at Subatmospheric Temperatures", Proj. No. 13, Joint ASME-ASTM Research Comm. on Effect of Temp. on Prop. of Metals, ASTM, Philadelphia, 1941.
15. Jaffe, L. D. and J. F. Wallace, Discussion, Trans. ASM, V. 40, 1948, 809-811.
16. Zackay, V. F., E. R. Parker, R. D. Goolsby and W. E. Wood, "Untempered Ultra-high Strength Steels of High Fracture Toughness", Natural Physical Science, V. 236, April 1972, 108-109.
17. Zackay, V. F., E. R. Parker, and W. E. Wood, "Influence of Some Microstructural Features on the Fracture Toughness of High Strength Steels", Proc. 3rd Int. Conf., Strength of Metals and Alloys, Institute of Metals, V. 1, Cambridge, 1973, 175-179.
18. Jolley, W. and E. H. Kottcamp, "A Study of the Toughness Differences Between Aluminum-Killed and Semikilled Steels", ASM Trans., V. 59, 1966, 439-456.
19. Bullens, D. K., Steel and Its Heat Treatment, V. 1, John Wiley and Sons, Inc., New York, 1948.
20. Derge, G. A., R. Kommel and R. F. Mehl, "Some Factors Influencing Austenite Grain Size in High Purity Steels", ASM Trans., V. 26, 1938, 153-166.
21. Herty, C. H., Discussion, J. Iron and Steel Inst., V. 134, 1936, 535-537.
22. Swinden, T. and G. R. Bolsover, "Controlled Grain Size in Steel", J. of Iron and Steel Inst., V. 134, 1936, 457-486.
23. Dorn, J. E. and O. E. Harder, "Relation of Pre-treatment of Steels to Austenitic Grain Growth", ASM Trans., V. 26, 1938, 106-132.
24. Beeghly, H. F., "Determination of Aluminum Nitride Nitrogen in Steel", Analytical Chemistry, V. 21, 1949, 1513-1519.
25. Solter, R. L. and C. W. Beattie, "Grain Structure of Aluminum-Killed Low Carbon Steel Sheets", AIME Trans., 1951, 721-726.
26. Leslie, W. C., R. L. Rickett, C. L. Dotson and C. S. Walton, "Solution and Precipitation of Aluminum Nitride in Relation to the Structure of Low Carbon Steels", ASM Trans., V. 46, 1954, 1470-1497.
27. Darken, L. S., R. P. Smith and E. W. Eiler "Solubility of Gaseous Nitrogen in Gamma Iron and the Effect of Alloying Constituents - Aluminum Nitride Precipitation", AIME Trans., V. 191, 1951, 1174-1179.

28. Grange, R. A., "Strengthening Steel by Austenite Grain Refinement", ASM Trans., V. 59, 1966, 26-48.
29. Phillips, R., G. Storey and K. J. Fussell, "Rapid Heat Treatments", The British Iron and Steel Research Association, London, 1964.
30. Claussen, E., "The Diffusion of Elements in Solid Iron", ASM Trans., V. 24, 1936, 640-648.
31. Dieter, G. E., Mechanical Metallurgy, McGraw-Hill, New York, 1961.
32. Low, John R., Jr., "Influence of Mechanical Variables", Behavior of Metals at Low Temperatures, ASM, Metals Park, Ohio, 1953, 39-70.
33. Gross, J. H., "Effect of Strength and Thickness on Notch Ductility", Impact Testing of Metals, ASTM STP 466, 1970, 21-52.
34. Smith, R. L. and J. L. Rutherford, "Tensile Properties of Zone Refined Iron in the Temperature Range from 298 to 4.2°K.", AIME Trans., V. 209, 1957, 857-864.
35. Huang, Der-Hung and G. Thomas, "Structure and Mechanical Properties of Tempered Martensite and Lower Bainite in Fe-Ni-Mn-C Steels", Met. Trans., V. 2, 1971, 1587-1598.
36. Holloman, J. H., L. D. Jaffee, D. E. McCarthy and M. R. Norton, "Effect of Microstructure on Mechanical Properties of Steel", ASM Trans., V. 38, 1947, 807-847.
37. Gensamer, M., "Brittle Fracture of Metals", Fracture of Engineering Materials, ASM, Metals Park, Ohio, 1957, 1-17.
38. Davenport, E. S., E. L. Roff and E. C. Bain, "Microscopic Cracks in Hardened Steel, Their Effects and Elimination", Trans. ASM, V. 22, 1934, 289-310.
39. Hehemann, R. F., V. J. Luhan and A. R. Troiano, "The Influence of Bainite on Mechanical Properties", ASM Trans., V. 49, 1957, 409-26.
40. Hyam, E. D. and J. Nutting, "The Tempering of Plain Carbon Steels", Jour. Iron and Steel Inst. (London), V. 184, 1956, 148-165.
41. Ludwik, P., "Die Bedeutung des Gleit und Reisswiderstandes fur die Werkstoff-prufung", Z. Ver. deut. Ing., V. 71:2, 1927, 1532-1538, (as cited in Ref. 5 and 31).
42. Honeycombe, R. W. K., The Plastic Deformation of Metals, St. Martin's Press, New York, 1968.

43. Cottrell, A. H., Dislocations and Plastic Flow in Crystals, Oxford University Press, London, 1953.
44. Griffith, A. A., "The Phenomena of Rupture and Flow in Solids", *Phil. Trans., Roy. Soc.*, London, V. 221, 1920, 163-198.
45. Orowan, E., "Fundamentals on the Brittle Behavior of Metals", Conf. on the Fatigue and Fracture of Metals, MIT, June 1950.
46. Zener, "The Micro-mechanism of Fracture", Fracturing of Metals, ASM, Metals Park, Ohio, 1948.
47. Stroh, A. N., "Crack Nucleation in Body-Centered Cubic Metals", Fracture, Proc. of Conf. on Fracture, Swampscott, Mass., John Wiley and Sons, Inc., New York, 1959, 117-122.
48. Stroh, A. N., "Brittle Fracture and Yielding", *Phil. Mag.*, V. 46, 1955, 968-972.
49. Cottrell, A. H., "Theoretical Aspects of Fracture", Fracture, Proc. of Conf. on Fracture, Swampscott, Mass., John Wiley & Sons, Inc., New York, 1959, 20-53.
50. Petch, N. J., "The Ductile-Cleavage Transition in Alpha-Iron", Fracture, Proc. of Conf. on Fracture, Swampscott, Mass., John Wiley and Sons, Inc., New York, 54-67.
51. Fractography and Atlas of Fractographs, ASM Handbook, V. 9, 1974.
52. "Basic Research Problems of the U. S. Army", Dept. of The Army, Durham, North Carolina, June 1974.
53. "Determining the Inclusion Content of Steel", E45 ASTM Standards, Part 31, 1970.
54. "Notched Bar Impact Testing of Metallic Materials", ASTM Spec. E23-66, ASTM Standards, V. 31, 1970, 285-301.
55. Fundamentals of Instrumented Impact Testing, Effects Technology, Inc., Santa Barbara, California, 1973.
56. Hoyt, S. L., "Notched-Bar Impact Tests", ASM Handbook, 1948, 112-115.
57. "The Selection of Steel for Notch Toughness", ASM Handbook, 1961, V. 1, 225-243.
58. Fahey, Norbert H., "Effects of Variables in Charpy Impact Testing", *Materials Research & Standards*, November 1961, 872-876.
59. "Impact Testing No. 1", Watertown Arsenal Laboratory, U. S. Dept. of Commerce, Watertown, Mass., 1958.

60. Tardif, H. P. and H. Marquis, "Impact Testing With an Instrumented Machine", *Metal Progress*, February 1964, 79-82.
61. Tardif, H. P. and H. Marquis, "Force Measurements in the Charpy Impact Test", *Canadian Metallurgical Quart.*, V. 2, No. 4, Oct.-Dec. 1963, 373-397.
62. Wullaret, R. A., "Applications of the Instrumented Charpy Impact Test", Impact Testing of Metals, ASTM STP 466, 1970, 148-164.
63. Erasmus, L. A., "Effect of Aluminum Additions on Forgeability, Austenite Grain Coarsening Temperature and Impact Properties", *Jour. of Iron & Steel Inst.*, January 1964, 32-41.
64. Petch, N. J., "The Cleavage Strength of Polycrystals", *Journ. of Iron & Steel Institute*, V. 174, 1953, 25-28.
65. Duckworth, W. E., M. J. May and J. J. Irani, "The Fracture of Martensite", *Proc. of 1st Inter. Conf. on Fracture (Japan)*, V. 2, 1965.
66. Rellick, J. R., C. J. McMahon, Jr. and H. L. Marcus, "Further Information on Oxygen Induced Intergranular Brittleness in Iron", *Met. Trans.*, V. 2, 1971, 342-344.
67. Stein, D. F., R. E. Weber and P. W. Palmberg, "Auger Electron Spectroscopy of Metal Surfaces", *Jour. of Metals*, February 1971.
68. "Family of Formable Steels Ready to Make It's Debut", Iron Age, March 17, 1975, 66-67.
69. "Tentative Method of Test for Plane-Strain Fracture Toughness of Metallic Materials", *ASTM Standards*, Part 31, 1971, E399-70T.
70. Holloman, J. H., "The Notched-Bar Impact Test", *AIME Trans.*, V. 158, 1944, 310-322.
71. Clausing, D. P., "Effect of Plane-Strain Sensitivity on the Charpy Toughness of Structural Steels", *International Journal of Fracture Mechanics*, V. 6, No. 1, March 1970.
72. Barsom, J. M. and S. T. Rolfe, "Correlations Between  $K_{IC}$  and Charpy V-Notch Test Results in the Transition-Temperature Range", Impact Testing of Metals, ASTM STP 466, 1970, 281-302.
73. Barsom, John M., "The Development of AASHTO Fracture-Toughness Requirements for Bridge Steels", *U. S.-Japan Cooperative Science Seminar*, Tohoku University, Sendai, Japan, August 1974.
74. Johnson, W. G. and Gilman, "Dislocation Velocities, Dislocation Densities and Plastic Flow in Lithium Fluoride Crystals", *Jour. of Appl. Physics*, V. 30, 1959, 129-144.

75. Wessel, E. T., "Abrupt Yielding and the Ductile-to-Brittle Transition in Body-Centered-Cubic Metals", AIME Trans., V. 209, 1957, 930-935.
76. Koistinen, D. P., U. S. Patent No. 3,461,002, August 12, 1969.
77. Richmond, O., W. C. Leslie and R. J. Sober, "Elimination of Yield Point in Steel by Rapid Temperature Change", Met. Trans., V. 3, 1972, 2593-2595.
78. Cohen, M., "Retained Austenite", ASM Trans., V. 41, 1949, 35-94.
79. Cottrell, A. H., An Introduction to Metallurgy, Edward Arnold, London, 1967.
80. Libsch, J. F., A. E. Powers and G. Bhat, "Temper Embrittlement in Plain Carbon Steels", ASM Trans., V. 44, 1952, 1058-1075.

MICHIGAN STATE UNIVERSITY LIBRARIES



3 1293 03143 3117